IDŐJÁRÁS

QUARTERLY JOURNAL
OF THE HUNGARIAN METEOROLOGICAL SERVICE

CONTENTS

VOL. 121 * NO. 1 * JANUARY – MARCH 2017

IDŐJÁRÁS

Quarterly Journal of the Hungarian Meteorological Service

Editorial Office: Kitaibel P.u. 1, H-1024 Budapest, Hungary
P.O. Box 38, H-1525 Budapest, Hungary
E-mail: journal.idojaras@met.hu
Fax: (36-1) 346-4669

Indexed and abstracted in Science Citation Index Expanded™ and Journal Citation Reports/Science Edition

Covered in the abstract and citation database SCOPUS®

Included in EBSCO's databases

Subscription by mail:
IDŐJÁRÁS, P.O. Box 38, H-1525 Budapest, Hungary
E-mail: journal.idojaras@met.hu

IDŐJÁRÁS

Quarterly Journal of the Hungarian Meteorological Service
Vol. 121, No. 1, January – March, 2017, pp. 1–28

Numerical simulation of sulfate formation in water drops: results of a box experiment

Gabriella Schmeller[1*] and **István Geresdi**[2]

[1]*University of Pécs, Faculty of Sciences*
Doctoral School of Earth Sciences
Ifjúság útja 6, 7624 Pécs, Hungary
E-mail: schg@gamma.ttk.pte.hu

[2]*University of Pécs, Faculty of Sciences*
Institute of Geography
Ifjúság útja 6, 7624 Pécs, Hungary
E-mail: geresdi@gamma.ttk.pte.hu

[*]*Corresponding author*

(Manuscript received in final form May 31, 2016)

Abstract—The purpose of the research was to investigate how sulfate formation depends on the drop size, and to find efficient scheme for the numerical integration of ODEs (ordinary differential equations) describing absorption and chemical reactions. A box model was developed to simulate how the water drops absorb the different compounds and to simulate formation of sulfate by oxidation processes. Results show, that the length of time step necessary for the accurate integration of the differential equation depends on the drop size and on the concentration of the trace gases in the environment of the water drop. Analysis of the data suggests that the time step should be at least 0.01 s if the drop size is smaller than 20 μm, and it can be 0.1 s above this size. The time evolution of the pH of solution and that of the concentration of different compounds inside of water drops significantly depend on the size of the drops. In the case of water drops smaller than 50 μm, the concentration of the compounds becomes steady state in time interval less than 20 s, that is absorption and oxidation processes occur at almost same rate. In the case of larger drops, it takes significantly longer time to reach this balance. In the polluted atmosphere, the mass of the condensation nuclei can increase significantly due to the chemical processes occuring inside of the water drops. The results of this research will be used in a two-dimensional model simulating these processes in stratocumulus clouds with bin microphysical scheme.

Key-words: cloud chemistry, numerical simulation, absorption, oxidation, sulfate formation

1. Introduction

The investigation of the chemical composition of rainwater has got into the focus of the research about atmospheric chemistry in the last decades. From the middle of the last century, the air pollution caused by the industry, traffic, agriculture, as well as households has endangered the natural environment and the human health. The increasing occurrence of acid rain and heavy air pollution related to smog have initiated researches about the role of cloud and precipitation elements in the accumulation of the pollution in the atmosphere and on the surface.

The emitted air pollutants show vertical and horizontal inhomogeneities in the atmosphere that depend on the characteristics of the emission (e.g., location and intensity of emission and chemical properties of the pollutants), the surface (topography), and atmosphere (e.g., temperature profile, wind speed, and cloud cover). The chemically inert gases can reach the stratosphere and can be transported to huge distances. The chemically active gases get into reactions with other chemicals both in gas and liquid phases. The rate of reaction depends on the characteristics of the atmospheric environment such as temperature, pressure, and relative humidity; and furthermore, on the type of the reaction. The liquid and solid phase hydrometeors not only absorb or desorb gases, but also numbers of chemical reactions can occur in these particles. This is the reason why clouds and precipitation play an important role in the transport (both in vertical and horizontal directions) and in the washout of air pollutants compounds. Broad scale of processes – from absorption of gases in micron-size water drops to transport of particles by kilometer-size updraft core – have to be studied to clarify the role of clouds in the transport of pollutants.

A number of researches over the past few decades have focused on the absorption of different trace gases by water drops, especially sulfur-dioxide (SO_2) and different oxidizing compounds, furthermore on the description of their chemical properties and reactions. *Diehl et al.* (2000) gives a comprehensive summary about the most important theoretical and laboratory studies and about the results of field experiments that have been accomplished. In the beginning of the 1980's, numerous field studies (e.g., *Hegg* and *Hobbs,* 1981, 1982; *Daum et al.,* 1983; *Hegg et al.,* 1984; *Barrie,* 1985) proved that a significant fraction (~ 60%) of sulfate (SO_4^{2-}) in drops is produced by absorption of sulfur-dioxide and converting it into sulfate by several chemical reactions, and the other part was formed by dissolution of aerosol particles.

Field measurements and chemical analysis of the collected precipitation samples gave a comprehensive overview about the chemical components inside the cloud and precipitation elements. These studies gave a correct description about the transport of pollutants in the lower atmosphere, but they provided less detail about physical and chemical processes occurring inside of water drops, and on the surface of ice particles.

A number of laboratory observations have been accomplished to study absorption and desorption of gases in water drops and on the surface of ice particles. Based on laboratory studies *Beilke* and *Georgii,* 1968, *Beilke,* 1970, *Barrie* and *Georgii,* 1976, and *Walcek et al.*, 1984 asserted, that the amount of absorbed SO_2 increased with increasing gas concentration and with the exposure time of the gas. It was asserted that molar concentration of SO_2 in water drops could reach a limiting equilibrium value if only SO_2 gas is present for long time period. In the case of drops smaller than diameter of 20 μm the solution is always in equilibrium with the gas phase in the environment. Chemical processes, e.g., dissociation of absorbed gases, oxidation of ions and the change of pH of solution have been investigated by several researchers. *Beilke et al.* (1975) determined the oxidation rate of dissolved 4-valence sulfur S(IV) species ($(SO_2)_{aq}$, HSO_3^-, and SO_3^{2-}) to 6-valence sulfur S(VI) species (HSO_4^- and SO_4^{2-}) in pure water drops. This rate was found to be rather slow ($\sim 10^{-5}$ % h^{-1}). *Seinfeld* (1986) showed that other chemical species can be also found in water drops, and some types of compounds may act as oxidizing agents (e.g., hydrogen-peroxide (H_2O_2) and ozone (O_3)). In drops containing these oxidizing agents, the total amount of sulfur in the liquid phase is continuously increasing with time (*Walcek et al.*, 1984; *Waltrop et al.*, 1991).

As a new research tool, numerical models have been developed to study the uptake of trace gases by water drops and the chemical reactions that occur inside of water drops. The results of these models have been verified mostly by laboratory experiments.

Description of absorption of gases into and out of water drops has been continuously improved since the middle of the last century. *Kronig* and *Brink* (1950), *Kronig et al.* (1951), *Johnson et al.* (1967), and *Watada et al.* (1970) solved the equation describing the convective diffusion inside the drop. *Walcek* and *Pruppacher* (1984) took into account the internal circulation in numerical simulation of diffusion of sulfur-dioxide occurred across the air-water interface. *Waltrop et al.* (1991), *Mitra et al.* (1992), *Hannemann et al.* (1995, 1996), and *Diehl et al.* (2000) carried out several laboratory experiments in a vertical wind tunnel and compared the results of observation with that of theoretical models. The unique of this type of measurement is that the drops are freely suspended in the vertical wind tunnel due to laminar or turbulent air flow, which mimics atmospheric conditions (*Diehl et al.,* 2011). In their laboratory experiments, *Waltrop et al.* (1991) investigated the uptake of SO_2 from the gas phase in the presence of H_2O_2 in the liquid phase. A simplified version of the theoretical model published by *Walcek* and *Pruppacher* (1984) was used (model for well-mixed drop) for the prediction of SO_2 diffusion into water drops. *Waltrop et al.* (1991) and *Mitra* and *Hannemann* (1993) published details about the equations used in the well-mixed model. In the case of millimeter sized drops, the results

of the laboratory experiments were in good agreement with that of the well-mixed model.

Hannemann et al. (1995, 1996) investigated the uptake and desorption of ammonia (NH_3) in the presence of carbon-dioxide (CO_2) and the simultaneous uptake of NH_3, SO_2 and CO_2, by water drops by using realistic vertical profile of these gases. In both cases the observed data agreed well with the results of the well-mixed model and with that of the Kronig-Brink model (details by *Walcek* and *Pruppacher,* 1984), that gives a sophisticated description about gas diffusion inside the drop. *Hannemann et al.* (1995) asserted that the slow hydration reaction of CO_2 must be taken into consideration in the model calculations, otherwise the amount of NH_3 is significantly overestimated. The model calculations were verified by observation of the simultaneous uptake of NH_3, SO_2, and CO_2 (*Hannemann et al.*, 1996). Important results were that the uptake of SO_2 strongly depended on the concentration of NH_3 and on the precipitation intensity, furthermore, they proved that if NH_3 and SO_2 are simultaneously present, their desorption is negligible. They also found that, the small drops more efficiently wash out these gases than the larger ones.

Several authors studied the role of ice crystals in the uptake and retention of trace gases (*Diehl et al.,* 1998; *v. Blohn et al.,* 2013), and also numerical models have been developed to study this process in the case of frozen drops (*Stuart* and *Jacobson,* 2005). They also proved that the direct uptake of gases by ice particles is not as efficient as by water drops. The most effective process to uptake of gases by ice particles is the riming.

In Hungary, the first attempts about precipitation chemistry were made in the early 60th. The setting of the surface network allowed the observation of chemical characteristics of precipitation (e.g., pH, electrical conductivity, sodium, potassium, magnesium, calcium, ammonium, sulfate, nitrate, nitrite, chloride, and orthophosphate ion content). The early precipitation chemistry measurements were accomplished by open samplers, which frequently overestimated the concentration of different ions by 100%. To avoid this high sampling failure rate, an automatic sampling network was established (*Horváth,* 1981). The accuracy of the data measured by this network – using automatic collectors - was analyzed in the early 80th. A suggestion for the development of the precipitation chemistry station was published to significantly improve the spatial resolution of the observations in Hungary. The dramatically increased air pollution in Hungary initiated comprehensive researches about the atmospheric and precipitation chemistry in the early 70th. *Mészáros* (1976) studied the sources, concentration, and chemical reactions of sulfur-dioxide, furthermore the chemical composition of background aerosol particles. Observations, accomplished in different regions of the world, showed that the concentration of sulfur-dioxide strongly decreases as the distance from the source increases, and that the relative amount of sulfate related to sulfur-dioxide increases. This phenomenon can be explained partly by the removal of sulfur-dioxide from the

atmosphere and partly by the efficient conversion of sulfur-dioxide to sulfate or to other compounds. This process was widely observed during field measurement campaigns. *Mészáros* (1973, 1974) published results about the correlation between the sulfate concentration and different atmospheric parameters. They asserted that sulfate aerosol particles formed in different ways during summer and during winter. *Mészáros* and *Vissy* (1974) studied the properties of aerosol particles over the oceans in the southern hemisphere. They observed that the aerosol particles in the maritime air mass mainly consist of ammonium sulfate ($(NH_4)_2SO_4$) and mixture of ammonium sulfate and sea salt. *Mészáros* (1976) concluded that aside from the sea salt, the tropospheric background aerosol mainly consists of sulfur compounds.

Várhelyi (1977, 1980, 1982) developed several numerical models to simulate the annual (or daily) variation of sulfur budget over Hungary, and to estimate rainout and washout of sulfate particles and sulfur-dioxide. She compared the simulated data with data of field observations. The analysis of the data showed that while both in-cloud scavenging (washout) and below-cloud scavenging (rainout) played important role in the wet removal of SO_2, sulfate particles were mostly washed out by cloud droplets. NH_3 has a significant role in the wet removal of SO_2.

Numerous calculations were made to simulate the chemical processes occurring in water drops. *Horváth* and *Mészáros.* (1978) and *Horváth* (1977) determined the mechanisms and kinetic parameters for sulfur-dioxide to sulfate conversion. *Horváth et al.* (1978) determined the rate constant for sulfur-sulfate oxidation occurring during summer and in two seasons (winter + summer). The results showed that the transformation of SO_2 is slower during summer than during winter. *Várhelyi* (1975) published results about the development of a numerical model to simulate the absorption and oxidation of sulfur-dioxide in cloud and fog droplets in the presence of ammonia.

In the middle of the seventies, several research projects have been accomplished to study the characteristics of sulfate-particles in the lower troposphere, such as the size distribution, concentration, and residence time (*Mészáros* and *Várhelyi,* 1975). The calculation of condensational growth of cloud droplets on ammonium sulfate particles was studied by *Mészáros et al.* (1974). The concentration and distribution of CCN (cloud condensation nuclei) containing ammonium sulfate was established referring to the results of field measurements. The effect of oxidation of SO_2 inside of water drops on the growth of sulfate condensation nuclei was also studied by numerical simulations (*Várhelyi,* 1975). *Mészáros* and *Várhelyi,* (1975) concluded from the observation data that on regional scale, most of the sulfate particles are smaller than 0.2 μm. They also argued that wet deposition removed the sulfate particles from the atmosphere more efficiently than dry deposition. *Mészáros et al.* (1974) investigated how the characteristics of aerosol particles (act as condensation nuclei) affect the evolution of size distribution of water drops. These aerosol particles were classified in different categories according to their

mass and their effect on water drop concentration. *Várhelyi* (1975) found that the calculated radius of ammonium sulfate particles was in good agreement with the observed values, furthermore, the oxidation of SO_2 in the presence of NH_3 in cloud and fog droplets is one of the main processes producing ammonium sulfate particles. Comparison of the simulated size distributions with the observation data published by *Mészáros* (1971) showed a bias between the predicted (0.3 – 0.6 μm) and measured (< 0.1 – 3 μm) size ranges. This discrepancy made her to suggest, that other chemical reaction might take part in the formation of ammonium sulfate particles besides the oxidation of SO_2 occurring inside of the water drops as well.

2. Description of the model

A box model was developed to simulate physical and chemical processes occurring in clouds. This type of box model does not allow us to simulate the scavenging of gases. The focus of our research is on looking for accurate and efficient solution of the ordinary differential equations (ODEs) describing the absorption/desorption of chemical compounds through the surface of water drops, furthermore for that of chemical reactions equations for water drops, especially the oxidation mechanisms of sulfur-dioxide producing sulfate ions. Sensitivity test was made by repeating the numerical experiments at six different drop sizes (10 μm, 20 μm, 50 μm, 70 μm, 100 μm, and 500 μm). The diffusional growth of water drops and the accretion by collision-coalescence were not taken into consideration. The role of chemical characteristics and atmospheric concentration of the compounds of CO_2, SO_2, NH_3, O_3, and H_2O_2 were investigated in the formation of sulfate inside water drops of different sizes. In the presence of ammonium ion (NH_4^+), the effect of acidic compounds on the pH is compensated, and ammonium sulfate particles may form after the evaporation of water drops. Some oxidizing agents, e.g., ozone (O_3) and hydrogen-peroxide (H_2O_2) can also promote this process through pH-dependent reactions. Their concentration in the solution depends on their amount in the gas phase, on their chemical properties (e.g., Henry's law constant and dissociation constant), and on the size of the drops. The dissociation constants of these gases depend on the pH of the solution. There is also a strong interaction between the hydrogen ion concentration and the rate of chemical reactions. These are only a few examples of that the gases and the liquid water drops form rather complex chemical system. This complexity is enhanced by the size dependence of absorption rates and by that of the rates of chemical reactions.

The uptake of gases by water drops was calculated by a model, assuming that the compounds are well-mixed inside of water drops all the time. The diffusion of gases through the surface of water drops is given by the following formula (*Pruppacher* and *Klett,* 2010):

$$\frac{dc_l}{dt} = \frac{3 \cdot D_g}{r^2}\left(c_{g,\infty} - \frac{c_l}{K_H^* \cdot R \cdot T}\right) \cdot f_v \ , \qquad (1)$$

where c_l and $c_{g,\infty}$ are the gas concentration inside of the drop and far from the drop in M [mole litre^{-1}] and ppbv, respectively; D_g is the diffusion constant in m^2 s^{-1} depending on the type of the gas and on the temperature; r is the radius of the drop in m, f_v is the ventilation coefficient, K_H^* is the modified (due to the dissociation) Henry's law constant in M Pa^{-1}, R = 8.2·10^3 Pa M^{-1} K^{-1}, and T is the temperature in units of K. The dependence of the K_H^* on the pH of the solution is shown in *Fig. 1.* Low dissociation rate of the H_2O_2 reflects that K_H^* only slightly depends on the pH. In the case of CO_2, the K_H^* remains near constant only if the pH is less than 5.0. K_H^* strongly depends on pH both in the cases of SO_2 and NH_3. The plots in *Fig. 1* also suggest that NH_3 is more efficiently absorbed at low pH values than at larger ones, and vice versa, SO_2 is more efficiently absorbed at larger pH values than at smaller ones.

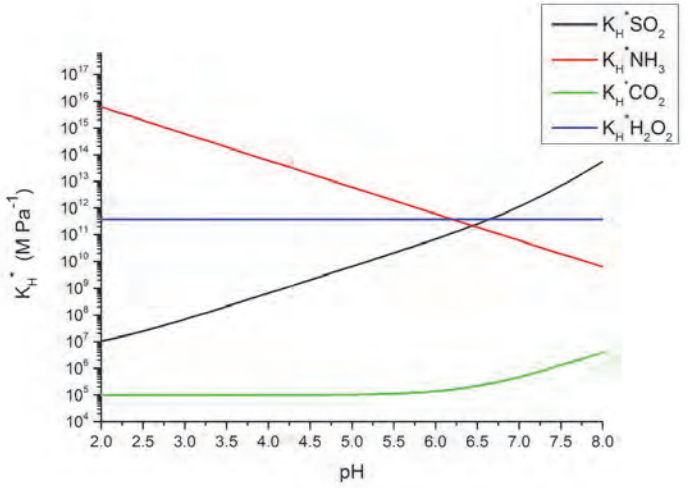

Fig. 1. Dependence of modified Henry's law constant (K_H^*) on pH in the case of different compounds.

If the dissolved gases completely dissociate in the drop, $k_H^* = k_H \cdot K_1 / c_l$, for $[H^+] << K_1$ and $[H^+] \approx c_l$, where k_H^* and k_H are dimensionless and considered as $k_H = K_H \cdot R \cdot T$ with R = 8.2·10^3 Pa M^{-1} K^{-1}. T is the temperature in units of K, $[H^+]$ is the hydrogen ion concentration in M, K_H is the Henry's law constant in M Pa^{-1}, and K_1 is the dissociation constant of the given chemical species in water in M. In this case Eq. (1) can be modified into the following form:

$$\frac{dc_l}{dt} = \frac{3 \cdot D_g}{r^2}\left(c_{g,\infty} - \frac{c_l^2}{k_H \cdot K_1} \right) \cdot f_v \,. \tag{2}$$

The advantage of this equation is that it does not involve the pH dependence of the modified Henry's law constant, so it can be solved analytically for the gases whose K_H^* depends on the pH. Unfortunately, the above mentioned conditions are not fulfilled for NH_3 and CO_2.

The oxidation mechanism of S(IV) species to S(VI) by O_3 and H_2O_2 are calculated by the formulas given by *Seinfeld* and *Pandis* (2006). H_2O_2 is a very soluble gas in water, and under typical atmospheric conditions, the OH radical produced from H_2O_2 oxidizes mainly the HSO_3^- ions as principal reactive S(IV) species (*McArdle* and *Hoffmann,* 1983). So the rate of oxidation can be given by the following equation (*Hoffmann* and *Calvert*, 1985):

$$-\frac{d\left[S(IV)\right]}{dt} = \frac{k \cdot \left[H^+\right] \cdot \left[H_2O_2\right] \cdot \left[HSO_3^-\right]}{1 + K \cdot \left[H^+\right]}, \tag{3}$$

where $k = 7.5 \pm 1.16 \cdot 10^7\, M^{-2} s^{-1}$ and $K = 13\, M^{-1}$ at 298 K. The concentration of HSO_3^- ion can be given as a function of absorbed SO_2 (sum of $\left[(SO_2)_{aq}\right]$, $\left[HSO_3^-\right]$ and $\left[SO_3^{2-}\right]$):

$$\left[HSO_3^-\right] = \frac{\left[S(IV)\right]}{\left[1 + \frac{\left[H^+\right]}{K_1} + \frac{K_2}{\left[H^+\right]}\right]}, \tag{4}$$

where K_1 and K_2 are the first and second dissociation constants of $(SO_2)_{aq}$ in unit of M, respectively. Substituting Eq. (4) into Eq. (3) the oxidation rate can be given as a function of the concentration of absorbed H_2O_2 and SO_2:

$$-\frac{d[S(IV)]}{dt} = \frac{k \cdot [H^+] \cdot [H_2O_2] \cdot [S(IV)]}{\left(1 + K \cdot [H^+]\right) \cdot \left(1 + \frac{[H^+]}{K_1} + \frac{K_2}{[H^+]}\right)} = [H_2O_2] \cdot [S(IV)] \cdot \frac{k \cdot [H^+]}{\left(1 + K \cdot [H^+]\right) \cdot \left(1 + \frac{[H^+]}{K_1} + \frac{K_2}{[H^+]}\right)} \,. \tag{5}$$

The aqueous phase concentration of H_2O_2 is about six orders of magnitude higher than that of O_3 under typical ambient conditions. Although it dissolves fast, its dissociation constant is rather small ($1.58 \cdot 10^{-12}$).

O_3 reacts in a different way with S(IV) species, than the H_2O_2 does. Oxidation reaction occurs with SO_3^{2-} with HSO_3^- and $(SO_2)_{aq}$ as well. The oxidation rate of O_3 is increasing by increasing pH, as it follows the presence of the above mentioned ions. It can oxidize all S(IV) species (*Seinfeld* and *Pandis*, 2006):

$$-\frac{d[S(IV)]}{dt} = \left(k_0 \cdot \left[(SO_2)_{aq}\right] + k_1 \cdot \left[HSO_3^-\right] + k_2 \cdot \left[SO_3^{2-}\right]\right) \cdot [O_3] \quad . \qquad (6)$$

The concentration of $(SO_2)_{aq}$, HSO_3^-, and SO_3^{2-} ions can be given as a function of the absorbed SO_2:

$$\left[(SO_2)_{aq}\right] = \frac{[S(IV)]}{\left[1 + \frac{K_1}{[H^+]} + \frac{K_1 \cdot K_2}{[H^+]^2}\right]} \quad , \qquad (7)$$

$$\left[HSO_3^-\right] = \frac{[S(IV)]}{\left[1 + \frac{[H^+]}{K_1} + \frac{K_2}{[H^+]}\right]} \quad , \qquad (8)$$

$$\left[SO_3^{2-}\right] = \frac{[S(IV)]}{\left[1 + \frac{[H^+]}{K_2} + \frac{[H^+]^2}{K_1 \cdot K_2}\right]} \quad , \qquad (9)$$

Substituting Eqs. (7), (8), and (9) into Eq. (6), the oxidation rate can be given as a function of the concentration of absorbed O_3 and that of absorbed SO_2:

$$-\frac{d[S(IV)]}{dt} = \left(k_0 \cdot \frac{[S(IV)]}{\left[1 + \frac{K_1}{[H^+]} + \frac{K_1 \cdot K_2}{[H^+]^2}\right]} + k_1 \cdot \frac{[S(IV)]}{\left[1 + \frac{[H^+]}{K_1} + \frac{K_2}{[H^+]}\right]} + k_2 \cdot \frac{[S(IV)]}{\left[1 + \frac{[H^+]}{K_2} + \frac{[H^+]^2}{K_1 \cdot K_2}\right]} \right) \cdot [O_3] =$$

$$[S(IV)] \cdot [O_3] \cdot \left(\frac{k_0}{\left[1 + \frac{K_1}{[H^+]} + \frac{K_1 \cdot K_2}{[H^+]^2}\right]} + \frac{k_1}{\left[1 + \frac{[H^+]}{K_1} + \frac{K_2}{[H^+]}\right]} + \frac{k_2}{\left[1 + \frac{[H^+]}{K_2} + \frac{[H^+]^2}{K_1 \cdot K_2}\right]} \right) \quad . \qquad (10)$$

Using Eq. (5) and Eq. (10), the coefficients for oxidation rates can be plotted as the function of the pH (*Fig. 2.*).

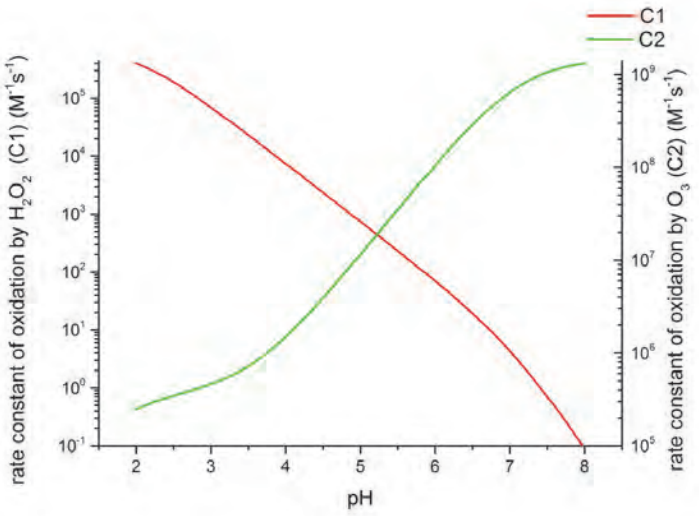

Fig. 2. The dependence of rate constants of S(IV) to S(VI) oxidation on the pH in the cases of oxidation by O_3 (green curve) and by H_2O_2 (red curve).

Although the rate constant related to the oxidation by O_3 is about five orders larger than in the case of oxidation by H_2O_2, the oxidation rate by H_2O_2 is about one-two orders larger, because the concentration of the H_2O_2 inside the water drops is about six orders larger than the concentration of O_3.

2.1. Description of the numerical techniques

Numerical modeling of absorption and that of chemical reactions occurring inside of water drops is a rather complex issue. The absorption/desorption rate of gases depends not only on their concentration in the ambient atmosphere, but on the turbulent mixing of the gases inside of the water drops, and the value of pH also affects the uptake of gases. The accurate and efficient numerical solution of the coupled differential equations describing the chemical reactions is also crucial. In the next phase of the research, we intend to implement these processes in a numerical cloud model, so it is important to find efficient numerical technique to solve the equations describing the above mentioned processes. Because both the rate of absorption and that of chemical reactions are sensitive on the value of pH, the accurate calculation of this diagnostic variable is also important.

2.1.1. Numerical solution of the absorption equations

In the case of O_3 and H_2O_2 gases, the analytical solution of Eq. (1) is possible because of the absence of dissociation (O_3) or due to very small dissociation rate (H_2O_2). The analytical solution of Eq. (2) can be applied to give the amount of absorbed SO_2 at some environmental conditions. Unfortunately, in the case of NH_3 and CO_2, there is no analytical solution to describe their absorption/desorption. In their cases, the numerical solution of Eq. (1) is used to evaluate the amount of the absorbed gases.

The Euler method is rather frequently applied for the solution of ordinary differential equations (ODEs) like Eq. (1). In this method, it is supposed that neither the concentration of dissolved gases in the liquid phase (c_l), nor the value of K_H^* change during the time step of Δt. The disadvantage of this method is that the above mentioned conditions can be hold if the time step used for integration is small enough. The other problem about the Euler method is that it causes large numerical dispersion (*Geresdi* and *Weidinger,* 1989).

To avoid these problems, a quasi-analytical method was chosen to solve Eq. (1). In this case, only the concentration of the hydrogen ions is supposed to remain constant during the time step of Δt, and by the end of the time step, the concentration of the gases in the liquid drop (c_l) is given by the following equation:

$$c_l\left(t+\Delta t\right) = c_{l,sat} - \left(c_{l,sat} - c_l\left(t\right)\right)\cdot e^{-const\cdot\Delta t}, \tag{11}$$

where $c_{l,sat}$ is the so called saturated concentration of the gas inside of the water drops in M:

$$c_{l,sat} = K_H^* \cdot R \cdot T \cdot c_g, \tag{12}$$

where c_g is the initial gas concentration inside of the drop in M calculated from the gas mixing ratio in the environment and the parameter *const* in s^{-1} is given by:

$$const = D_g \cdot \frac{3 \cdot f_V}{r^2 \cdot K_H^* \cdot R \cdot T}, \tag{13}$$

where D_g is the diffusion constant in $m^2\ s^{-1}$; f_v is the ventilation coefficient, r is the radius of the drop in m, K_H^* is the modified Henry's law constant in M Pa^{-1}, $R = 8.2\cdot10^3$ Pa M^{-1} K^{-1}, and T is the temperature in units of K.

Stability of this type of solution was investigated at different drop sizes and by varying the concentration of different gases in the ambient air. *Table 1*

summarizes the investigated cases and contains the time steps that are necessary to use for the accurate solution of Eq. (1) different drop sizes and at different environmental conditions. The calculations were repeated at three different time steps (1.0, 0.1, and 0.01 s). The data suggest that the time step has to be as small as 0.1 s. Even more, in some cases smaller time step (0.01 s) is necessary for the stable solution.

Table 1. Critical time steps (s) for numerical solution of differential equations describing the absorption of different trace gases at different drop sizes.

Case	Mixing ratio [ppbv]				Drop size [μm]					
	SO_2	NH_3	O_3	H_2O_2	10	20	50	70	100	500
					time step (s)					
01a	0.1	1	2	2	10^{-2}	10^{-1}	10^{-1}	10^{-1}	10^{-1}	10^{-1}
1a	1	2	2	2	10^{-2}	10^{-1}	10^{-1}	10^{-1}	10^{-1}	10^{-1}
2a	2	0	2	0	10^{-1}	10^{-1}	10^{-1}	10^{-1}	10^{-1}	10^{-1}
2b	2	0	2	2	10^{-1}	10^{-1}	10^{-1}	10^{-1}	10^{-1}	10^{-1}
2c	2	5	2	2	10^{-2}	10^{-2}	10^{-1}	10^{-1}	10^{-1}	10^{-1}
4a	4	2	2	2	10^{-1}	10^{-1}	10^{-1}	10^{-1}	10^{-1}	10^{-1}
5a	5	0	2	2	10^{-1}	10^{-1}	10^{-1}	10^{-1}	10^{-1}	10^{-1}
5b	5	2	2	0	10^{-1}	10^{-1}	10^{-1}	10^{-1}	10^{-1}	10^{-1}
5c	5	2	2	2	10^{-1}	10^{-1}	10^{-1}	10^{-1}	10^{-1}	10^{-1}
5d	5	5	2	2	10^{-2}	10^{-1}	10^{-1}	10^{-1}	10^{-1}	10^{-1}
10a	10	5	2	2	10^{-1}	10^{-1}	10^{-1}	10^{-1}	10^{-1}	10^{-1}
20a	20	10	2	2	10^{-1}	10^{-1}	10^{-1}	10^{-1}	10^{-1}	10^{-1}
30a	30	10	2	2	10^{-2}	10^{-1}	10^{-1}	10^{-1}	10^{-1}	10^{-1}
50a	50	10	2	2	10^{-2}	10^{-1}	10^{-1}	10^{-1}	10^{-1}	10^{-1}

2.1.2. Numerical solution of the chemical reaction equations

A quasi-analytical method was applied to solve the ordinary differential equations (Eqs. (5) and (10)) describing the oxidation processes occur inside of water drops:

$$\int_{[S(IV)]_0}^{[S(IV)]} \frac{d[S(IV)]}{[S(IV)]} = \int_{t_0}^{t_0+\Delta t} -C_1 \cdot [H_2O_2]_{t_0} \cdot \Delta t \quad , \tag{15}$$

$$\int_{[S(IV)]_0}^{[S(IV)]} \frac{d[S(IV)]}{[S(IV)]} = \int_{t_0}^{t_0+\Delta t} -C_2 \cdot [O_3]_{t_0} \cdot \Delta t \quad , \tag{16}$$

where $C_1 = \frac{k \cdot [H^+]}{\left(1 + K \cdot [H^+]\right) \cdot \left(1 + \frac{[H^+]}{K_1} + \frac{K_2}{[H^+]}\right)}$ is from Eq. (5) and $C_2 = \frac{k_0}{\left[1 + \frac{K_1}{[H^+]} + \frac{K_1 \cdot K_2}{[H^+]^2}\right]} + \frac{k_1}{\left[1 + \frac{[H^+]}{K_1} + \frac{K_2}{[H^+]}\right]} + \frac{k_2}{\left[1 + \frac{[H^+]}{K_2} + \frac{[H^+]^2}{K_1 \cdot K_2}\right]}$ is from Eq. (10) in $M^{-1}\ s^{-1}$.

These integrals can be solved analytically if some conditions are met. It is supposed that the concentration of H_2O_2 and O_3 remains constant during the time step. Although the coefficients C_1 and C_2 depend on the pH of the solution (*Fig. 2*), they can be also considered to be constant during the time step, if time step is small enough. If these conditions are met, the change of the sulfate concentration due to oxidation processes can be given by the following equations:

$$\begin{aligned}
\Delta[S(IV)]_1 &= [S(IV)]_{t_0+\Delta t} - [S(IV)]_{t_0} = [S(IV)]_{t_0} \cdot (e^{-C_1 \cdot [H_2O_2]_{t_0} \cdot \Delta t} - 1) \\
\Delta[S(IV)]_2 &= [S(IV)]_{t_0+\Delta t} - [S(IV)]_{t_0} = [S(IV)]_{t_0} \cdot (e^{-C_2 \cdot [O_3]_{t_0} \cdot \Delta t} - 1) \\
\Delta[S(IV)] &= \Delta[S(IV)]_1 + \Delta[S(IV)]_2
\end{aligned} \quad , \tag{17}$$

where the values of $[S(IV)]$ and $\Delta[S(IV)]$ are in M. The accuracy of these solutions strongly depends on the appropriate choose of the time step. The application of small time step may result in accurate solution, but it significantly reduces the efficiency of the numerical model. Numerical experiments were made to find the appropriate time step.

The calculation of pH is done by the iteration method developed by *Hannemann et al.* (1995).

3. Results

3.1. Absorption

Fig. 3 shows the time evolution of the pH of water drops at different drop sizes and different composition of the ambient air (see *Table 1*). (Not all of the

investigated cases are plotted, a few of them were chosen to show the typical time evolution of pH in the water drops.)

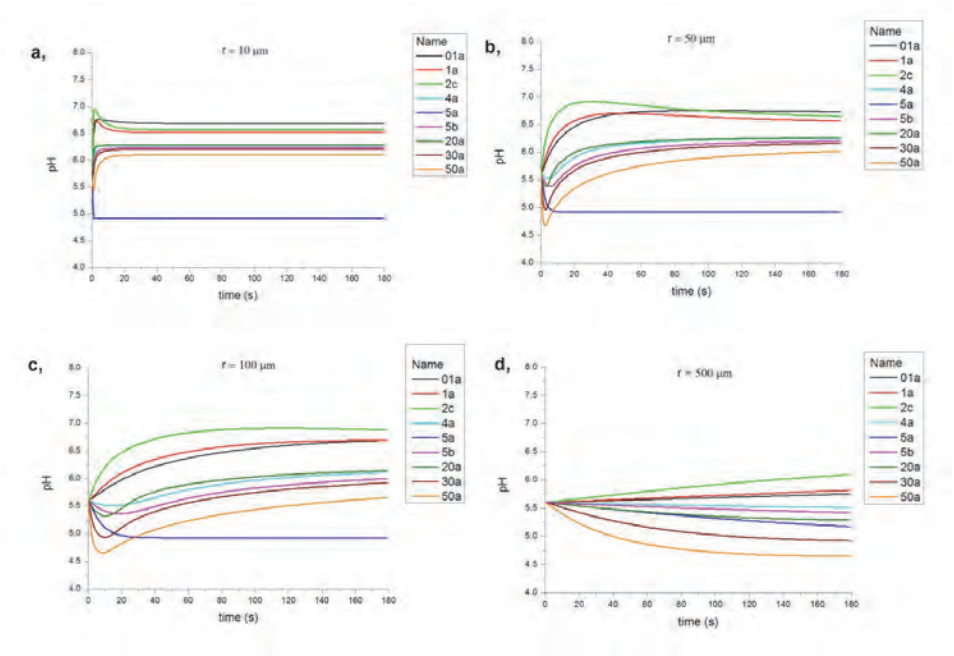

Fig. 3. Time evolution of the pH of the solution at different environmental conditions and different drop sizes: (a) $r = 10$ μm; (b) $r = 50$ μm; (c) $r = 100$ μm, and (d) $r = 500$ μm. The applied time step was equal to 0.01 s in the case of smallest drop size, and it was equal to 0.1 s in the other cases.

In the case of small water drops ($r \leq 20$ μm), the pH of the solution and the concentration of different compounds inside of water drops reach a steady state value in a rather short time period (*Fig. 3a*). This time period is less than 1 s if the concentrations of the trace gases in the ambient air are small, and it remains below 10 s even in the case of extremely polluted atmosphere (concentration of SO_2 and that of NH_3 are high as in the cases of 20a, 30a, 50a). This allows us to suppose that in the case of the small water drops (less than 20 μm), the concentrations of different compounds are equal to the saturated values.

The presence of NH_3 in the ambient air necessitates the reduction of the time step. The increased sensitivity of the solution on the time step was the consequence of the different dependence of K_H^* of SO_2 and NH_3 on the

concentration of hydrogen ion (*Fig. 1*). If the pH is increasing, the K_H^* of SO_2 is increasing, so SO_2 is getting more efficiently absorbed by water drops. The increased amount of the absorbed SO_2 reduces the pH, which promotes the more efficient absorption of NH_3 gas, and due to the more efficient depletion of NH_3, the pH of the solute starts to increase. If the time step is not appropriately chosen, the amounts of the absorbed gases are overestimated and, as a consequence, not only the concentration of both SO_2 and NH_3 but also the pH of the solution fluctuate in wide range (*Fig. 4*). As the surface-mass ratio inversely depends on the drop size, the instable solution of Eq. (1) due to the overestimation of the amount of absorbed gases mostly occur in the case of smaller drop sizes (10 μm, 20 μm). If the absorption of NH_3 was not taken into consideration (case 5a), longer time step was enough to get stable solution even in the case of the smaller water drops. In this case, the negative feedback between pH and K_H^* of SO_2 controls the absorption of SO_2.

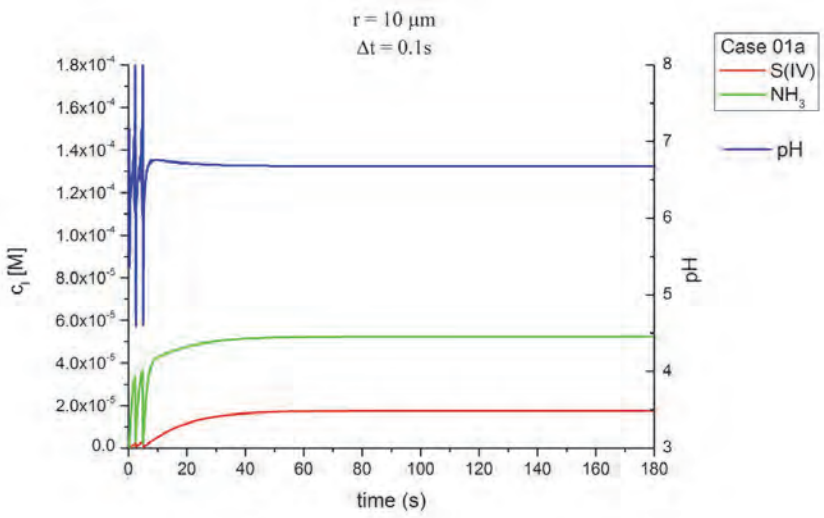

Fig. 4. Time evolution of the pH of the solute (blue curve) and concentration of S(IV) (red curve) and NH_3 (green curve) in the case of the 10-μm-size drop if time step was too long.

In the case of larger drops (50 μm ≤ r ≤ 100 μm), the absorption increases the gas concentration with smaller rate than in the case of the smaller ones. Thus, the above mentioned feedback due to absorption of both SO_2 and NH_3 is weaker. If the case when the ambient air does not contain NH_3 (case 5a) is not considered, the pH of solution changes in wider interval in the case of larger drops than in the case of smaller ones. If the environmental conditions are the

same, the pH of the solution in the case of larger drops is smaller compared to the pH of smaller drops. The size dependence of the pH is getting weaker as more SO_2 is absorbed due to the higher concentration of SO_2 in the ambient air (*Figs. 3b* and *c*). If in the environmental air the amount of NH_3 was in excess comparing to SO_2 (01a, 1a, 2c cases), the pH of the solution increased more slowly in time because of the counter effect of the dissolved CO_2 (formation of $(CO_2)_{aq}$, HCO_3^-, CO_3^{2-}), but it reached a higher value (near 6.5). If SO_2 was in excess, the pH decreased, but it reached constant value in shorter time period. If the absorption of NH_3 was not taken into consideration (case 5a), in the case of drops smaller than 500 μm, the pH of the solution reached a constant value in the first 20 s. This stems from the fact that only gases with acidic properties are absorbed at these environmental conditions. If the atmosphere is strongly polluted (20a, 30a, 50a cases), the evolution of pH is not a monotonic function of time. The pH of the solute decreases in the first 10 s of the simulation, and it starts to increase after reaching the minimum value at about the 10th s of the simulation. The larger the drop size, the longer the time period needed to increase the pH. The value of the pH does not become steady state even by the end of the simulation if the environment is extremely polluted.

In the case of large water drops (r = 500 μm), the absorption rate is not large enough to reach the steady state either in the less polluted cases. The pH of the solution continuously decreases during the simulation time, even if only acidic gases were absorbed (*Fig. 3d*). It is interesting to note, that the time evolution of pH is different from the case of smaller drops if the atmosphere is polluted (curves 20a, 30a, 50a). In the cases of smaller drops, the solution becomes rather acidic in a short time period. Later, the pH starts to increase (see *Figs. 3b* and *c*). In the case of larger water drops, the pH continuously decreases during the simulation time geting near to 5.0–4.5 by the end of the simulation (see *Fig. 3d*). The explanation of the dependence of time evolution of pH on the drop size is given in followings:

(i) Due to its larger concentration in gas phase the absorption of SO_2 gas is the dominant process in the first time period. The sharp decrease of pH (see *Fig. 3b*) significantly increases the absorption rate of NH_3, and near the same amount of both gases were absorbed by the end of the simulation time if drop radius is smaller than 100 μm (*Figs. 5a* and *b*). (Note, that the concentration of SO_2 was larger than that of NH_3 in the ambient air.) The larger concentration of NH_3 inside of the drops finally resulted in larger pH.

(ii) In the case of larger drops the concentration of neither SO_2 and nor NH_3 become steady state even in the less polluted cases. The absorption of gases is controlled by their chemical properties (furthermore, the pH) and by their concentration in the ambient air. Although NH_3 dissolves better than SO_2, the smaller concentration of NH_3 in the ambient air results in smaller uptake rate if the drop radius is larger than 100 μm.

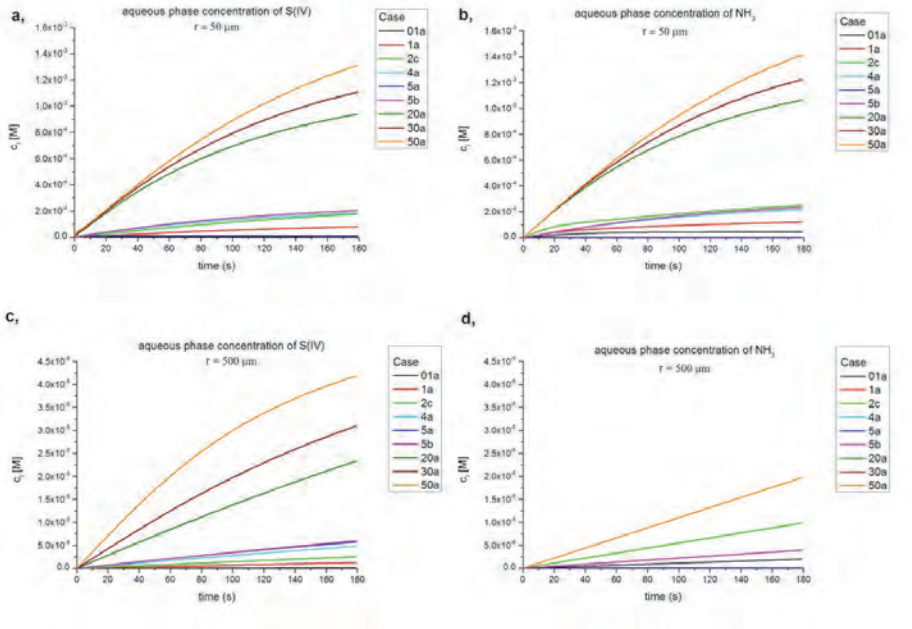

Fig. 5. Time evolution of concentration of S(IV) and NH_3 in the case of two different drop sizes and different environmental conditions.

The analysis of the output data shows (it is not plotted) that aqueous phase concentration of H_2O_2 reaches a constant value in the first 20 s if the radius of the water drop was smaller than 20 μm. Its concentration depends on the concentration of the H_2O_2 in the ambient air, and it has not been affected by the presence of the other compounds. This finding corresponds with the independence of the K_H^* of H_2O_2 on the pH of the solution (see *Fig. 1*). Similar results were found in the case of O_3. Its concentration increases very fast in the drops, and reaches its maximum value within a few seconds even in the case of water drop with radius of 500 μm. The concentration of O_3 does not depend on the concentration of other dissolved gases or on the size of the drop.

3.2. Absorption and oxidation

Smaller time steps comparing with the values in *Table 1* were used to avoid the overestimation of the depletion of O_3 due to the oxidation process. The concentration of O_3 inside of the drops was much smaller than the concentration of other species, so the application of too large time step may results in the inaccurate calculation of O_3. *Fig. 6* shows the time evolution of O_3 inside the

water drops with radius of 10 and 50 μm at different time steps. It was found that the time step should be at least 0.001 s to avoid the fluctuation of O_3 concentration caused by the overestimation of the oxidation (see *Figs. 6b* and *d*). The evolution of aqueous phase concentration of O_3 is plotted at greater (0.01 s) and smaller (0.001 s) time steps to demonstrate the fluctuations (*Fig. 6*). In the case of smaller drops significant reduction of the time step was necessary even at lower concentration of sulfate (cases 4a and 5a).

The presence of dissolved NH_3 impacts the aqueous phase concentration of O_3 (*Figs. 6a* and *c*). If there is no NH_3 gas in the ambient air (case 5a), the pH of the solution is smaller, so the oxidation rate by O_3 is also smaller (see *Fig. 2*). In any other cases, O_3 is more efficiently depleted by the oxidation, and its concentration is reduced by about factor of two. Considering the other species, their concentration inside of the water drops is not so sensitive to the value of the time step. The critical time steps defined for absorption were found to be adequate for the numerical integration of the differential equations that describe the oxidation processes if the time evolution of O_3 is not considered.

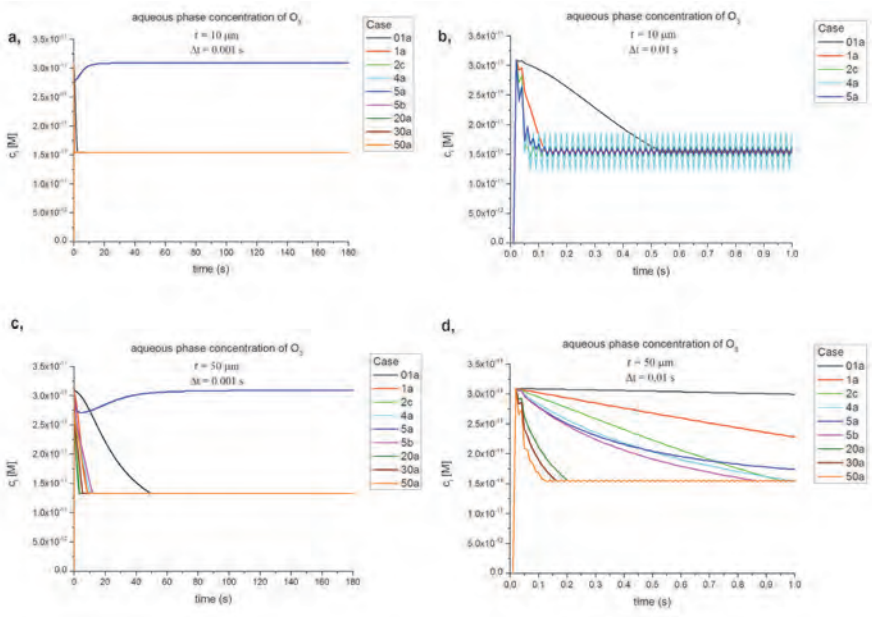

Fig. 6. Time evolution of O_3 at two different drop sizes at time step of 0.01 and 0.001 s. A shorter time period is used for the time evolution of O_3 to demonstrate the effect of too long time step (b, d).

Figs. 7–10 show how the oxidation affects the time evolution of pH and that of the concentration of different compounds in the solution at different drop sizes and different environmental conditions. The results are summarized in the followings:

(i) The most significant effect can be observed in the case of smallest water drops. If only the absorption is taken into consideration, the pH of the solution becomes constant in a very short time interval. The oxidation of S(IV) significantly impacts the time evolution both of pH and concentrations of different compounds inside of water drops. In the smallest drops, the amount of dissolved SO_2 and NH_3 sharply increases in the first 10–20 s of the simulation (*Figs. 7b* and *c*). By the end of this short time period the concentration of the dissolved H_2O_2 reaches its maximum value, and efficient oxidation of S(IV) to S(VI) results in the reduction of the S(IV). The formation of sulfate results in decrease of pH, and as a consequence, the concentration of the NH_3 further increases. The concentration of H_2O_2 reaches a constant value in a short time period. However, the values of constant concentrations depend on the environmental conditions (*Fig. 7d*). This effect is the consequence of the oxidation. The largest oxidation rate in case 50a results in the smallest H_2O_2 concentration in the water drop. Due to the efficient uptake of H_2O_2 by water drops, the absorption balances the depletion by oxidation at relatively large concentrations (*Fig. 7d*). If SO_2 dominates over NH_3 in the ambient atmosphere, the pH decreases more significantly due to the oxidation. The most dramatic decrease can be observed when no NH_3 gas is present (case 5a). In the other cases, the presence of NH_3 mitigates the decrease of the pH. If NH_3 dominates (case 01a), the efficiency of the oxidation by H_2O_2 is smaller due to the larger pH (see *Fig. 2*), furthermore, the low concentration of O_3 limits the oxidation by O_3.

(ii) The absence of NH_3 gas in the environment (case 5a) results in very small concentration of S(IV) at each drop size (see *Figs. 7b, 8b, 9b,* and *10b*). The low absorption rate of this gas due to the small pH (see *Figs. 7a, 8a, 9a* and *10a*) and oxidation by H_2O_2 restrict the accumulation of SO_2 inside water drops.

(iii) The main characteristics of the time evolutions of concentrations of dissolved compounds hardly depend on the drop size if the drop radius is larger than 20 μm (*Figs. 8–10*). The concentration of the dissolved compounds continuously increases. Except for the extremely polluted cases, even the concentration of H_2O_2 increases during the simulation. The continuous increase of the compounds suggests that the absorption rates exceed the oxidation rates, and it takes longer time to get these processes in balance.

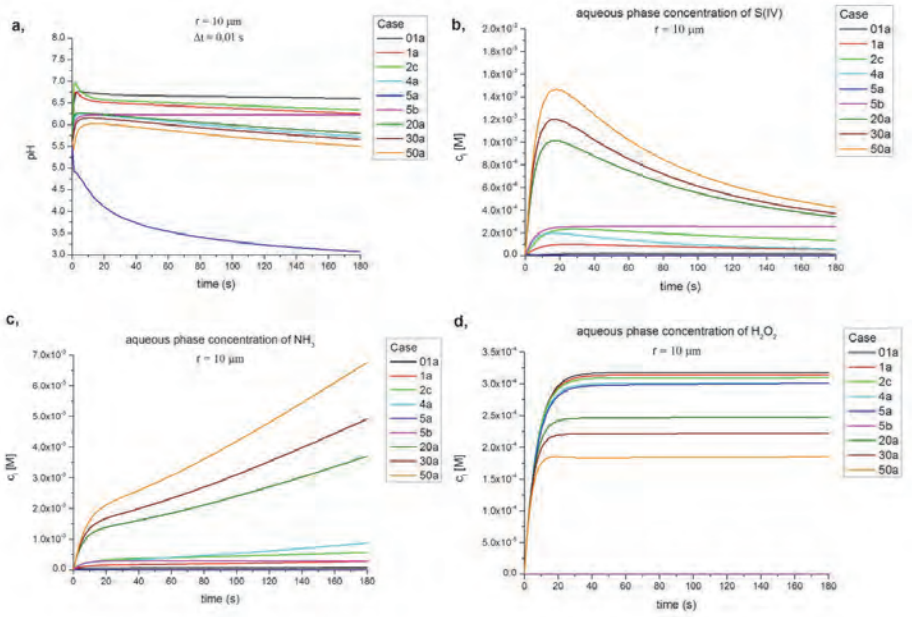

Fig. 7. Time evolution of pH and the concentration of S(IV), NH_3, and H_2O_2 in case of 10 μm drop size (both absorption and oxidation were taken into consideration).

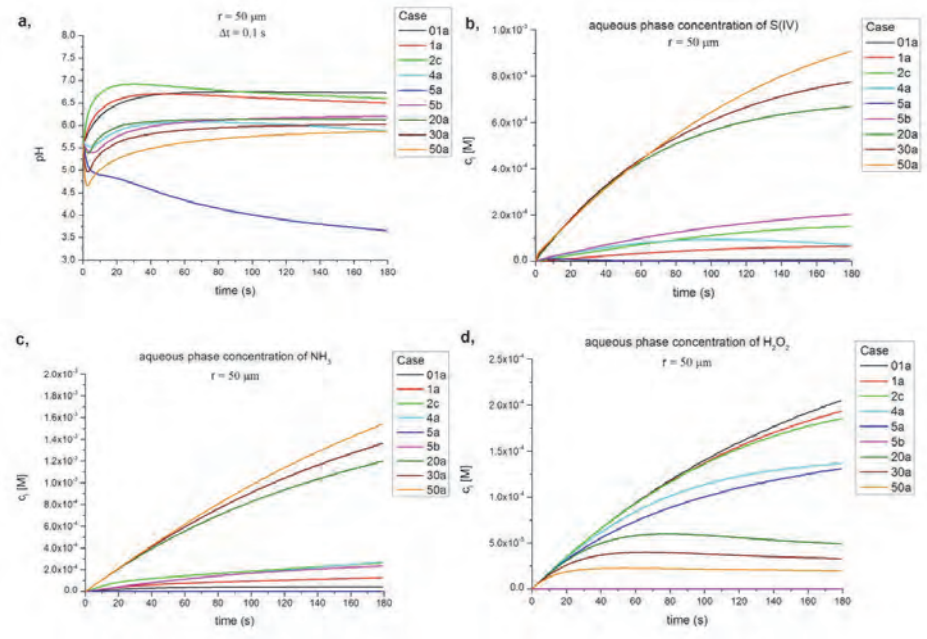

Fig. 8. Same as *Fig. 7* for 50 μm drop size.

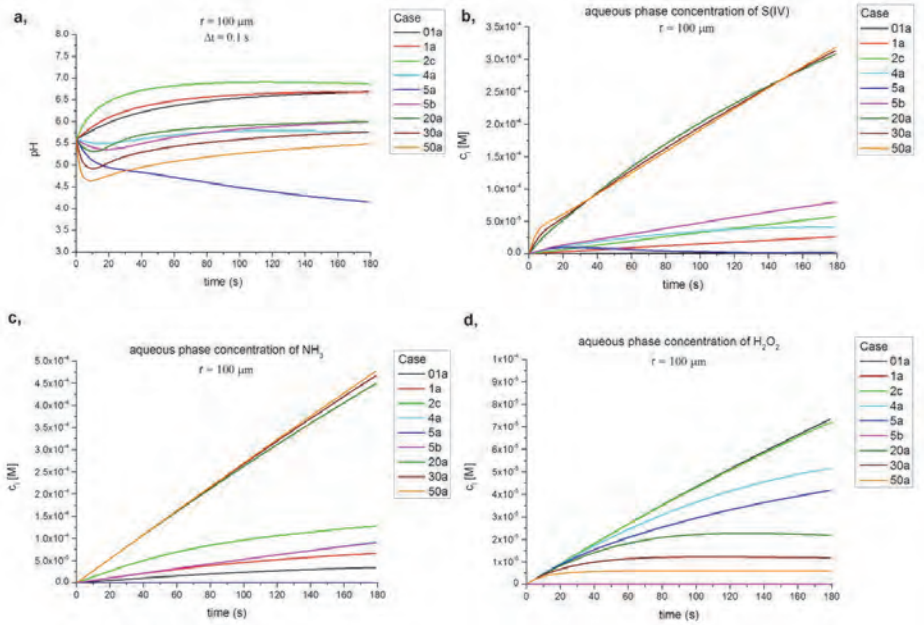

Fig. 9. Same as *Fig. 7* for 100 μm drop size.

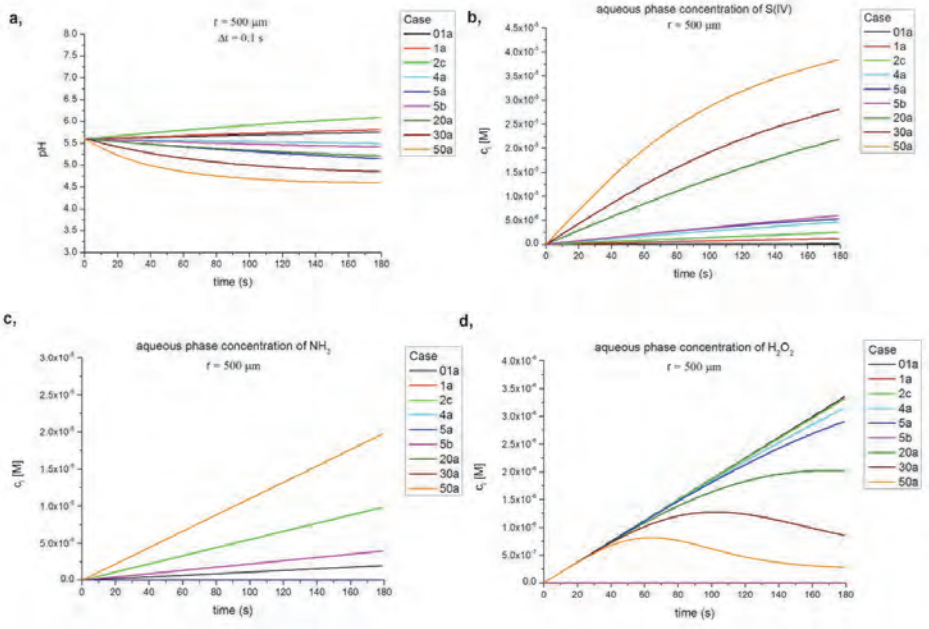

Fig. 10. Same as *Fig. 7* for 500 μm drop size.

Fig. 11 shows the time evolution of S(VI) concentrations in water drops at four different drop sizes. The concentrations of S(VI) continuously increase in every case. The fastest increase occurs inside of the smallest drop, and the rate of production of this compound is inversely proportional to the drop size. Another interesting characteristics of the S(VI) production is that the larger the drop size, the larger the delay for the start of the efficient oxidation. While in the case of the smallest drop the concentration of S(VI) starts to increase noticeably after a few seconds, in the case of the largest drop and polluted atmosphere, there is an about 40 s delay. S(VI) formed in the largest concentration in the case of the polluted environment, and the absence of H_2O_2 restrains the formation of S(VI). However, in the case of water drop with radius of 500 μm, the sulfate production was constrained by the low SO_2 concentration, rather than by the absence of H_2O_2 (case 5b and case 01a in *Fig. 11d*).

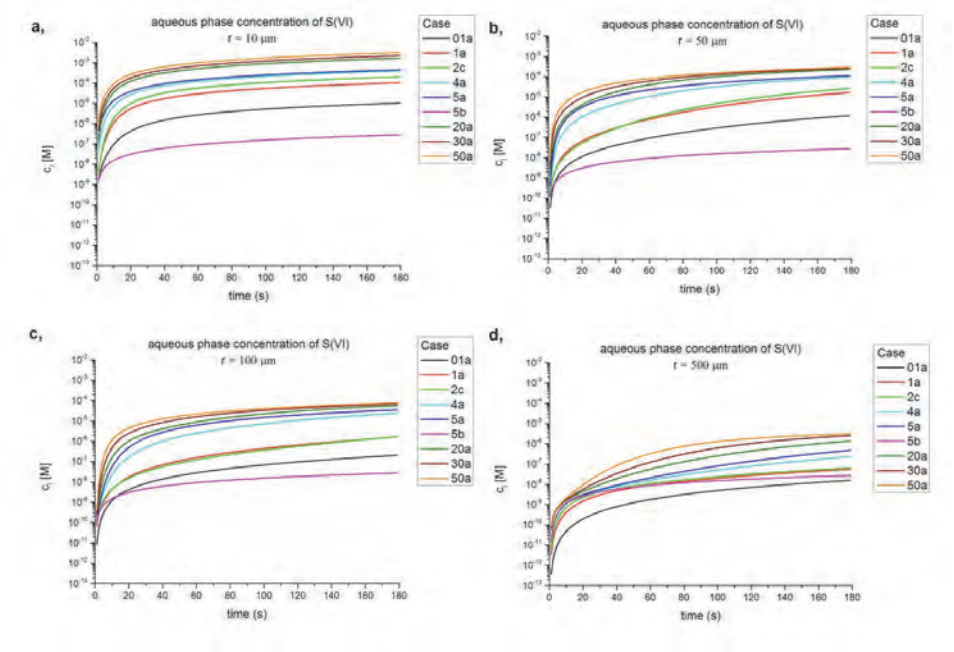

Fig. 11. Time evolution of concentration of S(VI) at different environmental conditions in the case of four different drop sizes.

3.3. Calculation of the produced $(NH_4)_2SO_4$

Tables 2–5 summarize the results of the numerical experiments about the oxidation processes (Eq. (16)). The amount of $(NH_4)_2SO_4$ is calculated from the final aqueous phase concentrations of SO_4^{2-} and NH_4^+ ions for each drop size and environmental condition (*Tables 2–5*). Smaller time steps comparing with Table 1 were used during the calculations to obtain the most accurate mass production of $(NH_4)_2SO_4$. Except in case when no NH_3 is present in the ambient air (case 5a), the mass of $(NH_4)_2SO_4$ formed inside the drops increases with increasing SO_2 gas concentration and with increasing drop size. About one – two order larger amount of ammonium sulfate forms in a polluted atmosphere than in a clean atmosphere. The absence of H_2O_2 (case 5b) had the largest effect on the production of $(NH_4)_2SO_4$. If the concentration of H_2O_2 is zero, the $(NH_4)_2SO_4$ amount is very small. In this case O_3 becomes the dominant oxidant. Results shows that at environmental conditions used in this research, H_2O_2 is more effective oxidant of S(IV) than O_3. Significant increase of O_3 concentration in the atmosphere is necessary for the oxidation by O_3 to overwhelm the oxidation by H_2O_2.

Table 2. Calculated amount of compounds at the end of the simulation in the case of 10 μm drop size

Case	time step [s]	amount of substance [mol]			mass [g]
		SO_4^{2-}	NH_4^+	$(NH_4)_2SO_4$	$(NH_4)_2SO_4$
01a	0.001	$5.28\cdot10^{-17}$	$2.72\cdot10^{-16}$	$5.28\cdot10^{-17}$	$6.97\cdot10^{-15}$
1a	0.01	$4.31\cdot10^{-16}$	$1.15\cdot10^{-15}$	$4.31\cdot10^{-16}$	$5.70\cdot10^{-14}$
2c	0.01	$8.50\cdot10^{-16}$	$2.39\cdot10^{-15}$	$8.50\cdot10^{-16}$	$1.12\cdot10^{-13}$
4a	0.001	$1.68\cdot10^{-15}$	$3.61\cdot10^{-15}$	$1.68\cdot10^{-15}$	$2.22\cdot10^{-13}$
5a	0.01	$2.21\cdot10^{-17}$	0.0	0.0	0.0
5b	0.01	$1.16\cdot10^{-18}$	$1.24\cdot10^{-15}$	$1.16\cdot10^{-18}$	$1.54\cdot10^{-16}$
20a	0.001	$6.95\cdot10^{-15}$	$1.54\cdot10^{-14}$	$6.95\cdot10^{-15}$	$9.18\cdot10^{-13}$
30a	0.001	$9.46\cdot10^{-15}$	$2.05\cdot10^{-14}$	$9.46\cdot10^{-15}$	$1.25\cdot10^{-12}$
50a	0.001	$1.32\cdot10^{-14}$	$2.82\cdot10^{-14}$	$1.32\cdot10^{-14}$	$1.74\cdot10^{-12}$

Table 3. Same as *Table 2* for 50 μm drop size

Case	time step [s]	amount of substance [mol]			mass [g]
		SO_4^{2-}	NH_4^+	$(NH_4)_2SO_4$	$(NH_4)_2SO_4$
01a	0.01	$7{,}59 \cdot 10^{-16}$	$2.40 \cdot 10^{-14}$	$7.59 \cdot 10^{-16}$	$1.00 \cdot 10^{-13}$
1a	0.01	$8{,}63 \cdot 10^{-15}$	$6.75 \cdot 10^{-14}$	$8.63 \cdot 10^{-15}$	$1.14 \cdot 10^{-12}$
2c	0.01	$1{,}42 \cdot 10^{-14}$	$1.38 \cdot 10^{-13}$	$1.42 \cdot 10^{-14}$	$1.87 \cdot 10^{-12}$
4a	0.01	$5{,}12 \cdot 10^{-14}$	$1.43 \cdot 10^{-13}$	$5.12 \cdot 10^{-14}$	$6.76 \cdot 10^{-12}$
5a	0.01	$6{,}06 \cdot 10^{-14}$	0.0	0.0	0.0
5b	0.01	$1{,}45 \cdot 10^{-16}$	$1.22 \cdot 10^{-13}$	$1.45 \cdot 10^{-16}$	$1.92 \cdot 10^{-14}$
20a	0.01	$1{,}22 \cdot 10^{-13}$	$6.28 \cdot 10^{-13}$	$1.22 \cdot 10^{-13}$	$1.61 \cdot 10^{-11}$
30a	0.01	$1{,}39 \cdot 10^{-13}$	$7.17 \cdot 10^{-13}$	$1.39 \cdot 10^{-13}$	$1.83 \cdot 10^{-11}$
50a	0.01	$1{,}53 \cdot 10^{-13}$	$8.06 \cdot 10^{-13}$	$1.53 \cdot 10^{-13}$	$2.02 \cdot 10^{-11}$

Table 4. Same as *Table 2* except for 100 μm drop size

Case	time step [s]	amount of substance [mol]			mass [g]
		SO_4^{2-}	NH_4^+	$(NH_4)_2SO_4$	$(NH_4)_2SO_4$
01a	0.1	$8.50 \cdot 10^{-16}$	$1.43 \cdot 10^{-13}$	$8.50 \cdot 10^{-16}$	$1.12 \cdot 10^{-13}$
1a	0.1	$6.74 \cdot 10^{-15}$	$2.78 \cdot 10^{-13}$	$6.74 \cdot 10^{-15}$	$8.91 \cdot 10^{-13}$
2c	0.1	$6.95 \cdot 10^{-15}$	$5.35 \cdot 10^{-13}$	$6.95 \cdot 10^{-15}$	$9.18 \cdot 10^{-13}$
4a	0.01	$1.03 \cdot 10^{-13}$	$3.88 \cdot 10^{-13}$	$1.03 \cdot 10^{-13}$	$1.36 \cdot 10^{-11}$
5a	0.01	$1.49 \cdot 10^{-13}$	0.0	0.0	0.0
5b	0.01	$1.16 \cdot 10^{-15}$	$3.82 \cdot 10^{-13}$	$1.16 \cdot 10^{-15}$	$1.53 \cdot 10^{-13}$
20a	0.01	$2.42 \cdot 10^{-13}$	$1.89 \cdot 10^{-12}$	$2.42 \cdot 10^{-13}$	$3.20 \cdot 10^{-11}$
30a	0.01	$2.92 \cdot 10^{-13}$	$1.97 \cdot 10^{-12}$	$2.92 \cdot 10^{-13}$	$3.86 \cdot 10^{-11}$
50a	0.01	$3.22 \cdot 10^{-13}$	$2.01 \cdot 10^{-12}$	$3.22 \cdot 10^{-13}$	$4.25 \cdot 10^{-11}$

Table 5. Same as *Table 2* except for 500 μm drop size

Case	time step [s]	amount of substance [mol]			mass [g]
		SO_4^{2-}	NH_4^+	$(NH_4)_2SO_4$	$(NH_4)_2SO_4$
01a	0.1	$8.16 \cdot 10^{-15}$	$1.03 \cdot 10^{-12}$	$8.16 \cdot 10^{-15}$	$1.08 \cdot 10^{-12}$
1a	0.1	$2.93 \cdot 10^{-14}$	$2.06 \cdot 10^{-12}$	$2.93 \cdot 10^{-14}$	$3.87 \cdot 10^{-12}$
2c	0.1	$3.29 \cdot 10^{-14}$	$5.14 \cdot 10^{-12}$	$3.29 \cdot 10^{-14}$	$4.34 \cdot 10^{-12}$
4a	0.1	$1.21 \cdot 10^{-13}$	$2.06 \cdot 10^{-12}$	$1.21 \cdot 10^{-13}$	$1.60 \cdot 10^{-11}$
5a	0.1	$2.49 \cdot 10^{-13}$	0.0	0.0	0.0
5b	0.1	$1.43 \cdot 10^{-14}$	$2.06 \cdot 10^{-12}$	$1.43 \cdot 10^{-14}$	$1.89 \cdot 10^{-12}$
20a	0.1	$7.11 \cdot 10^{-13}$	$1.03 \cdot 10^{-11}$	$7.11 \cdot 10^{-13}$	$9.40 \cdot 10^{-11}$
30a	0.1	$1.32 \cdot 10^{-12}$	$1.03 \cdot 10^{-11}$	$1.32 \cdot 10^{-12}$	$1.75 \cdot 10^{-10}$
50a	0.1	$1.62 \cdot 10^{-12}$	$1.03 \cdot 10^{-11}$	$1.62 \cdot 10^{-12}$	$2.15 \cdot 10^{-10}$

4. Conclusions

A box model was developed to simulate absorption and chemical reactions that occur inside water drops. The purpose of the research was to investigate how sulfate formation depends on the drop size, and to find efficient scheme for the numerical integration of ODEs which describe absorption and chemical reactions. To focus on these processes, the diffusional growth of water drops and the accretion by collision-coalescence were not taken into consideration. Results are summarized in the followings:

(i) The accurate solution of the differential equations describing the absorption of gases through the surface of water drops needs rather small time step. The value of the critical time step depends on the environmental conditions and the size of the drop. The presence of NH_3 in the ambient air reduces the value of the critical time step. As a rule of thumb, time step of 0.01 s is suggested to apply if the drop radius is smaller than 20 μm, and of 0.1 s if the drop radius is above this size.

(ii) The numerical solution of the differential equations needs further reduction of the time step if the concentration of one of reacting compounds is small comparing to the other compounds.

(iii) The time evolution of pH and that of the concentration of different species depends on the drops size. In the case of small water drops, both the pH of the solution and the concentration of the chemical compounds become steady state in a short time period of about 10 s. In the case of the larger drops, this time period can become significantly longer depending on the pollution of the ambient air and on the drop size. The only exception is the concentration of H_2O_2. The concentration of this gas becomes steady state before the end of the simulation even in the extremely polluted cases.

(iv) The oxidation significantly impacts the amount of absorbed gases. The reduction of pH due to the formation of sulfate slightly increase the amount of absorbed NH_3, and the depletion of S(IV) and H_2O_2 by oxidation allows further absorption of both SO_2 and H_2O_2 gases. While in the case of drops with size of 10 μm, the absorptions and chemical reactions get into balance during the simulated time period, in the case of larger drops, the concentration of different species continuously increases.

(iv) The sulfate formation is significantly impacted by the environmental conditions and the drop size. The fastest increase of mole concentration of sulfate occurs inside the smallest drop, and the rate of increase is the smallest in the cases of the largest drop.

(v) Significant amount of ammonium sulfate can be produced by oxidation inside of water drops, which increases the mass of the CCN after the evaporation of water drops. In the case of polluted atmosphere, the mass of

ammonium sulfate formed by this way is comparable to the mass of CCN that the drops formed on.

(vi) Strong size dependence of sulfate production suggests that application of the bin microphysical scheme may give a more accurate description of the chemical processes than the bulk schemes which are currently used to simulate these processes. The application of the bin scheme is limited by the large computer capacity required by this scheme.

In the next phase of the research, these results will be applied to simulate the absorption and chemical reactions in stratocumulus clouds by using two-dimensional cloud model with bin microphysical scheme.

Acknowledgment: The contribution to this research by *I. Geresdi* was supported by Hungarian Scientific Research Found (Number: OTKA K116025).

References

Barrie, L.A. and *Georgii, H.W.,* 1976: An experimental investigation of the absorption of sulfur dioxide by water drops containing heavy metal ions. *Atmos. Environ. 10,* 743–749.

Barrie, L.A., 1985: Features of the atmospheric cycle of aerosol trace elements and sulfur dioxide revealed by baseline observations in Canada. *J. Atmos. Chem. 3*,139–152.

Beilke, S. and *Georgii, H.W.,* 1968: Investigation on the incorporation of sulfur dioxide into fog and raindrops. *Tellus 20,* 435–441.

Beilke, S., 1970: Laboratory investigations of washout trace gases. In (Eds.: *Engelmann, R.J.* and *Slinn, W.G.N.*) Precipitation Scavenging (1970). U.S. Atomic Energy Commission, AEC symposium series 22, 261–267.

Beilke, S., Lamb, D. and *Müller, J.,* 1975: On the oxidation of SO_2 in aqueous systems. *Tellus 20,* 435–441.

Daum, P.H., Schwartz, S.E. and *Newman, L.,* 1983: Studies of the gas and aqueous phase composition of stratiform clouds. In (Eds.: *Pruppacher, H.R., Semonin, R.G.* and *Slinn, W.G.N.*) Precipitation Scavenging, Dry Deposition, and Resuspension, Volume 1. Elsevier Science Publishing Co., New York, 31–51.

Diehl, K., Mitra, S.K. and *Pruppacher, H.R.,* 1998: A laboratory study on the uptake of HCl, HNO_3 and SO_2 gas by ice crystals and the effect of these gases on the evaporation rate of the crystals. *Atmos. Res. 47–48,* 235–244.

Diehl, K., Vohl, O., Mitra, S. K. and *Pruppacher, H. R*., 2000: A laboratory and theoretical study on the uptake of sulfur dioxide gas by small water drops containing hydrogen peroxide under laminar and turbulent conditions. *Atmos. Environ. 34* 2865–2871.

Diehl, K., Mitra, S. K., Szakáll, M., v. Blohn, N. , Borrmann, S. and *Pruppacher, H.R.,* 2011: The Mainz Vertical Wind Tunnel facility–a review of 25 years of laboratory experiments on cloud physics and chemistry. In (Eds.: *Justin D. Pereira*) Wind Tunnels: Aerodynamics, Models and Experiments. Nova Science Publishers, United States.

Geresdi, I. and *Weidinger, T.,* 1989: A meteorológiai folyamatok modellezésében alkalmazott numerikus módszerek. *Időjárás 93*, 100–114.

Hannemann, A., 1995: Eine experimentelle und theoretische Untersuchung zur gekoppelten ufnahme von NH_3, CO_2 und SO_2 in Wassertropfen. Zugl. Mainz, Universiẗat, Diss., Shaker Verlag GmbH, Aachen.

Hannemann, A.U., Mitra, S.K. and *Pruppacher, H.R.,* 1995: On the Scavenging of Gaseous Nitrogen Compounds by Large and Small Rain Drops I. A Wind Tunnel and Theoretical Study of the Uptake and Desorption of NH_3 in the Presence of CO_2. *J. Atmos. Chem. 21*, 293–307.

Hannemann, A.U., Mitra, S.K. and *Pruppacher, H.R.,* 1996: On the Scavenging of Gaseous Nitrogen Compounds by Large and Small Rain Drops: II. Wind Tunnel and Theoretical Studies of the simultaneous Uptake of NH_3,SO_2 and CO_2 by Water Drops. *J. Atmos. Chem. 24*, 271–284.

Hegg, D.A. and *Hobbs, P.V.,* 1981. Cloud water chemistry and chemical production of sulfates in clouds. *Atmos. Environ. 15*, 1597–1604.

Hegg, D.A. and *Hobbs, P.V.,* 1982. Measurements of sulfate production in natural clouds. *Atmosp. Environ. 16*, 2663–2668.

Hegg, D.A., Hobbs, P.V. and *Raschke, L.F.,* 1984: Measurements of the scavenging of sulfate and nitrate in clouds. *Atmos. Environ. 18*, 1939–1946.

Hoffmann, M.R. and *Calvert, J.G.,* 1985: Chemical Transformation Modules for Eulerian Acid Deposition Models, Vol. 2, The Aqueous-Phase Chemistry, EPA/600/3-85/017, U.S. Environmental Protection Agency, Research Triangle Park, NC.

Horváth, L., 1977: A légköri kén-dioxid szulfáttá alakulásának mechanizmusa és kinetikája. *Időjárás 81*, 5, 280–287. (In Hungarian)

Horváth, L. and *Mészáros, E.,* 1978: Determination of the kinetic parameters of sulfur-dioxide - sulfate conversion on the basis of atmospheric measurements. *Időjárás 82*, 2, 58–62.

Horváth, L., 1981: A csapadékvíz kémiai összetétele Magyarországon. *Időjárás 85*, 4, 201–212. (In Hungarian)

Johnson, A.I., Hamielec, A.E. and *Houghton, W.T*., 1967: An experimental study of mass transfer with chemical reaction from single gas bubbles. *Canadian J. Chem. Engin. 45*, 140–144.

Kronig, R. and *Brink, J.C.,* 1950: On the theory of the extraction from falling drops, *J. Appl. Sci. Res. A2,* 142–154.

Kronig, R., Vanderveen, B. and *Ijzerman, P*., 1951: On the theory of extraction from falling droplets. II. *J. Appl. Sci. Res. A3*, 103–110.

McArdle, J.V. and *Hoffmann, M.R.,* 1983: Kinetics and mechanism of the oxidation of aquated sulfur dioxide by hydrogen peroxide at low pH. *J. Phys. Chem. 87*, 5425–5429.

Mészáros, Á. and *Vissy, K.,* 1974: Concentration, size distribution and chemical nature of atmospheric aerosol particles in remote oceanic areas. *J. Aerosol Sci. 5*, 101–110.

Mészáros, E., 1971: The size distribution of water soluble particles in the atmosphere. *Időjárás 75*, 308–314.

Mészáros, E., 1973: Evidence of the role of indirect photochemical processes in the formation of atmospheric sulphate particulate. *J. Aerosol Sci. 4*, 429–434.

Mészáros, E., 1974: On the formation of atmospheric sulphate particulate in the winter months. *J. Aerosol Sci. 5*, 483–485.

Mészáros, E., Sas, É. and *Mészáros, Á.,* 1974: Felhőcseppek kondenzációs növekedése ammónium-szulfát magvakon. *Időjárás 78*, 333–341.

Mészáros, E. and *Várhelyi, G.,* 1975: On the concentration, size distribution and residence time of sulfate particles in the lower troposhere. *Időjárás 79*, 267–273.

Mészáros, E., 1976: A kén körforgalma a légkörben. *Időjárás 80*, 1, 42–47. (In Hungarian)

Mitra, S.K. and *Hannemann, A.U.,* 1993: On the Scavenging of SO_2 by Large and Small Rain Drops: V. A Wind Tunnel and Theoretical Study of the Desorption of SO_2 from Water Drops Containing S(IV). *J. Atmos. Chem.* 16, 201–218

Mitra, S.K., Waltrop, A., Hannemann, A., Flossmann, A. and *Pruppacher, H.R.,* 1992: A wind tunnel and theoretical investigation to test various theories for the absorption of SO_2 by drops of pure water and water drops containing H_2O_2 and $(NH_4)_2SO_4$. In: Schwartz, S.E. and Slinn, W.G.N. (eds.), Precipitation Scavenging and Atmosphere – Surface Exchange, Vol. 1. Hemisphere Publishing, Washington, DC, 123–141.

Pruppacher, H.R. and *Klett, J.D.,* 2010: Microphysics of Clouds and Precipitation. Second revised and expanded edition, Springer Science+Business Media B.V., Springer Dordrecht Heidelberg London New York.

Seinfeld, J.H. and *Pandis, S.N.,* 2006: Atmospheric Chemistry and Physics. John Wiley & Sons, Inc., Hoboken, New Jersey

Seinfeld, J.H., 1986: Atmospheric Chemistry and Physics of Air Pollution. John Wiley & Sons, Inc., New Jersey.

Stuart, A.L. and *Jacobson, M.Z.,* 2006: A Numerical Model of the Partitioning of Trace Chemical Solutes during Drop Freezing. *J. Atmos. Chem. 53* (2006), 13–42

Várhelyi, G., 1977: Wet removal of tropospheric sulfur compounds. *Időjárás 81*, 85–93.

Várhelyi, G., 1980: Dry deposition of atmospheric sulfur and nitrogen oxides. *Időjárás 84*, 15–20.

Várhelyi, G., 1982: On the atmospheric sulfur budget over Hungary. *Időjárás 86*, 333–337.

Várhelyi, G., 1975: A kén-dioxid abszorpciója és oxidációja felhő- és ködcseppekben. *Időjárás 79*, 360–365. (In Hungarian)

v. Blohn, N., Diehl, K., Nölscher, A., Jost, A., Mitra, S. K. and *Borrmann, S.,* 2013: The retention of ammonia and sulfur dioxide during riming of ice particles and dendritic snow flakes: laboratory experiments in the Mainz vertical wind tunnel. *J. Atmos. Chem. 70,* 131–150.

Walcek, C.J. and *Pruppacher, H.R.,* 1984: On the scavenging of SO_2 by cloud and rain drops. I: a theoretical study of SO_2 absorption and desorption for water drops in air. *J. Atmos. Chem. 1,* 269–289.

Waltrop, A., Mitra, S.K., Flossmann, A.I. and *Pruppacher, H.R.,* 1991: On the scavenging of SO_2 by cloud and rain drops: IV. A wind tunnel and theoretical study on the adsorption of SO_2 in the ppb(v) range by water drops containing H_2O_2. *J. Atmos. Chem. 12,* 1–17.

Watada, H., Hamielec, A.E. and *Johnson, A.I.,* 1970: A theoretical study of mass transfer with chemical reaction in drops. *Canadian J. Chem. Engin. 48,* 255–261.

IDŐJÁRÁS

Quarterly Journal of the Hungarian Meteorological Service
Vol. 121, No. 1, January – March, 2017, pp. 29–41

Analyses of long-term and multi-site floral phenological observations of apple cultivars in comparison with temperature datasets

Panna Sepsi[*1], **Márta Ladányi**[2], and **Magdolna Tóth**[3]

[1] *Department of Soil Science and Water Management*
Faculty of Horticultural Science Szent István University
Villányi út 29-43. H-1112 Budapest, Hungary
and
Hungarian Meteorological Service
Kitaibel Pál utca 1. H-1024 Budapest, Hungary
E-mail: sepsi.p@met.hu

[2] *Department of Biometrics and Agricultural Informatics*
Faculty of Horticultural Science Szent István University
Villányi út 29-43. H-1112 Budapest, Hungary
E-mail:Ladanyi.Marta@kertk.szie.hu

[3] *Department of Pomology*
Faculty of Horticultural Science Szent István University
Villányi út 29-43. H-1112 Budapest, Hungary
E-mail: Toth.Magdolna@kertk.szie.hu

[*] *Corresponding author*

(Manuscript received in final form July 7, 2016)

Abstract—Three flowering stages were available for seven old apple cultivars in the database of Hungarian Meteorological Service. These old apple cultivars have more and more important role in the fruit production. The aim of this work is to describe the main flowering characteristics of these cultivars. Understanding the temporal nature and causes of phenological changes of such fruit trees is potentially valuable in the context of local climate change and associated yields, and more particularly for establishing appropriate horticultural management structures to ensure suitable future yields under changing orchard formation processes.

Key-words: apple cultivars, weather impact, phenology, flowering, heat accumulation

1. Introduction

1.1. Importance of old apple cultivars

In the Carpathian basin, a highly diverse fruit cultivar assortment could by enjoyed for a long time. Commercial fruit production, monocultures threatens biodiversity. In order to preserve biodiversity, cultivar collections are maintained in gene banks. Old cultivars are getting more and more attention for several reasons (*Tóth,* 2013).

Nowadays, people have nostalgic feeling about old apple cultivars. Old varieties have historical and cultural importance, they are part of the natural treasures and cultural heritage. They also have an important role in landscape aesthetic and nature protection.

Breeders use them as parent cultivars in order to reach their breeding purposes. Some of the old cultivars have exceptional size, shape, surface, or not light colored flesh. They have an important role to increase nutritional content, consuming values, and health benefits of future cultivars.

Other aim of selection is to increase resistance and tolerance to the most dangerous diseases (*Hevesi, et al.,* 2004; *Tóth et al.,* 2012). Several cultivars shows sufficient tolerance to the most biotic and abiotic stress factors (*Tóth, et al.,* 2005).

Old cultivars are suitable for growing systems with closed or opened plantation, self-supporting house gardens, complex agroforestry systems, furthermore, in traditional orchards or in tree lines.

1.2. Description of examined cultivars

For this study, the phenological observations of old apple cultivars (*Table 1*) (‘Nyári fontos’, ‘Asztrahán i piros’, ‘Téli aranyparmen’, ‘Batul’, ‘Húsvéti rozmaring’, ‘Jonathan’, ‘Starking’) from the Hungarian Meteorological Service (OMSZ) were used. Data were available from 1952 to 1964. At that time, they used traditional growing and training methods in the orchards, trees were planted in large spacing. Apple trees were mostly grown on seedlings or in some cases on M.4 rootstock.

1.3. Spring phenology

The growth cycle of the apple trees includes all events occurring normally every year. The main processes - budburst, flowering, extension growth, fruit set and development, extension growth cessation, flower-bud formation, leaf abscission, and winter dormancy - are interrelated and synchronized with the growth season.

Table 1. Examined old apple cultivars

	Blooming	Ripening	Harvest	Edible maturity	Production region
Asztraháni piros	early-mid	July	early-season	July-August	Northern Transdanubia, Southern Transdanubia, Danube-Tisza Plain, Transtisza, Nyírség
Batul	late-mid	October	late-season	November-March	Nyírség, Upper Hungary
Húsvéti rozmaring	early-mid or late-mid	October	late-season	December-June	Western Transdanubia, Southern Transdanubia, Danube-Tisza Plain, Transtisza, Nyírség
Jonathan	late-mid	September	late-season	October-March	Northern Transdanubia, Western Transdanubia, Southern Transdanubia, Danube-Tisza Plain, Transtisza, Nyírség
Nyári fontos	early	August	early-season	August	Southern Transdanubia, Danube-Tisza Plain, Transtisza, Nyírség
Starking	late-mid	September-October	late-season	November-March	Northern Transdanubia, Western Transdanubia, Southern Transdanubia, Danube-Tisza Plain, Transtisza, Nyírség
Téli aranyparmen	early-mid or late-mid	August-September	mid-season	September-January	Western Transdanubia, Transtisza, Nyírség, Upper Hungary

In early spring, as a response to chilling temperatures during the preceding winter, high proportion of buds emerge from dormancy (*Webster,* 2005). As the air temperature reaches a certain level, these buds are ready to develop (*Faust,* 1989). Buds with flower primordia normally open first and develop flower clusters that pass through a series of phenological stages.

Flowering in apple trees comprises floral induction, initiation, differentiation, and anthesis (*Hanke et al.,* 2007).

Temperature has direct and indirect effects on flowering. Warm temperatures advance flower initiation, cool temperatures retard it (*Abbott,* 1984). Indirectly, high temperatures stimulate shoot growth and so influencing flowering negatively *(Tromp, 1984)*.

2. Materials and methods

2.1. Phenology data

Stages in the developments from flowers to fruitlets were recorded in various locations in Hungary (*Figs. 1–7*) between 1952 and 1964. The assessments of floral dates was made by experienced observers.

Phenological database covers three stages during the flowering period: beginning of flowering, full flower, and petal fall.

The beginning of flowering can be defined several ways. *Maliga* (1958), *Singh, et al*. (2002), and *Soenen et al.* (1978) describe as the time in the year, when at some places of the plant, the first flowers have opened completely. According to *Faust* (1989), it is defined as the time when the rate of opened flowers is 12–15%.

The stage of full flower can be defined as the time when about 80% of the flowers are flowering, petal fall signals the end of flowering period, followed by the early fruitlet (*Wertheim,* 1996).

Soltész (1992) describes the end of flowering period when the pistils are not able to function anymore. *Faust* (1989) and *Nyéki* (1989) mentioned the 95–100% rate of overblown flowers as the end of flowering period.

Fig 1. Phenological observations ‘Asztraháni piros’.

Fig 2. Phenological observations ‘Batul’.

Fig 3. Phenological observations‘Húsvéti rozmaring’.

Fig 4. Phenological observations ‘Jonathan’.

Fig 5. Phenological observation ‘Nyári fontos’.

Fig 6. Phenological observations ‘Starking’.

Fig 7. Phenological observation ‘Téli aranyparmen’.

2.2. Temperature data

Temperature database stems from the meteorological observational stations in Hungary during 1952–1964. At that time, synoptic measurements were carried out in 19 weather stations (*Fig. 8*).

Fig 8. Synoptic stations.

Temperature data from the station closest to each phenological observation point were taken into account during the calculation of growing degree days.

Meteorological database was checked to detect errors due to missing observational data. Daily gaps in the temperature database were filled by linear interpolation between existing records. In case of significant gaps and missing periods, the closest stations were taken into account with different weight.

2.3. Calculation of growing degree days (GDD)

The accumulation of the active temperature values above the base temperature is a widespread method to classify the environmental conditions in phenological analysis (*Szász,* 2013).

In order to evaluate the relationship between the different developmental processes in the tree's annual growth cycle and temperature, in terms of accumulation of heat, growing degree days were calculated by the following formula:

$$GDD = \frac{T_{max}+T_{min}}{2} - T_{base},$$

where T_{max} and T_{min} are the mean daily maximum and minimum temperature, and T_{base} is the threshold temperature below which development does not progress.

2.4. Statistical analyses

All statistical analyses were performed using IBM SPSS Statistics 22.0 software.

For identifying univariate outliers, z score method was used (*Schiffler,* 1988). Any observation with a z score less than -1.96 or greater than +1.96 is considered an outlier.

Detection of multivariate outliers was performed by calculating Mahalanobis' distances (*Mahalanobis,* 1936), which identifies observations that lies far from the center of the data cloud. Less weight was given to those variables with large variances or to groups of highly correlated variables.

Data were analyzed using one-way analysis of variance (ANOVA) for the separation of means with a confidence interval of 95%. Grouping information was obtained by comparing means using Tukey's method in case of homogeneity of variance.

In cases flowering period, the strength of relationships between beginning of the flowering and the time of petal fall was measured by Pearson correlation analysis.

2.5. Mapping

Generic Mapping Tools (GMT) was used for creating maps with contours. The optimal Delaunay triangulation is performed (using *Shewchuk's* (1996) method). After eliminating outliers, for all sites the average dates were calculated. Maps are based on these average phenological data.

3. Results

3.1. Beginning of flowering

In the database, 2538 observations were available for beginning of flowering. After eliminating the outliers (61 data), maps were designed with 2477 data. In the examined period, the average date of beginning of flowering was in the second half of April. In general, it was the 117th day of the year (April 26). The standard deviation was 8.911, and the range was 38. Significant spatial differences can be observed in the start date (*Fig. 9*).

After splitting the dataset by cultivars, another outlier detection was carried out. In this case, 2.52% of the data was marked as outlier. ANOVA showed significant cultivar effect ($F(6, 2467) = 3.337$, $p = 0.003$). The results of post hoc test can be seen in *Table 2*. Significant differences were detected between the cultivars ($p < 0.05$). Summer cultivars ('Asztraháni piros' and 'Nyári fontos') flowered exceptionally early.

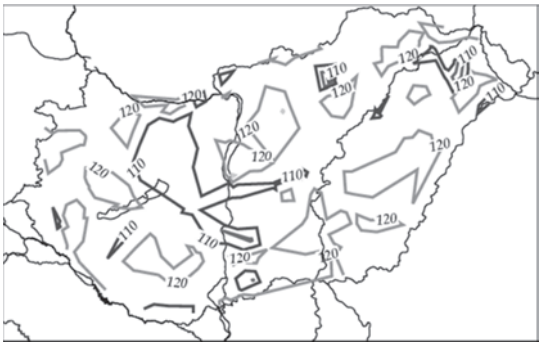

Fig 9. Spatial distribution of beginning of flowering.

After splitting the dataset by cultivars, another outlier detection was carried out. In this case, 2.52% of the data was marked as outlier. ANOVA showed significant cultivar effect ($F(6, 2467) = 3.337$, $p = 0.003$). The results of post hoc

test can be seen in *Table 2*. Significant differences were detected between the cultivars ($p < 0.05$). Summer cultivars (‘Asztraháni piros’ and ‘Nyári fontos’) flowered exceptionally early.

Table 2. Average date of beginning of flowering by cultivars and the results of the post hoc test

Cultivar	DOY	Date	Sample size	Post hoc test*
Asztraháni piros	113.63	April 22.	183	a
Batul	115.56	April 24.	342	ab
Húsvéti rozmaring	116.56	April 25.	364	bc
Jonathan	117.52	April 26.	782	bc
Nyári fontos	113.39	April 22.	167	a
Starking	118.13	April 27.	201	c
Téli aranyparmen	117.43	April 26.	435	bc

*: means marked with the same letter are not different from each other at $p<0.05$ significance level

3.2. Full bloom

In the database, 2544 observations were available for full bloom. After eliminating the outliers (65 data), maps were designed with 2468 data. In the examined period, the average date of full flower was at the end of April or in the very beginning of May. In general, it was the 122nd day of the year (May 1). The standard deviation was 8.437, and the range was 35. Significant spatial differences can be observed in the start date (*Fig. 10*).

Fig 10. Spatial distribution of full bloom.

After splitting the dataset by cultivars, another outlier detection was carried out. In this case, 3.04% of the data was marked as outlier. ANOVA showed significant cultivar effect ($F(6, 2449) = 20.502$, $p < 0.001$). The results of the post hoc test can be seen in *Table 3*. Significant differences were detected between the cultivars ($p < 0.05$). Like beginning of flowering, full flower can be observed earlier in the case of summer cultivars ('Asztraháni piros' and 'Nyári fontos').

Table 3. Average date of full bloom by cultivars and the result of post hoc test

Cultivar	DOY	Date	Sample size	Post hoc test*
Asztraháni piros	118.04	April 27.	182	a
Batul	120.82	April 29.	340	b
Húsvéti rozmaring	121.72	April 30.	366	bc
Jonathan	123.02	May 2.	779	cd
Nyári fontos	117.67	April 26.	165	a
Starking	124.05	May 3.	196	d
Téli aranyparmen	122.91	May 1.	428	ab

*: means marked with the same letter are not different from each other at p<0.05 significance level

3.3. Flowering period

The average length of flowering period can be calculated in 2524 cases. Outlier detection marked 98 cases as outlier. The average length of flowering period was 15 days. The standard deviation was 4.875, the range was 23.

After splitting the dataset by cultivars, another outlier detection was carried out. In this case, 4.08% of the data was marked as outlier. ANOVA showed significant cultivar effect ($F(6, 2414) = 4.026$, $p < 0.001$). The results of the post hoc test can be seen in *Table 4*. Significant differences were detected within the cultivars ($p < 0.05$).

Table 4. Average length of flowering period by cultivars and the results of the post hoc test

Cultivar	Mean	Sample size	Post hoc test*
Asztraháni piros	14.43	178	ab
Batul	14.89	330	ab
Húsvéti rozmaring	15.22	359	ab
Jonathan	15.42	767	b
Nyári fontos	14.11	161	a
Starking	14.04	198	a
Téli aranyparmen	14.63	428	ab

*: means marked with the same letter are not different from each other at p<0.05 significance level

3.4. Relationship between beginning of flowering and petal fall dates

In the database, there were 2524 cases when both beginning of flowering and petal fall dates were available. Outliers were detected based on Mahalanobis' distances. 26 cases were eliminated. The relationship between the two phenological stages can be seen in *Fig. 11*. Strong correlation was observed ($r=0.818$, $p<0.001$). If the flowering begins later, it also ends later.

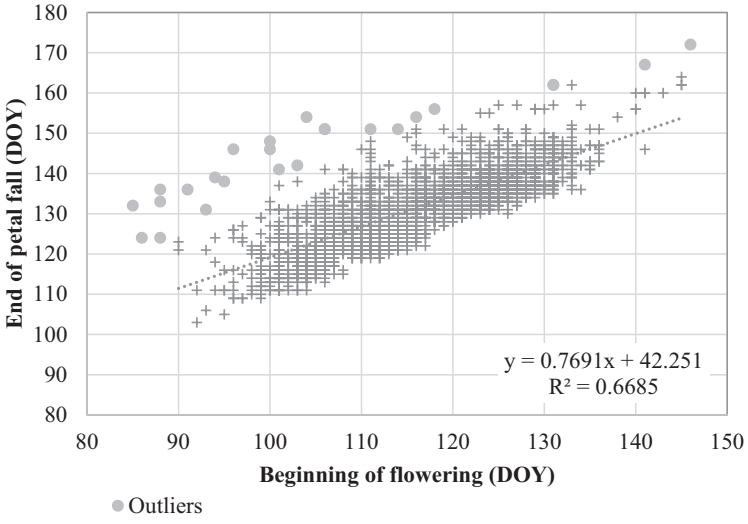

Fig 11. Relationship between beginning of flowering and end of petal fall.

3.5. The role of temperature indices in the timing of the beginning of flowering and the duration of flowering

For the entire database, four temperature indices were examined before the date of beginning of flowering. Significant relationship was observed (*Table 5*). The average minimum temperature and average temperature amplitude have remarkable impact on the timing of beginning of flowering.

These above mentioned indices were calculated during the flowering period (*Table 6*). Significant connection was found in this case, too.

Table 5. Temperature indices before the flowering period and correlations between these indices and the timing of beginning of flowering

Period	10-day		20-day		30-day	
	Average	Pearson correlation	Average	Pearson correlation	Average	Pearson correlation
Mean temperature	12.70 °C	0.213**	11.38 °C	0.152**	10.28 °C	0.163**
Maximum temperature	18.78 °C	0.109**	17.30 °C	–0.004**	16.17 °C	–0.096**
Minimum temperature	6.75 °C	0.348**	5.70 °C	0.310**	4.71 °C	0.384**
Temperature amplitude	12.03 °C	–0.176**	11.60 °C	–0.333**	11.47 °C	–0.458**

**: at $p<0.001$ significance level

Table 6. Temperature indices during the flowering period and the correlations between these indices and flowering duration

	Average	Pearson correlation
Mean temperature	13.90 °C	–0.389**
Maximum temperature	19.83 °C	–0.403**
Minimum temperature	8.10 °C	–0.343**
Temperature amplitude	11.73 °C	–0.271**

**: at $p<0.001$ significance level

Growing degree days were determined for the period before the bud break: for the 10-day-long period the value was 67.74 °C, for the 20-day-long one it was 112.06 °C, and finally, for 30-day-long period it was 141.10 °C. The effect of these values was measured by the linear correlation coefficient between the timing of beginning of flowering and the growing degree days (*Fig. 12*). The role of the 30-day-long period is the highest. The optimal choice of base temperature is 5.1 °C.

During the flowering period, the average value of growing degree days calculated with 5.1 °C base temperature was 126.21 °C. In case of markedly longer flowering period, this value was larger.

These findings indicate that the relationship between phenology and temperature is significant, but may not necessarily be linear, and thus, apple cultivars may respond differently to temperature change.

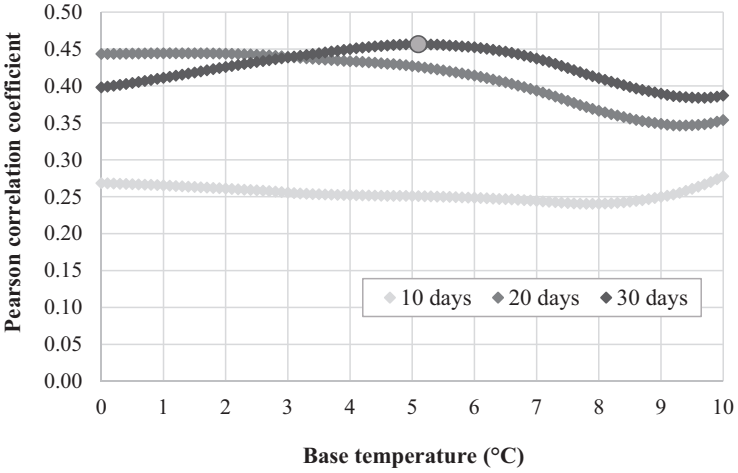

Fig. 12. Correlation between the timing of beginning of flowering and growing degree days.

4. Summary and conclusion

The time required for a crop to pass through its various stages of development is useful in estimating yield (*Hunkár et al.,* 2012) and in describing the effects of climate change. This interval is effected by the weather conditions. Our results prove the importance of temperature on timing of phenological phases. Newertheless, GDD calculation disprove the long-standing statement that the higher amount of heat accumulation shortens the flowering period.

Acknowledgements: This work has been supported by TÁMOP-4.2.1/B-09/1/KMR-2010-0005 and TÁMOP-4.2.2.B-10/1-2010-0023.

References

Abbott, D. L., 1984: The Apple Tree: Physiology and Management, London, Grower Books

Faust, M., 1989: Physiology of temperate zone fruit trees. New York: Wiley. 338 pp.

Hanke, M.V., Flachowsky, H., Peil, A., and *Hättasch, C.,* 2007: No flower no fruit — genetic potentials to trigger flowering in fruit trees. *Genes, Genomes and Genomics 1*, 1–20.

Hevesi, M., Göndör, M., Kása, K., Honty, K. and*, Tóth, M.,* 2004: Traditional and commercial apple and pear cultivars as sources of resistance to fireblight. Eur. Plant Protect. Organis.Bull., *34*, 377–380.

Hunkár, M., Vincze, E., Szenyán, I., and *Dunkel, Z.*, 2012: Application of phenological observations in agrometeorological models and climate change research. *Időjárás, 116,* 195–209.

Mahalanobis, P.C., 1936: On the generalized distance in statistics. *Proc. Nat Inst. Sci. India 2,* 49–55.
Maliga, P., 1958: A gyümölcsfák termékenysége és terméketlensége. In: (Ed.: *M. Mohácsy*) A körte termesztése és nemesítése. Budapest: Pátria. (In Hungarian)
Nyéki, J., 1989: Csonthéjas gyümölcsűek virágzása és termékenyülése. Budapest: MTA. (In Hungarian)
Shewchuk, J.R., 1996: Triangle: Engineering a 2D Quality Mesh Generator and Delaunay Triangulator, First Workshop on Applied Computational Geometry (Philadelphia, PA), 124–133.
Shiffler, R.E., 1988: Maximum Z Scores and Outliers. *Amer. Statist. 42*, 79–80.
Singh, D., Sharma, S.D. and *Kumar, K.,* 2002: Flowering and Cross-sompatibility in Apple Cultivars Growing in the Kullu Valley of India. *J. Amer. Pomologic. Soc., 56,* 46–50.
Soenen, A., Paternotte, E. and *Verheyden, C*., 1978: Phenology and climate during preflowering and flowering time in fruit trees (apple and pear). *Fruit Belge 46* (381), 33.
Soltész, M., 1992: Virágzásfenológiai adatok és összefüggések hasznosítása az almaültetvények fajtatársításában. Budapest: MTA, Doctor of MTA thesis. (In Hungarian)
Szász, G., 2013: Agrometeorological research and its results in Hungary (1870–2010). *Időjárás 117*, 315–358.
Tóth, M., 2005: Régi magyar almafajták, mint a rezisztencia nemesítés génforrásai és a környezettudatos külterjes gyümölcsösök elemei. In (Ed.: *Tóth M.*) A fajtaválaszték fejlesztése a kertészetben. Mezőgazdasági Kiadó Kft, Budapest, 23–31. (In Hungarian)
Tóth, M., 2013: Régi gyümölcsfajták szerepe a modern gyümölcsészetben. Bevezető tanulmány. in: Tolnay Gábor (szerk.): Bereczki-Dörgő levelezés. II. kötet, Budapest. http://portal.vfmk.hu /07_00000185. (In Hungarian)
Tóth, M., Balikó, E., and *Szani, Zs.,* 2005: Evaluation of fruit quality of old apple cultivars originating from the foot of the Charpatian Mountains, for utilization in breeding and in ecological farming. *Int. J. Horticult. Sci. 11*, 15–21.
Tóth M., Ficzek G., Király I., Honty K., and *Hevesi M.,* 2012: Evaluation of old Carpathian apple cultivars as genetic resources of resistance to fire blight (Erwinia amylovora). *Trees – Structure and Functions 27,* 597–605.
Tromp, J., 1984: Flower-Bud formation in apple as affected by air and root temperature, air humidity, light intensity, and day length. *Acta Horticulturae 149*, 39–48.
Webster, A.D., 2005: Shoot growth. In (Eds.: *Webster, A.D., Wertheim, S.J.* and *Tromp, J*.) Fundamentals of Temperate Zone Tree Fruit Production, Leiden, The Netherlands: Backhuys, 120–135.
Wertheim, S.J., 1996: Methods for cross pollination and flowering assessment and their interpretation. *Acta Horticulturae 423.,* 237–242.

IDŐJÁRÁS

Quarterly Journal of the Hungarian Meteorological Service
Vol. 121, No. 1, Januar – March, 2017, pp. 43–62

The effect of climate change on heat-related excess mortality in Hungary at different area levels

János Bobvos[1*], **Tibor Málnási**[1], **Tamás Rudnai**[1], **Dóra Cserbik**[2], and **Anna Páldy**[1]

[1]*National Public Health Center*
Albert Flórián u. 2-6, H-1097 Budapest, Hungary

[2] *Maastricht University,*
Minderbroedersberg 4-6, 6211 LK Maastricht, Netherlands

E-mails: bobvos.janos@oki.antsz.hu; malnasi.tibor@oki.antsz.hu; rudnai.tamas@oki.antsz.hu; c.cserbik@student.maastrichtuniversity.nl; paldy.anna@oki.antsz.hu

**Corresponding author*

(Manuscript received in final form August 31, 2016)

Abstract— According to the 5th Assessment Report of IPCC, one of the greatest health impacts of climate change will be the heat-related excess mortality. In Hungary, the National Adaptation Geo-Information System (NAGiS) helps the adaptation process of climate change. Within CRIGiS project, which was initiated to extend the NAGiS, our special subtask was the assessment of heat-related excess mortality at different area levels in the present and for two predicted future periods. This assessment is described in this paper.

The Hungarian Central Statistical Office provided the daily mortality data for the period of May 1 – Sep 30, 2005–2014. The observed daily mean temperature data for the same period at small area level (NUTS 4, Nomenclature of territorial units for statistics) were provided by the Hungarian Meteorological Service (HMS). The modeled daily mean temperature data at NUTS 4 level based on the ALADIN-Climate model for three periods, May 1 – Sep 30 of 1991–2020, 2021–2050, and 2071–2100, were also provided by HMS.

The heatwave days were defined by the 90th percentile of the frequency distribution of daily mean temperatures at different area levels. The excess mortality was computed by extracting the mean daily mortality of cool days from the number of deaths on heatwave days. As we found a difference between the frequency distributions of observed and modeled present periods, a correction was done assuring that the yearly sums of excess mortality were the same in the observed and modeled present periods. Based on the corrected threshold values the changes in the future could be predicted.

During 2005–2014, the range of daily threshold temperature was between 22.3 °C and

25.4 °C, the mean excess mortality was 15.8% on the heatwave days at NUTS 4 level. At national level, daily mortality was higher by 51 cases on heatwave days than on cool days, which corresponded to an excess of 783 death cases per year in average. According to the climate model, the number and intensity of heatwave days will increase in relation to the present situation. Assuming the same population and level of sensitivity, for 2021–2050 a 2.6-fold, for 2071–2100 a 7.4-fold increase of excess deaths is predicted causing 2030 and 5800 cases per year, respectively.

The prediction of excess mortality at different area levels in the NAGiS database will help stakeholders to prepare adaptation measures to climate change.

Key-words: heatwave, heat-related excess mortality, heat-health warning system, climate change, health effects of climate change

1. Introduction

Generally, the climate depends on natural and anthropogenic substances and processes that influence the Earth's energy budget (*Le Treut et al*., 2007). However, climate change occurred over the last decades is primarily driven by human actions, posing a major source of health threat for the 21th century (*McMichael et al*., 2012).

Climate extremes such as heatwaves, cold snaps, droughts, and floodings have become more frequent due to global warming. These extreme weather conditions are not only environmental issues, but they pose unique challenges to human health, both directly and indirectly (*Costello et al*., 2009; *IPCC*, 2014; *McGregor*, 2005).

Direct physiological effects include higher rates of mortality and morbidities, including respiratory, cardiovascular, and metabolic diseases. Indirect effects on health include changing disease vectors of foodborne, waterborne, and airborne diseases, as well as other pathways mediated through human systems like under-nutrition, migration *(Costello et al.*, 2009; *McMichael et al*., 2006; *Patz et al.*, 2014). Additionally, climate extremes pose an additional threat to health professionals and health systems due to the related increase in the demand for health services (*European Commission*, 2013a).

Numerous studies have been published analyzing the impact of heat-related mortality for the last 20 years. *Basu* (2009) reviewed the epidemiological studies dealing with the association of ambient temperature and mortality from a methodological point of view published in the period of 2001–2008.

Several indicators are used to characterize the daily temperature in the national and international literature. The use of simple indicators like daily maximum, minimum, and mean temperature is rather common, but complex indices including humidity, windspeed are also used, however no preferable indicator was recommended (*Barnett et al*., 2010; *Kalkstein* and *Valimon,* 1986; *Kim et al*., 2011).

The definition of heatwaves and the indicator of "high temperature" are not harmonized in practice. A common definition of heatwaves in Europe, including Hungary is the period of three or more consecutive days with temperature above a threshold value. However, mortality increases above the threshold temperature even on one day, therefore, several authors investigated this effect as well in the latest publications (*Hajat et al.*, 2006; *Rocklöw* and *Forsberg*, 2008).

The temperature thresholds also showed great variability in the literature, some studies applied the 95th percentile (*Ishigami et al*., 2008; *Kysely et al*., 2011). *Pascal et al*. (2013) evaluated the excess mortality above the thresholds of 97th, 98th, and 99th percentiles pointing to the problem that the different percentiles defined different days and excess mortalities. The use of the 90th percentile as threshold is now applied by multicenter studies (*De'Donato et al*., 2015) allowing the comparison of the results by cities.

Several papers were published analyzing the temperature-mortality relationship in Budapest (*Paldy et al.*, 2005; *Hajat et al.*, 2006; *Gosling et al.*, 2007; *Ishigami et al.*, 2008; *Baccini et al.*, 2008 and *D'Ippoliti et al.*, 2010). The predicted heat-related excess mortality due to climate change was assessed by few study groups (*Gosling et al.*, 2009; *Baccini et al.*, 2011 and *Bobvos et al.*, 2011) using regional climate models.

In order to manage the above-mentioned risks on human health, adaptation strategies are essential to minimize the impact of climate change on the population's vulnerability (*McMichael et al.*, 2012). Thus, according to the World Health Organization, the most important and urgently needed measures, strategies, and policies regarding climate change adaptation and capacity building should address the reinforcement of public health infrastructures (*McMichael et al*., 2003).

The European Union addressed concerns about the impacts of the environment on public health with special regard to climate change in the European Environment & Health Action Plan 2004–2010, which was further supported by close collaboration with the WHO (*European Commission*, 2007). It was followed by the EU Strategy on Adaptation to Climate Change in 2013, with the aim to contribute to a more climate-resilient Europe. The Strategy launched the European Climate Adaptation Platform (Climate-ADAPT) in 2012 as a tool to provide the best available information for decision-making (*European Commission*, 2013b).

Hungary developed the National Climate Change Strategy in 2008 following the amendment of UNFCCC and Kyoto Protocol. The 2013 revision of the Strategy was developed by the National Adaptation Center of the Geological and Geophysical Institute of Hungary, which determined a timeline from 2014 to 2025, with an outlook to 2050. The strategy uses the National Adaptation Geo-information System (*NAGiS*, 2015) as a tool to facilitate decision-making process and policy-making regarding impact assessments and adaptation measures of climate change. NAGiS established a country-wide

database, indicators, input data to serve the methodological basis for modeling the local and regional exposure, sensitivity, and adaptive capacity for different climate hazards.

Based on existing dataset of the NAGiS, the Vulnerability and Impact Studies on Tourism and Critical Infrastructure (*CRIGiS*, 2015) project aimed to prepare indicators for the assessment of climate change vulnerability. In CRIGiS, our special subtask was the assessment of heat-related excess mortality at different area levels in the present and for two predicted future periods using the ALADIN-Climate model and SRES A1B (IPCC Special Report on Emission Scenarios) scenario as default criteria in the CRIGIS project. The methods and results are described in this paper.

2. Data and methods

2.1. Observed heat-related mortality in the present period

It is very important to choose the proper spatial resolution for the statistical analysis. The daily mortality data at settlement level are not accessible due to the protection of personal data stated by law (5th Law of 2013 on Civil Book of Laws). Beyond this protection, the analysis of daily data at settlement level is not relevant due to the small number of population and the great variance of mortality data, therefore, the chosen smallest territorial unit is the so-called "small area" level (NUTS 4-Nomenclature of territorial units for statistics, 175 small areas). The assessments were carried out separately at higher levels of territorial aggregation (NUTS 3 – twenty counties, NUTS 2 – seven regions, NUTS 1 – three great regions, NUTS 0 - country level). These assessments are not the sums of the results gained at small area level, but separate analyses related to the given spatial level assuring that the assessments of heat-related mortality are uniform at the given spatial level.

Daily total mortality data were gained from the Hungarian Central Statistical Office at NUTS 4 level for the summer periods (May 1–Sept 30) of 2005–2014 for Hungary. Choosing the time frame of ten years is sufficient and enough, while during ten years the long-term change of mortality can not be detected, therefore a correction for the trend is not necessary.

In the analysis, we evaluated not only the impact of heatwaves – a period of three or more consecutive days with daily mean temperature over the threshold defined in our previous paper (*Paldy* and *Bobvos*, 2012) – but also the impact on excess mortality of high temperature of even one day. Based on the study related to Budapest (*Bobvos et al*., 2015), the simple daily mean temperature indicator was chosen because its measurement and prediction is simpler than those of the complex indices, moreover, it is a basic, not calculated parameter of climate models. The observed daily mean temperature data for the same period at NUTS 4 level were provided by the Hungarian Meteorological Service (HMS). At

higher levels of territorial aggregation, the daily mortality data were summed, daily temperature data at NUTS 4 level were averaged. As the methods of computation were the same concerning each area of the different NUTS levels, we described them in general formulas.

In order to represent the effect of heatwaves on daily mortality, daily mean excess mortality (EM_j) was defined. It can be computed for each area of the five NUTS levels described above as the mean of difference of the daily mortality during heatwave days and mean mortality during cool days at the identified area j by Eq.(1):

$$EM_j = N^{-1} * \sum_{i=1}^{1530} \left(MH_{ij} - MC_j\right) \quad if \quad T_{ij} > TT_j \qquad \text{[cases per day]}, \quad (1)$$

where MH_{ij} represents the daily mortality cases on day i (10 years, 1530 days), MC_j is the daily mean mortality on days under threshold temperarture, N is the number of days over threshold temperature, T_{ij} is the daily mean temperature on day i, and TT_j, the threshold temperature at the given area j.

The yearly mean excess death cases can be computed as daily mean excess mortality cases multiplied by the yearly mean number of heatwave days. The number of heatwave days depends on the chosen temperature threshold. The yearly mean excess death cases decreased by the increase of threshold values, as the number of identified heatwave days decreased. On the other hand, the daily mean excess mortality cases on heatwave days increased in relation to threshold values. To define the proper threshold, the product function of the corresponding values of the two curves can be used (*Bobvos et al*., 2015). At the maximum range of the product curve, the two opposite processes were equally considered (*Fig. 1*). By analyzing the aggregated data at national level, the frequency distribution shows a maximum at the 90th percentile.

Based on the above mentioned analysis, the heat-related excess mortality was modeled by the 90th percentile of the frequency distribution of the daily mean temperatures (TP90) at the given area level (*Fig. 2.*).

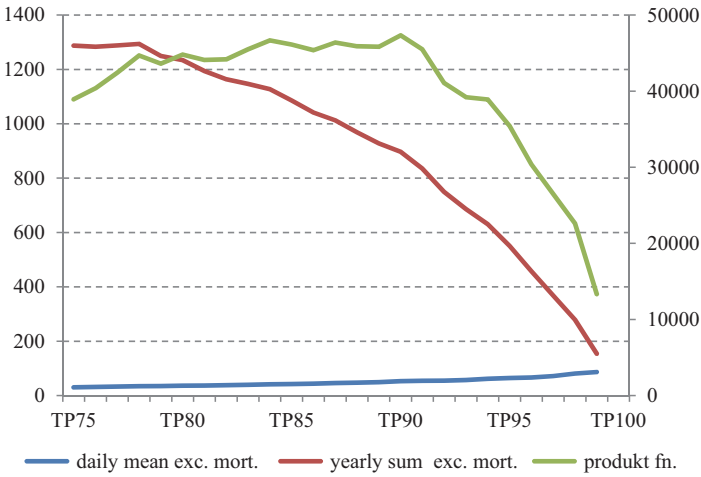

Fig. 1. The yearly mean excess mortality (case), the daily mean excess mortality on heatwave days (case) above different thresholds (TP%), as well as their product function at national level in Hungary, in the period 2005–2014.

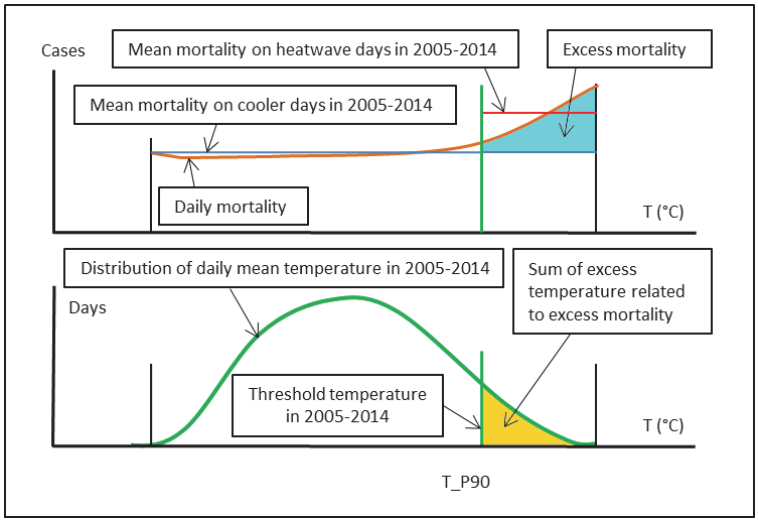

Fig. 2. Scheme of the methodological process of calculation of heat-related excess mortality.

To ensure comparability, the relative excess mortality was also computed, defining the per cent increase of mortality during the heatwaves for each area of the five NUTS levels. The relative daily mean excess mortality ($EM\%_j$) on heatwave days can be computed by Eq.(2):

$$EM\%_j = 100 * EM_j * MC_j^{-1} \qquad [\%\ \text{per day}], \qquad (2)$$

where EM_j represents the daily mean excess mortality cases and MC_j is the daily mean mortality on days under threshold temperarture at the given area j.

The numbers of days above the 90th percentile of daily mean temperature in the areas at each NUTS level are equal (153 days in 10 years); however, the sum of excess temperature ($TSUM_j$) above the threshold is different due to the different distributions of daily temperature on these days. This excess temperature causing excess mortality can be computed by Eq.(3). Dividing it by ten we get the mean yearly excess temperature.

$$TSUM_j = \sum_{i=1}^{1530} \left(T_{ij} - TT_j\right) \qquad if\ \ T_{ij} > TT_j \quad \left[^{\circ}\text{C per ten year}\right], \qquad (3)$$

where T_{ij} represents the daily mean temperature on day i and TT_j is the threshold temperature at the given area j.

The excess mortality related to excess temperature can be expressed as relative risk ($RR1°C_j$). It can be computed by using the daily mean excess mortality cases on days over the thresholds and the excess temperature measured on these days. This value is the percent excess mortality per 1 °C increase of temperature, it can be regarded as heat-related vulnerability indicator in present period in each area of the five NUTS levels Eq.(4):

$$RR1°C_j = N * EM_j * TSUM_j^{-1} \qquad [\%\ \text{per}\ ^{\circ}\text{C}], \qquad (4)$$

where N represents the number of days over the threshold temperature, EM_j indicates the daily mean excess mortality cases, and $TSUM_j$ is the sum of excess temperature above the threshold at the given area j.

The result curve of multiplication necessary to determine the proper threshold range can also be used for diagnostic purposes. In case of small areas with few daily death cases where the relative standard deviation is greater, the

result has low confidence. Therefore, a systematic analysis was carried out in order to establish an indicator of reliability with four categories:

- Category 1 (high reliability): includes those areas, where the multiplication curve had the maximum value around the 90th percentile, similarly to the curve of national level data.
- Category 2 (moderate reliability): containes those areas, where the maximum of the multiplication curve was not at the 90th percentile, although the curve had a monotonous line and the excess mortality values belonging to the 90th percentile were exact.
- Category 3 (informative): includes those areas, where the maximum of the multiplication curve was not at the 90th percentile and the shape of the curve was not monotonous. This category gives information about the possibility to define excess mortality, although the value is not reliable.
- Category 4 (unreliable): includes those areas, where the maximum of the multiplication curve was not at the 90th percentile, the shape of the curve was not monotonous, and negative values of excess mortality could be detected. Due to the great uncertainty, the data of excess mortality were not presented.

2.2. Heat-related mortality in the climate model

In order to assess the climate change related excess mortality, the modeled daily mean temperature data at NUTS 4 level based on the ALADIN-Climate model (SRES A1B) for three periods (May 1 – Sep 30 of 1991–2020, 2021–2050, and 2071–2100) were provided also by HMS.

The period of 1991–2020 can be regarded as present period of the climate model. Our aim was to relate the results of the observed present period (2005–2014) to the present period of the climate model (1991–2020). As the two periods did not have equal length, we assumed that the results of observed present period represent the whole 30 years period. As we found a difference between the frequency distribution of observed temperature and the temperature of the present period of the climate model, a correction was done. We chose a new threshold temperature in the modeled present period assuring that the mean yearly excess temperatures contributing to excess mortality were the same in the two present periods (*Fig. 3*).

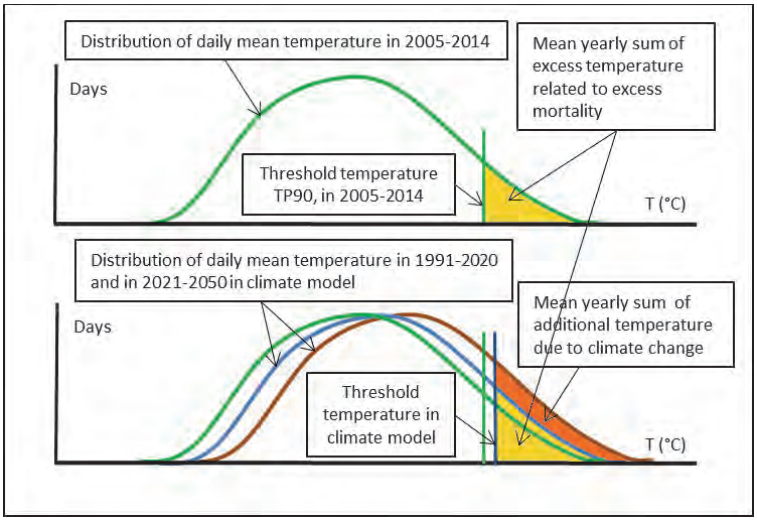

Fig. 3. Scheme of the methodological process of calculation of heat-related excess mortality in the climate model.

Based on the corrected threshold values of the modeled present period, the changes in the future could be predicted. The changes of the number and intensity of heatwave days together define the level of increasing mean yearly excess temperature, which is the additional exposure due to climate change. Assuming the same population and sensitivity level (RR1°C) in the future, this additional exposure will cause the same level of increase in excess mortality.

The calculated yearly mean excess mortality cases, which are the same in both present periods can be regarded as heat-related baseline sensitivity indicator, from the point of climate change. The excess mortality due to the increase of heat exposure predicted by the climate model serves as a potential impact indicator and (regardless to changes of adaptive capacity) as a vulnerability indicator of the heat-related mortality due to climate change.

3. Results

3.1. Characteristics of population, daily mortality data, and temperature indicators in the present period

Fig. 4 demonstrates the distribution of the mean population at NUTS 4 and NUTS 3 levels between 2005 and 2014. The mean population ranged from 6,900

(Őriszentpéter) to 1,691,000 (Budapest) at smaller area level, the mean population (excluding Budapest) was 48,000, areas belonging to cities had much bigger population. During the studied period, less than 15,000 inhabitants lived in 18 small areas. The mean population ranged from 211,000 (Nógrád) to 1,691,000 (Budapest) at NUTS 3 level, the mean population of the counties was 444,000 without Budapest.

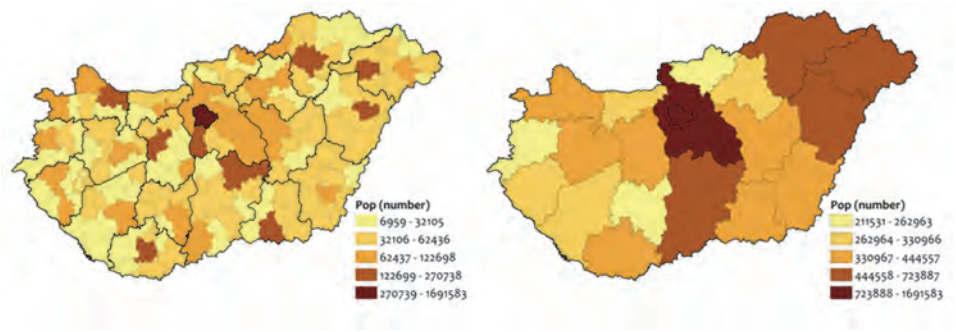

Fig. 4. Distribution of mean population (Pop, number) at NUTS 4 and NUTS 3 levels in Hungary, in the period of 2005–2014.

The mean daily mortality data on cool days at NUTS 4 and NUTS 3 levels of the investigated period is shown in *Fig. 5*. The spatial distribution of mean mortality, basically defined by the number of population is similar to the distribution of the population. The mean daily mortality ranged from 0.3 (Őriszentpéter) to 55.6 (Budapest) at NUTS 4 level. The mean mortality at NUTS 4 level without Budapest was 1.6 cases. Less than one mean daily death cases occurred in 67 small areas. The mean daily mortality ranged from 7.7 (Nógrád) to 55.6 (Budapest) at NUTS 3 level, the mean mortality was 14.3 cases without Budapest.

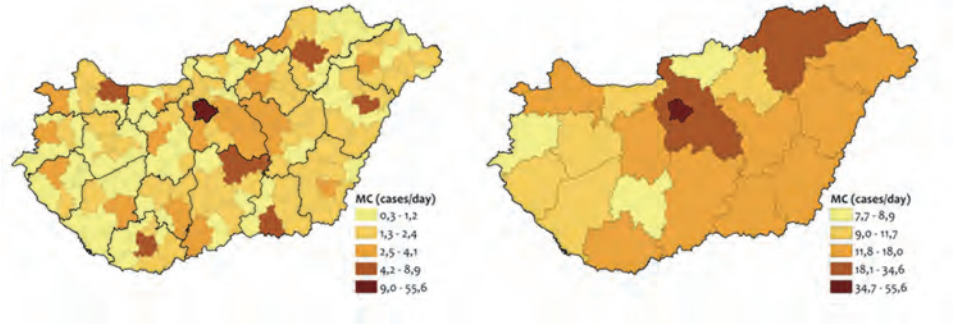

Fig. 5. Distribution of mean daily mortality on cool days (MC, cases/day) at NUTS 4 and NUTS 3 level in Hungary, in the period of 2005–2014.

The 90th percentile of the frequency distribution of the daily mean temperature at NUTS 4 and NUTS 3 levels of the investigated period is shown in *Fig. 6*. The spatial distribution of the threshold temperature was in a range of 22.3 °C and 25.4 °C at NUTS 4 level. Small areas with threshold temperature over the mean (24.3 °C) could be detected in the Great Plain and Small Plain. The highest values were registered in counties Csongrád and Békés.

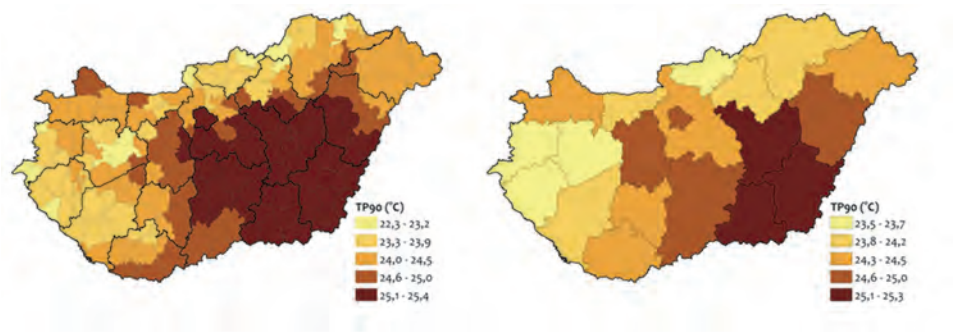

Fig. 6. The 90th percentile of the frequency distribution of the daily mean temperature (TP90, °C) at NUTS 4 and NUTS 3 level in Hungary, in the period of 2005–2014.

Maps of *Fig. 7* demonstrate the mean excess temperature of the days above the threshold in the period of 2005–2014. The number of days above the 90th percentile was 153 days in each area during the studied 10-year period, meaning 15.3 heatwave days as yearly average. The mean excess temperature was between 1.45°C and 1.82 °C at NUTS 4 level and between 1.5 °C and 1.78 °C at NUTS 3 level, respectively.

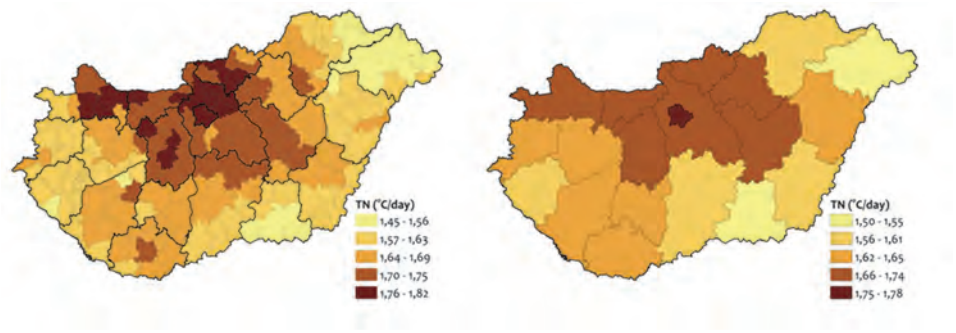

Fig. 7. The mean excess temperature above the threshold temperature (TN, °C/day) on heatwave days at NUTS 4 and NUTS 3 level in Hungary, in the period of 2005–2014.

3.2. Characteristics of heat-related excess mortality in the present and predicted future periods

The relative increase (EM%) of daily mean excess mortality on days above the 90th percentile of daily mean temperature is shown in *Fig. 8.* The mean increase of mortality on heatwave days was 15.7%/°C at national level, it was between 0.5% and 45% at NUTS 4 level and between 9% and 20% at NUTS 3 level, respectively. The excess mortality at small area level does not show a typical spatial pattern. At NUTS 3 level, the highest excess mortality can be observed in Budapest and in Veszprém county.

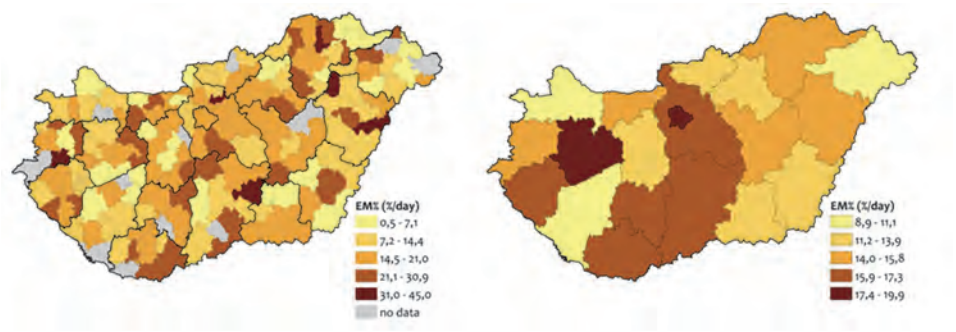

Fig. 8. The mean excess mortality above the threshold temperature on heatwave days (EM%, %/day) at NUTS 4 and NUTS 3 level in Hungary, in the period of 2005–2014.

The spatial distribution of relative excess mortality by 1 °C (RR1 °C) showed similar pattern as the relative excess mortality (*Fig. 9*). The mean increase of mortality on heatwave days was 9.5%/°C at national level, it was between 0.3%/°C and 27.4%/°C at NUTS 4 level and between 5.5%/°C and 11.2%/°C at NUTS 3 level, respectively.

According to the reliability categories at NUTS 4 level, the number of areas belonging to categories 1 and 2 was 152 (87%), while 9 small areas (5%) fell into category 3 (*Fig. 10*). 14 small areas (8%) could not be evaluated, the excess mortality data are not given, they are grouped into category 4. Regarding the analyses of higher area levels, each of the results met the criteria of category 1.

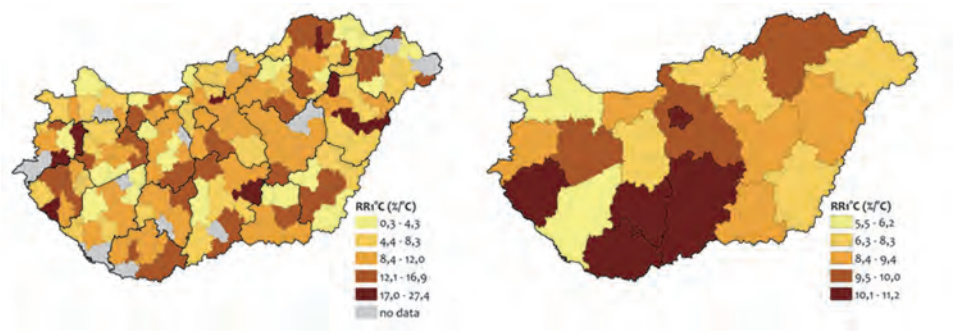

Fig. 9. The mean excess mortality per 1°C increase of temperature above the threshold on heatwave days (RR1°C, %/°C) at NUTS 4 and NUTS 3 level in Hungary, in the period of 2005–2014.

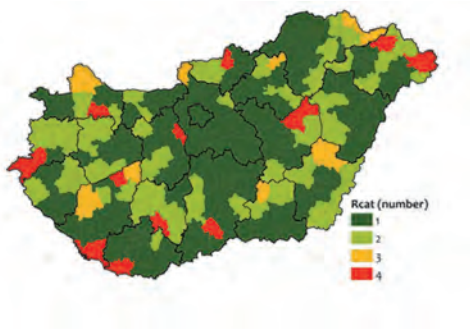

Fig. 10. Categories (Rcat, number 1 to 4) of reliability at NUTS 4 level.

At NUTS 4 level, according to the climate model, the number of yearly heatwave days will increase in relation to the present situation by 57–98% on average between 2021–2050, while the intensity (daily mean excess temperature above threshold) of heatwaves will increase by 27–55% on average (*Fig. 11*).

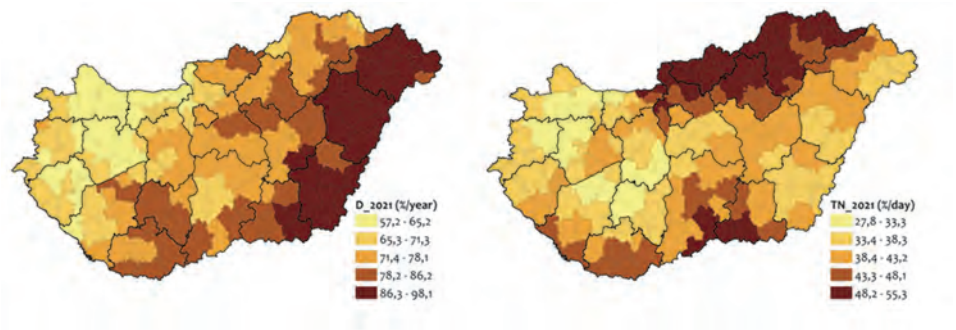

Fig. 11. Change of the number (D_2021, %/year) and intensity (TN_2021, %/day) of heatwave days in the period of 2021–2050 of the climate model in relation to 1991–2020.

At NUTS 4 level, according to the climate model, the number of yearly heatwave days will increase in relation to the present situation by 195–270% on average between 2071–2100, while the intensity (daily mean excess temperature above threshold) of heatwaves will increase by 80–133% on average (*Fig. 12*).

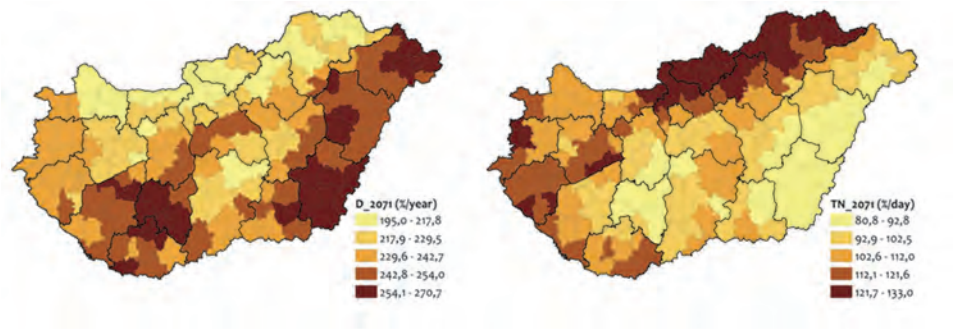

Fig. 12. Change of the number (D_2071, %/year) and intensity (TN_2071, %/day) of heatwave days in the period of 2071–2100 of the climate model in relation to 1991–2020.

The changes of the number and intensity of heatwave days together will increase for 2021–2050 in relation to the present situation, defining the level of additional heat exposure and excess mortality. The range of increase of excess death cases per year at NUTS 4 level will be between 107% and 182% compared to the period of 1991–2020. For 2071–2100, climate projection shows a change of excess mortality in the range of 531% and 668% regarding increasing exposure (*Fig. 13*).

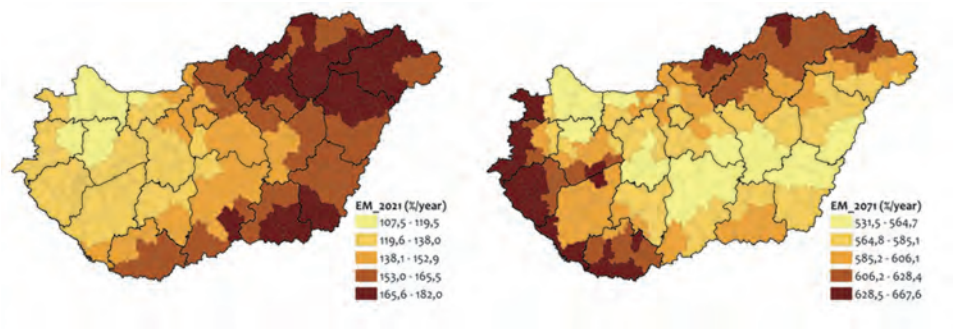

Fig. 13. Change of heatwave related mortality in the periods of 2021–2050 (EM_2021, %/year) and 2071–2100 (EM_2071, %/year)of the climate model in relation to 1991–2020 at NUTS 4 level.

At NUTS 3 level, according to the climate model, the number of yearly heatwave days will increase in relation to the present situation by 62-95% on average between 2021–2050, while the intensity (daily mean excess temperature above threshold) of heatwaves will increase by 31–51% on average (*Fig. 14*).

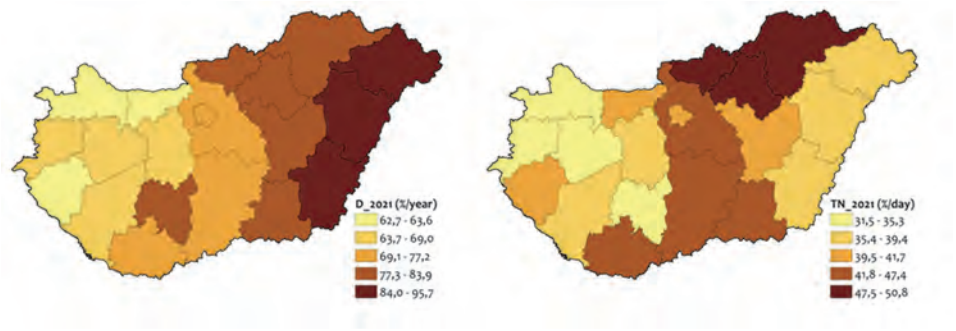

Fig. 14. Change of the number (D_2021, %/year) and intensity (TN_2021, %/day) of heatwave days in the period of 2021–2050 of the climate model in relation to 1991–2020.

At NUTS 3 level, according to the climate model, the number of yearly heatwave days will increase in relation to the present situation by 214–264% on average between 2071–2100, while the intensity (daily mean excess temperature above threshold) of heatwaves will increase by 86–127% on average (*Fig. 15*).

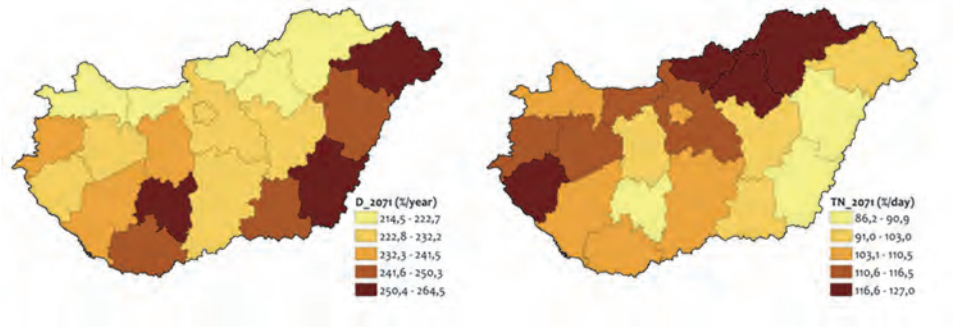

Fig. 15. Change of the number (D_2071, %/year) and intensity (TN_2071, %/day) of heatwave days in the period of 2071–2100 of the climate model in relation to 1991–2020.

The changes of number and intensity of heatwave days together will increase for 2021–2050 in relation to the present situation, defining the level of additional heat exposure and excess mortality. The range of increase of excess death cases per year at NUTS 4 level will be between 114% and 173% compared to the period of 1991–2020. For 2071–2100, climate projection shows a change of excess mortality in the range of 559% and 638% regarding increasing exposure (*Fig. 16*).

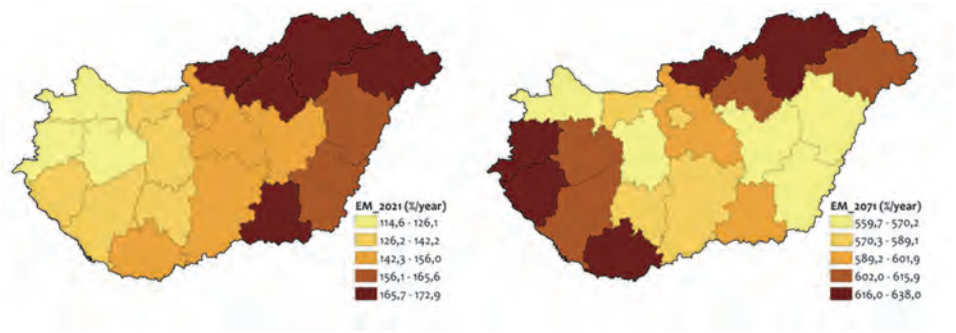

Fig. 16. Change of heatwave related mortality in the periods of 2021–2050 (EM_2021, %/year) and 2071–2100 (EM_2071, %/year) of the climate model in relation to 1991–2020 at NUTS 3 level.

3.3. Results of higher aggregated area levels

The results reported previously will be available for the experts, decision makers and laypeople in the NAGiS system. The data at regional, great regional, and national levels are necessary for long term strategic planning; they do not require regular accessibility. Therefore, the data aggregated at higher levels are summarized in *Table 1*.

At national level, daily mortality was higher by 51 cases (EM%=15.65%) on heatwave days (15.3 days/years) than on cool days, which corresponded to an excess of 783 death cases per year. According to the climate model, the number and intensity of heatwave days (D_2021, TN_2021) will increase in the period 2021-2050 in relation to the present situation, these together define the rate of increase of exposure (EM_2021=159%). Assuming the same population and sensitivity level in the future, this additional exposure will cause the same level of increase in excess mortality. For 2021–2050, a 2.6-fold increase of excess deaths is predicted causing 2,030 cases per year. For 2071–2100, climate projection shows a change of excess mortality by 640% (EM_2071), meaning a 7.4-fold increase at national level, which corresponds to 5,800 yearly excess death cases.

Table 1. Results of higher aggregated area levels

Name	NUTS code	MC	TP90	TN	EM %	RR1°C	D _2021	TN _2021	EM _2021	D _2071	TN _2071	EM _2071
		case /day	°C	°C/day	%/day	%/°C	%/year	%/day	%/year	%/year	%/day	%/year
KMR	HU10	90.16	24.51	1.74	18.43	10.61	72.51	46.35	152.4	226.6	114.1	599.5
KDR	HU21	34.97	24.25	1.64	15.11	8.99	73.36	33.99	132.2	239.7	106	599.8
NyDR	HU22	32.49	23.80	1.61	13.83	8.56	64.74	37.12	125.8	231.1	119.1	625.7
DDR	HU23	32.93	24.20	1.61	13.95	8.64	76.99	38.17	144.5	252.4	105.1	623.0
ÉMR	HU31	43.88	23.91	1.63	14.05	8.63	80.75	49.92	170.9	225.7	123.1	626.9
ÉAR	HU32	48.03	24.72	1.57	13.70	8.72	89.29	42.64	170.0	247.8	102.1	603.2
DAR	HU33	46.08	25.18	1.57	15.48	9.86	84.49	43.95	165.5	251.1	98.24	596.1
KMR	HU1	90.16	24.51	1.74	18.43	10.61	72.51	46.35	152.4	226.6	114.1	599.5
DR	HU2	99.25	24.08	1.60	14.16	8.79	73.19	36.82	137.0	242.5	112.8	629.4
AÉR	HU3	138.0	24.54	1.59	13.80	8.63	80.45	50.66	171.8	227.9	119.7	620.8
MO	HU	327.3	24.28	1.60	15.65	9.78	77.14	46.25	159.0	232.6	122.6	640.7

4. Conclusion

The final products of this analysis of the CRIGiS project are incorporated in the NAGiS database to meet the needs of different users: decision makers, experts, planners, and people having personal interest. The dataset includes maps, datasheets, descriptions of use and limitations, as well as examples.

The uncertainties of the predictions for the future can be decreased by repeating the assessments using different climate models and emission scenarios. This can easily be done, because the NAGiS database has been updated by three more climate models.

In the latest period, increasing emphasis is put on the identification of socioeconomical factors influencing heat-related excess mortality, to which the results of this study can serve as a basis.

The results computed at a yearly basis may allow the risk assessment of the heat-related excess mortality. The risk estimates can be compared to other environment-related risk estimates, helping the correct evaluation of heat-related mortality risk and the additional risk attributed to climate change and can easily be integrated in a risk assessment and management system.

Aknowledgements: This research was supported by the CRIGiS project (Vulnerability and Impact Studies with focus on Tourism and Critical Infrastructures - EEA-C12-13). The authors acknowledge the highly appreciated help by the colleagues of the Hungarian Meteorological Service: *Zita Bihari, Tamás Kovács, Mónika Lakatos, Annamária Marton,* and *Tamás Szentimrey*.

References

Baccini, M., Biggeri, A., Accetta, G., Kosatsky, T., Katsouyanni, K., Analitis, A., Anderson, H.R., Bisanti, L., D'Ippoliti, D., Danova, J., Forsberg, B., Medina, S., Paldy, A., Rabczenko, D., Schindler, C., and *Michelozzi, P.,* 2008: Heat effects on mortality in 15 European cities. *Epidemiology 19,* 711–719.

Baccini M., Kosatsky T., Analitis A., Anderson H.R., D'Ovidio M., Menne B., Michelozzi P., and *Biggeri A.,* 2011: PHEWE Collaborative Group. Impact of heat on mortality in 15 European cities: attributable deaths under different weather scenarios. *J. Epidemiol. Community Health 65,* 64–70.

Barnett, A.G., Tong, S., and *Clements, A.CA.,* 2010: What measure of temperature is the best predictor of mortality? *Environ. Res. 110,* 604–611.

Basu, R., 2009: High ambient temperature and mortality: a review of epidemiologic studies from 2001 to 2008. *Environ. Health 8,* 40.

Bobvos, J. and *Paldy, A.,* 2009: Impact of Heat on the Urban and Rural Population in Hungary. *Epidemiology 20,* S127.

Bobvos, J., Solymosi, N., and *Paldy, A.,* 2011: Climate change and heat-related mortality in Budapest - comparative methods of impact estimation of temperature change. *Environ. Health Perspect.* Available at: http://ehp.niehs.nih.gov/isee/isee2011/, accessed 15 Jun 2016.

Bobvos, J., Fazekas, B., and *Páldy, A.,* 2015: Assessment of heat-related mortality in Budapest from 2000 to 2010 by different indicators. *Időjárás 119,* 143–158.

Chen, K., Huang, L., Zhou, L., Ma, Z., Bi, J., and *Li, T.,* 2015: Spatial analysis of the effect of the 2010 heat wave on stroke mortality in Nanjing, China. *Sci. Rep. 2015 Jun 2;5:*10816.

Costello, A., Abbas, M., Allen, A., Ball, S., Bell, S., Bellamy, R., and *Patterson, C.,* 2009: Managing the health effects of climate change: Lancet and University College London Institute for Global Health Commission. *Lancet, 373(9676),* 1693–1733.

CRIGiS, 2015: Vulnerability and Impact Studies on Tourism and Critical Infrastructure. Available at: http://www.met.hu/KRITeR/en/kezdo/index.php, accessed 15 Jun 2016.

De' Donato, F.K., Leone, M., Scortichini, M., De Sario, M., Katsouyanni, K., Lanki, T., Basagaña, X., Ballester, F., Åström, C., Paldy, A., Pascal, M., Gasparrini, A., Menne, B., and *Michelozzi, P.,* 2015: Changes in the Effect of Heat on Mortality in the Last 20 Years in Nine European Cities. Results from the PHASE Project. *Int. J. Environ. Res. Public Health. 12,*15567–83.

European Commission, 2007: Communication from the Commission to the Council, the European Parliament and the European Economic and Social Committee - "Mid Term Review of the European Environment and Health Action Plan 2004–2010. Available at: http://eur-lex.europa.eu/legal-content/EN/ALL/?uri=CELEX:52007DC0314, accessed 15 Jun 2016.

European Commission, 2013a: Adaptation to climate change impacts on human, animal and plant health. Available at: http://ec.europa.eu/clima/policies/adaptation/what/docs/swd_2013_136_en.pdf, accessed 15 Jun 2016.

European Commission, 2013b: Communication from the Commission to the European Parliament, the Council, the European Economic and Social Committee, and the Committee of the Regions - An EU Strategy on adaptation to climate change. Available at: http://eur-lex.europa.eu/legal-content/EN/TXT/PDF/?uri=CELEX:52013DC0216&from=EN, accessed 15 Jun 2016.

Fouillet, A., Rey, G., Laurent, F., Pavillon, G., Bellec, S., Guihenneuc-Jouyaux, C., Clavel, J., Jougla, E., and *Hémon, D.,* 2006: Excess mortality related to the August 2003 heat wave in France. *Int. Arch. Occup. Environ. Health 80,*16–24.

Gosling, S.N., McGregor, G.R., and *Paldy, A.,* 2007: Climate change and heat-related mortality in six cities Part 1: model construction and validation. *Int. J. Biometeorol. 51,* 525–540.

Gosling, S.N., McGregor, G.R., and *Lowe, J.A.,* 2009: Climate change and heat-related mortality in six cities Part 2: climate model evaluation and projected impacts from changes in the mean and variability of temperature with climate change. *Int. J. Biometeorol. 53,* 31–51.

Hajat, S., Armstrong, B., Baccini, M., Biggeri, A., Bisanti, L., Russo, A., Paldy, A., Menne, B., and *Kosatsky, T.,* 2006: Impact of high temperatures on mortality: is there an added heat wave effect? *Epidemiology 17,* 632–638.

Hajat, S., Vardoulakis, S., Heaviside, C., and *Eggen, B.,* 2014: Climate change effects on human health: projections of temperature-related mortality for the UK during the 2020s, 2050s and 2080s. *J. Epidemiol. Commun. Health 68,* 641–648.

Huang, C., Barnett, A.G., Wang, X., Vaneckova, P., Fitzgerald, G., and *Tong, S.,* 2011: Projecting Future Heat-Related Mortality under Climate Change Scenarios: A Systematic Review. *Environ. Health Perspect. 119,*1681–1690.

IPCC, 2001: Technical Summary, Climate Change 2001: Impacts, Adaptation, and Vulnerability. In (Eds. *M. Manning, M. and Nobre, C.*) Report of Working Group II of the Intergovernmental Panel on Climate Change, Geneva, Switzerland, February 2001.

IPCC, 2013*:* Climate Change 2013: The Physical Science Basis. Summary for Policymakers*.* In (Eds. *Stocker, T.F., Qin, D., Plattner, G.K., Tignor, M., Allen, S.K., Boschung, J., Nauels, A., Xia, Y., Bex, V., Midgley, P.M.*) Contribution of Working Group I to the Fifth Assessment Report of the Intergovernmental Panel on Climate Change*.* Cambridge University Press, Cambridge, United Kingdom and New York, NY, USA.

IPCC. 2014: Climate Change 2014: Synthesis Report. Contribution of Working Groups I, II and III to the Fifth Assessment Report of the Intergovernmental Panel on Climate Change. (Core Writing Team, R. K. Pachauri, & L. A. Meye Eds.). Geneva, Switzerland: IPCC.

Ishigami, Ai., Hajat, S., Kovats, R.S., Bisanti, L., Rognoni, M., Russo, A., and *Paldy, A.,* 2008: An ecological time-series study of heat-related mortality in three European cities. *Environ. Health 7,* 5.

Kalkstein, L.S. and *Valimont, K.M.,* 1986: An evaluation of summer discomfort in the United States using a relative climatological index. *Bull. Am. Meteorol. Soc. 67*, 842–848.

Kim, Y.M., Kim, S., Cheong, H. K., and *Kim, E.H.*, 2011: Comparison of temperature indexes for the impact assessment of heat stress on heat-related mortality*. Environ. Health Toxicol. 26,* Available at: http://dx.doi.org/10.5620/eht.2011.26.e2011009, accessed 15 Jun 2016.

Kyselý, J., Plavcová, E., Davídkovová, H., and *Kynčl, J.,* 2011: Comparison of hot and cold spell effects on cardiovascular mortality in individual population groups in the Czech Republic. *Clim. Res. 49,*113–129.

KSH, 2008: Tájékoztató a kiemelten támogatott kistérségekről. Központi Statisztikai Hivatal, Budapest*.*

KSH, 2014: Szépkorúak és vének - október elseje, az idősek világnapja. *Statisztikai Tükör 103.*

Le Treut, H., Somerville, R., Cubasch, U., Ding, Y., Mauritzen, C., Mokssit, A., Prather, M., 2007: Historical Overview of Climate Change. *In Solomon,S., Qin M.D., Manning, Z.,Chen, M., Marquis, K.B., Tignor M.A.,* and *Miller H.L. (Eds.):* Climate Change 2007: The Physical Science Basis. Contribution of Working Group I to the Fourth Assessment Report of the Intergovernmental Panel on Climate Change*.* Cambridge University Press, Cambridge, United Kingdom and New York, NY, USA.

Martinez, G.S., Baccini, M., De Ridder, K., Hooyberghs, H., Lefebvre, W., Kendrovski, V., Scott, K., and *Spasenovska, M.,* 2016: Projected heat-related mortality under climate change in the metropolitan area of Skopje*. BMC Public Health. 16,*407.

McGregor, G., 2005: Projected changes in extreme weather and climate events in Europe. In (Eds*. K. Wilhelm, B. Menne, & R. Bertollini*) Extreme Weather Events and Public Health Responses. Berlin and Heidelberg, Germany: Springer-Verlag, 11–13.

McMichael, A.J., Campbell-Lendrum, D.H., Corvalán,C.F., Ebi ,K.L., Githeko,A., Scheraga J.D., and *Woodward, A.,*2003: Climate change and human health - risks and responses. WHO Geneva.

McMichael, A.J., Woodruff, R.E., and *Hales, S.,* 2006: Climate change and human health: present and future risks. *Lancet 367(9513),* 859–869.

McMichael, T., Montgomery, and *H., Costello, A.,* 2012: Health risks, present and future, from global climate change. *BMJ, 344,* e1359.

NAGiS, 2015: Newsletter 2015/1. Available at: http://nagis.hu/sites/nater.mfgi.hu/files/files/NAGIS_ Newsletter_2015_01.pdf, accessed 15 Jun 2016.

Pascal, M., Wagner, V., Le Tertre, A., Laaidi, K., Honoré, C., Bénichou, F., and *Beaudeau, P.,* 2013: Definition of temperature thresholds: the example of the French heat wave warning system. *Int. J. Biometeorol. 57,* 21–9.

Paldy, A., Bobvos, J., Vamos, A., Kovats, R. S., Hajat, S., 2005: The effect of temperature and heat waves on daily mortality in Budapest, Hungary, 1970–2000. In (Eds. *Kirch, W., Menne, B.,*

Bertollini, R.) Extreme weather events and public health responses. Springer, New York, 99–107.

Paldy A. and *Bobvos J.,* 2011: Predicted Impact of Climate Change on Daily Excess Mortality and Emergency Ambulance calls between 2021–2050 and 2071–2100. *Cent. Eur. J. Occupat. Environ. Med. 17*, 445–68.

Paldy, A., Juhasz, A., Bobvos, J., and *Nagy, CS.,* 2011: Modelling of the association of health impacts of exposure to 2007-heatwave and the effect modifiers at small area level in Hungary. *Environ Health Perspect.* Available at: http://ehp.niehs.nih.gov/isee/isee2011/, accessed 15 Jun 2016.

Paldy, A. and *Bobvos, J.,* 2012: Impact of Heat Waves on Excess Mortality in 2011 and 2012 in Hungary. *Cent. Eur. J. Occupat. Environ. Med. 18,*15–26.

Patz, J.A., Grabow, M.L., and *Limaye, V.S.,* 2014: When It Rains, It Pours: Future Climate Extremes and Health. *Ann. Glob. Health 80,* 332–344.

RKK, 2016: Long-term socio-economic forecasting for Hungary project. http://nater.rkk.hu, accessed 15 Jun 2016.

Rocklöv, J. and *Forsberg, B.*, 2008: The effect of temperature on mortality in Stockholm 1998-2003: a study of lag structures and heatwave effects. *Scand. J. Public Health 36,* 516–23.

Urban, A., Burkart, K., Kyselý, J., Schuster, C., Plavcová, E., Hanzlíková, H., Štěpánek, P., and *Lakes, T.*, 2016: Spatial Patterns of Heat-Related Cardiovascular Mortality in the Czech Republic. *Int. J. Environ. Res. Public Health 4*;13(3). pii: E284.

Vardoulakis, S., Dear, K., Hajat, S., Heaviside, C., Eggen, B., and *McMichael, A.j.*, 2014: Comparative Assessment of the Effects of Climate Change on Heat- and Cold-Related Mortality in the United Kingdom and Australia. *Environ. Health Perspect. 122,* 12.

IDŐJÁRÁS

Quarterly Journal of the Hungarian Meteorological Service
Vol. 121, No. 1, January – March, 2017, pp. 63–78

Analysis of precipitation time series at Keszthely, Hungary (1871–2014)

Tímea Kocsis[1*] and **Angéla Anda**[2]

[1] *Budapest Business School College of Commerce,*
Catering and Tourism Department of Methodology,
1054 Budapest, Alkotmány Str. 9–11., Hungary

[2] *University of Pannonia Georgikon*
Faculty Department of Meteorology and Water Management,
8360 Keszthely, Festetics Str. 7., Hungary

**Corresponding author e-mail: JakuschneKocsis.Timea@uni-bge.hu*

(Manuscript received in final form July 20, 2016)

Abstract—The results in the issue of local signs of global climate change at Keszthely (Hungary) are summarized and presented in this paper. The meteorological measurements at Keszthely have long history, a more than 140-year-long dataset of monthly amount of precipitation, provided by the University of Pannonia, is available for statistical analysis. The long-time series of precipitation amounts of Keszthely (Hungary) meteorological station was analyzed from the beginning of the observation (1871) until 2014, from the point of view of climate change. Simple climate-statistical analysis has been made in purpose to discover local climate alternations. Linear and exponential trends were fitted, and it was concluded that linear trends in every case had lower relative standard error than exponential trends, so linear changes were interpreted. Despite the fact that significant declining tendency was expected, the annual data does not show any modification in the tendency or variability, but other signs of the decreasing trend can be detected. Significant decreasing tendency was found in spring (–31.5 mm/100 years). Among the monthly sums, the precipitation amount of April (–14 mm/100 years) and October (–23.5 mm/100 years) showed statistically proved decreasing tendency. Variability is increasing significantly in September. These tendencies are unfavorable for the agricultural cultivation of the region.

Key-words: climate change, Keszthely, Hungary, precipitation, linear and exponential trend, box-plot

1. Introduction

Climate change is one of those serious problems that mankind should face in the 21st century. According to the last *IPCC* report (2013), 95% is the probability that human influence has been dominant on the present changes of climate system. This phenomenon will probably affect all parts of the Earth, and in the heart of Europe, the Carpathian-Basin will be affected too. This region is one of the most vulnerable and less understood areas in Europe. In some cases, the volume and direction of the changes in climate model simulations are not definite. Beside model predictions, it is interesting to search analogies of projected climate during the history of the Earth for better understanding of the processes. *Prista et al.* (2015) worked out chronostratigraphic analogies for IPCC scenarios, and stated that Pliocene (Mid Piacenzian Warm Period) is the best analogue for warming climate in Europe.

Precipitation in average over mid-latitude land areas of the Northern Hemisphere has increased from 1901 (medium confidence) according to *IPCC* AR5 (2013). Heavy precipitation events and increase in intensity and frequency is very likely (90% probability) over mid-latitude land masses (*IPCC*, 2013). This phenomenon can change run-off to lakes that is an income parameter for water budget. *Olichwer* and *Tarka* (2015) investigated water run-off changes in Poland due to climate change, and proved that there were no significant changes in total run-off (but there was reduction in groundwater run-off), and reduction in groundwater run-off in favor of increased surface run-off can be expected. Changing water cycle can strongly affect water balance of vulnerable areas, such as Lake Balaton in Hungary.

The prediction of the effects of climate change on the Carpathian Basin (Hungary) requires regional climate scenarios with adequate temporal and spatial resolution, capable of translating global phenomena to local scale. *Bartholy et al*. (2004) developed a stochastic-dynamic downscaling model to estimate the regional effects of climate change in the Lake Balaton–Sió Canal catchments' area, using ECHAM/GCM outputs. This catchments' area (which also includes Keszthely) is one of the most vulnerable regions in Hungary in terms of climate change. According to *Bartholy et al.* (2005), the amount of precipitation will decline by 25–35% in the summer half-year and by 0–10% in the winter half-year on the Lake Balaton-Sió Canal catchments' area.

The regional model runs for Carpathian Basin (RCMs) using the A2 and B2 global emission scenarios of the *IPCC* AR4 (2007) expect more than 2.5 and less than 4.8 °C temperature rise for all seasons and both scenarios (*Bartholy et al*., 2007). A 20–33% decrease in precipitation is predicted for the summer half-year, and there is high uncertainty for the rainfall for the winter half-year (*Bartholy et al*., 2007). The earlier results of the authors harmonizes with their latest projection carried out in PRUDENCE European Project's model application (*Bartholy et al.,* 2009). These statements were enhanced by *Bartholy*

et al. (2008) and by the *Hungarian Meteorological Service* (2010) according to further regional climate model simulations. According to the results of ENSEMBLES project, increasing tendency of the precipitation can be projected in winter and autumn, but strong decrease can be expected in summer, while the annual sum will not change significantly (*Pongrácz et al.,* 2011). *Kiss et al.* (2014) enhances these future tendencies, that climate circumstances will be drier is summer and wetter in winter. *Pongrácz et al.* (2014) project significant increase in drought-related indices in summer by the end of the 21st century. *Bartholy et al.* (2015) analyzed precipitation indices and project that frequency of extreme precipitation will increase in Central Europe, except of summer, when decreasing tendency is very likely.

The annual precipitation amount decreased by 11% between 1901 and 2004, according to the analysis of the Hungarian Meteorological Service (*Szalai et al.,* 2005). The biggest decline could be experienced in spring; it was 25% in the same period. *Bodri* (2004) suggested slow decrease of precipitation with a noticeable increase in precipitation variability for the 20th century. While the northern and western parts of Europe get more precipitation in parallel with the warming tendency, Hungary, similarly to the region of the Mediterranean Sea, gets less rainfall. The water balance has deficit, the difference between water income and outflow is increasing. Between 1901 and 2009, the highest precipitation decline over the territory of Hungary occurred in the spring, nearly 20% (*Lakatos* and *Bihari,* 2011). *Bartholy* and *Pongrácz* (2007, 2010) examined several precipitation extreme indices and their researches suggested that regional intensity and frequency of extreme precipitation increased in the Carpathian Basin in the second half of the last century, while the total precipitation decreased. The largest extremes for precipitation (monthly precipitation anomalies) tend to occur in summer (*Bartholy* and *Pongrácz,* 2005).

The goal of this study was to analyze the long-term data series of the meteorological measurements of precipitation amount at Keszthely (Trans-Danubia, Hungary, N 46°44', E 17°14', *Fig. 1*) from the point of view of climate and statistics. Keszthely is situated in the Lake Balaton catchments' area sheltered by hills from the north, and its climate is affected also by the lake. It is situated next to the inflow point of Zala stream, at north-western part of the shore. The Zala stream's sub-basin is the largest between the six sub-basins of the catchment area of Lake Balaton.

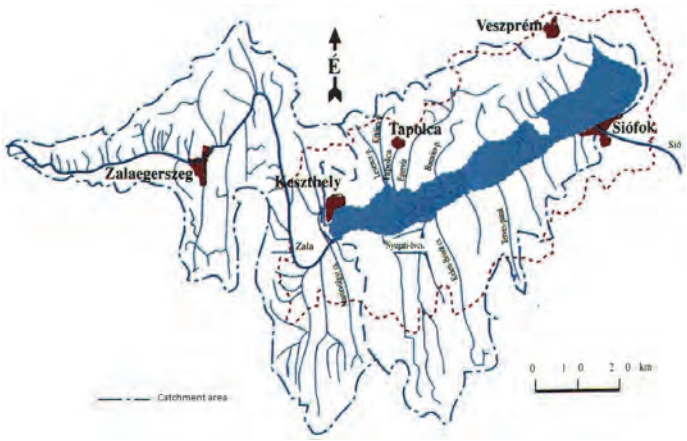

Fig. 1. Catchment area of Lake Balaton (source: website of the Hungarian Water Inspectorate, *https://www.vizugy.hu/index.php?module=content&programelemid=42*)

Our goal is to improve the knowledge about the changes in precipitation of Keszthely by expanding the data-set to 2014. *Lakatos* and *Bihari* (2011) detected higher decrease in precipitation sums in the Transdanubian Region than overall Hungary. Keszthely is situated in the center of this region, but precipitation changes cannot be proven clearly, and they are in contradiction to the regional tendencies. Other aim of this study is to highlight the application of some statistical methods in decision-making between the functions describing the tendencies of time series. Local analysis is presented in the paper, and beside the statistical methodological aspects, it highlights the phenomena that, probably in cause of microclimatic conditions, there can be areas that do not show the tendencies of the wider region.

2. Data and methods

Monthly amounts of precipitation were analyzed from 1871 to 2014 measured at first in the territory of the ancient Georgikon Academy of Agriculture at Keszthely, then at the meteorological station of the Hungarian Meteorological Service. The dataset was provided by the Department of Meteorology and Water Management of University of Pannonia Georgikon Faculty (Keszthely). This dataset is special because few stations in Hungary have continuous measurements of more than 140 years with detailed historical background (*Kocsis* and *Anda,* 2006). Data set was analyzed in three sessions: annual amounts, seasonal amounts, and monthly precipitation. Seasons were performed as common in meteorology, e.g., spring: March, April, May.

Trend analysis of time series from single point observations has often been used to define local climate trends (*Boyles* and *Raman,* 2003). During the

procession, the data set was analyzed by linear trend analysis and with running averages, which are widespread at the analysis of time series. 10 member-running averages ($k = 10$) were used based on computation of climate normal.

Simple statistical methods, such as linear trend, are useful for investigating changes in climatic patters. Slopes of the linear fits to the time series of climatic data provide a simple picture of changes that occurred in the examined period (*Boyles* and *Raman,* 2003). It is well known, that for simplification usually the tendencies in weather elements' time series are described by linear trend, but in reality the tendency is rarely linear. Estimation of the parameters of linear trend was according to the following equitations:

$$\hat{y}_t = b_0 + b_1 t \qquad t = 1, 2, \ldots, 144, \tag{1}$$

$$b_1 = \frac{\overline{t \cdot y} - \bar{t} \cdot \bar{y}}{\overline{t^2} - \bar{t}^2}, \tag{2}$$

$$b_0 = \bar{y} - b_1 \cdot \bar{t}, \tag{3}$$

where

$\hat{y}_t$ is the value estimated by the trend function at t period,
t is the code of time period,
b_0 is the value estimated by the trend function at $t = 0$,
b_1 is the slope of the linear, interpreted as absolute change in the phenomena over a time period unit,
$\bar{y}$ is the mean of the data set and
$\bar{t}$ is the mean of time codes.

Lakatos and *Bihari* (2011) stated that precipitation changes are shown better by exponential trend in % than by linear trend in mm. Exponential trend was also used to describe the tendencies in case of the annual and seasonal time series. Estimation of the parameters of exponential trend was according to the following equitations:

$$\hat{y}_t = b_0 \cdot b_1^t \qquad t = 1, 2, \ldots, 144, \tag{4}$$

$$\log b_1 = \frac{\overline{t \cdot \log y} - \bar{t} \cdot \overline{\log y}}{\overline{t^2} - \bar{t}^2}, \tag{5}$$

$$\log b_0 = \overline{\log y} - \log b_1 \cdot \bar{t}, \tag{6}$$

where

$\hat{y}_t$ is the value estimated by the trend function at t period,

t is the code of time period,

b_0 is the value estimated by the trend function at $t = 0$ period,

b_1 refers to the relative change in the phenomena over a time period unit (b_1-1 given in percent shows the relative change per time unit),

$\overline{\log y}$ is the mean of the logarithm of the dataset's values, and

$\bar{t}$ is the mean of time codes.

Sum of square error (SSE) was determined to decide which type of function is fitting the data set better:

$$SSE = \sum_{t=1}^{n} (y_t - \hat{y}_t)^2 , \tag{7}$$

where

t is code of the time period (t=1,2,3,…,144),

y_t is data of the time series at t period,

$\hat{y}_t$ is data of the time series at t period estimated by trend function.

Mean square deviation between real data and trend data is presented as relative standard error (V_e) of the trend function in percent:

$$V_e = \frac{\sqrt{\frac{SSE}{n}}}{\bar{y}_t} , \tag{8}$$

where $\bar{y}_t$ is the mean of the time series' dataset.

In case of linear trend, 5% of significance level was used to determine the significancy of the slope (b_1) by two tailed t-test. In every case the better fitting function was explained.

The mean values and the dispersion and distribution attributes were also determined. The following ones from the simplest climatic and statistical attributes were applied (*Péczely,* 1998): average, median, standard deviation, maximum and minimum values, upper and lower quartiles, and 5% and 95% percentiles. Distribution of the data is performed by box plot diagrams made by SPSS Statistics.

Climate fluctuation can have two interpretations: one of them is the difference between the certain value and the average of the data series (in an absolute value), the other one is the difference between the values following each other (*Varga-Haszonits,* 2003). Tendency in absolute deviation of the annual data from the mean of the dataset was used to describe changes in the variability.

3. Results

3.1. Annual data

The average of the dataset of the annual precipitation amount is 673 mm which at is a mean value for Hungary. Standard deviation is 138 mm. 25% of the data are higher than 772 mm, and 75% are higher than 580 mm. The lowest amounts (5% percentile is 456 mm) are of the years 2011, 2000, 1971, 1968, 1911, 1898, and 1967, in increasing order. The highest 5% are 1879, 2010, 1905, 1915, 1965, 1940, and 1937, in increasing order (95% percentile is 908 mm). The median is 654 mm, and dominancy of those data that are lower than the mean can be experienced. *Fig. 2* shows the box plot of annual data. Distribution shows slight asymmetry toward lower amounts.

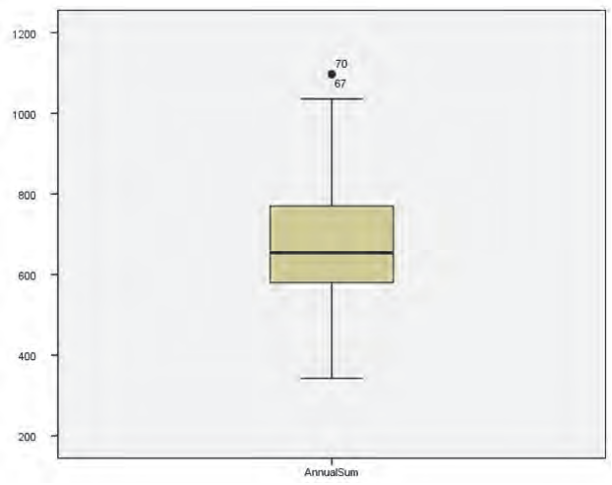

Fig. 2. Box plot of annual precipitation data of Keszthely (1871–2014)

(Lower line of the box is the lower quartile (25%), upper line of the box is the upper quartile (75%), the line in the box is the median (50%), upper end of the range is the maximum, and lower end is the minimum according to the box-plot algorithm. Values singed with dots over the range are time codes of outlier data that are more than 1.5 box lengths /interquartile range/ far from the hinge of the box.)

In the course of the analysis of the data series it can be concluded, that in the case of the annual amount of precipitation, neither significant linear decreasing tendency (*Fig. 3*) nor modification in the variability of the annual data (*Fig. 4*) can be shown. The linear trend gave a non-significant decreasing result (linear trend equitation is $\hat{y}_t = 709.2 + 0.4948t$), so the tendency was described also by running averages ($k = 10$). The declining tendency can be seen

in *Fig. 3*. Modification of the variability should be expected as an effect of climate change, numbers of extreme values should be enhanced, but the variability of the data did not change.

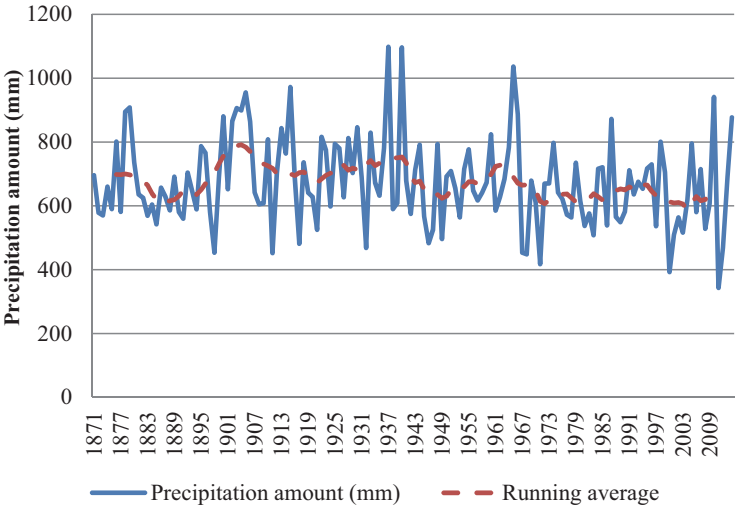

Fig. 3. Tendencies of annual precipitation sum at Keszthely (1871–2014) with running average.

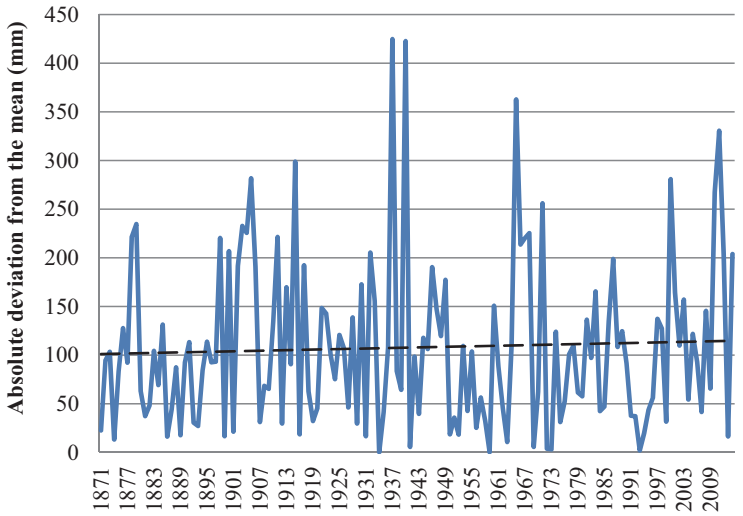

Fig. 4. Absolute deviation of the annual data from the mean precipitation and its linear tendency (linear trend equitation is $\hat{y}_t = 101.09 + 0.0949t$)

Szalai (2011) showed significant linear declining tendency of the annual precipitation amount in Hungary between 1901 and 2008. The annual rainfall sum decreased by 7% in this period. The declining tendency of the precipitation was enhanced in the Transdanubian Region (*Szalai,* 2011) where Keszthely station is situated, but no decreasing tendency could be found in the dataset of Keszthely.

Exponential trend was also determined (exponential trend equation is $\hat{y}_t = 699.86 * 0.99992^t$). It can be concluded that linear trend is fitting better the dataset, because the relative standard error is lower in case of this function. (Relative standard error is 20.18% for linear trend and 20.29% for exponential trend, respectively.) But linear trend is not significant (p-value is 0.0734), so changing tendency can not be described.

To get more information about the tendency of the annual precipitation sums, climate normals were applied (averages determined for 30 years, shifted by 10 years, following the WMO recommendations). Climate normals show that the amount of precipitation decreased in the second half of the 20th century. This tendency stopped in the first decade of the 21st century (*Fig. 5*).

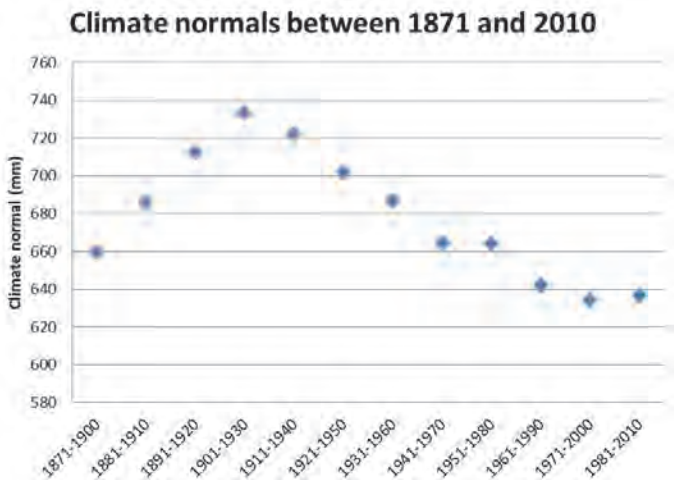

Fig. 5. Declining tendency of the climate normal.

3.2. Seasonal data

Mean precipitation sum in spring was 162 mm between 1871 and 2014. The average is 223 mm in summer, 177 mm in autumn, and 111 mm in winter. *Table 1* presents the descriptive statistics of the seasonal amounts. *Fig. 6* shows

the distribution of the seasonal data by box plot diagrams. In all seasons, those data have dominancy that are lower than the average.

Table 1. Descriptive statistics of the seasonal amounts of precipitation between 1871 and 2014

(mm)	Spring	Summer	Autumn	Winter
Mean	162	223	177	111
Standard deviation	54	77	68	42
Lower quartile	128	166	132	78
Median	153	216	179	110
Upper quartile	195	268	217	138
Range	302	373	367	198
5% percentile	85	104	65	47
95% percentile	268	374	294	187

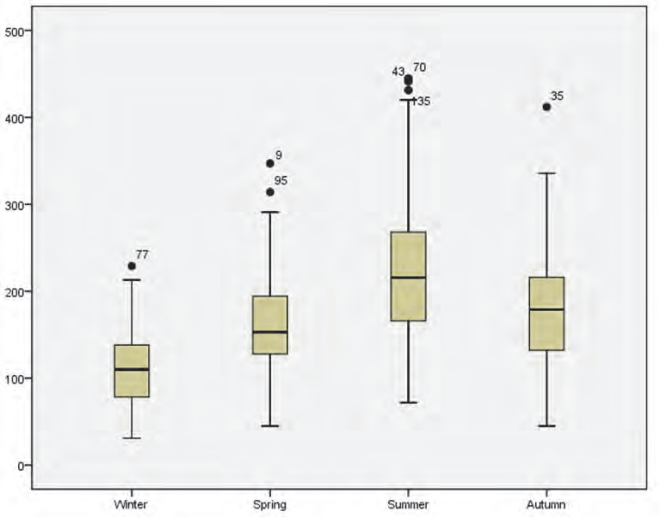

Fig. 6. Box-plots of the seasonal sums of precipitation at Keszthely

Linear and exponential trend was determined to analyze the tendencies of the seasonal sums of precipitation. *Table 2* gives the values of relative standard error of the functions. In all cases, linear trend is fitting the data better. *Table 3* contains the slopes of the linear tendencies of the seasons. The only significant

change can be found in case of spring precipitation sum. The decreasing tendency is significant at the 5% significance level, and it shows 31.5 mm decline in the precipitation sum in 100 years. Previous researches showed 35 mm significant decrease in 100 years between 1871 and 2000 (*Kocsis,* 2008). This tendency is not favorable for agricultural cultivation, especially for spring crops. No significant changes can be detected in the variability of seasonal amounts.

Table 2. Relative standard errors of linear and exponential trends

Relative standard error	**Spring**	**Summer**	**Autumn**	**Winter**
Linear trend	32.54%	34.54%	37.87%	37.10%
Exponential trend	33.00%	35.06%	38.69%	37.89%

Table 3. The slope of the linear tendency and empirical significance level (p-value) of the seasonal data series. * indicates significant modification at the 5% probability level

	Spring	**Summer**	**Autumn**	**Winter**
Slope (b1) of linear trend	**–0.315**	–0.075	–0.241	0.136
Empirical significance level of the slope (b_1)	**0.4%***	63.0%	7.8%	10.5%

3.3. Monthly data

The mean values of the monthly precipitations sums are shown in *Fig. 7.* In Hungary, the annual evaluation of the monthly precipitation has a minimum in February and a main maximum in June, and a secondary maximum in October. This secondary maximum in the autumn seems to disappear. It is not completely clear that it would be the disappearance of the secondary maximum or a shift in it, but according the averages of the 144-year-long data set, the monthly amounts of precipitation in the fall are nearly the same. The continuous measurements of the further decades will probably answer this question. *Fig. 8* shows the distribution of the monthly data by box plot analyses.

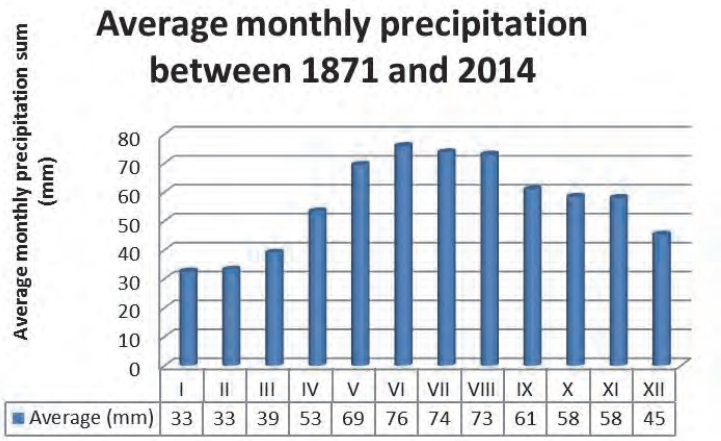

Figure 7. Monthly precipitation sums (1871–2014)

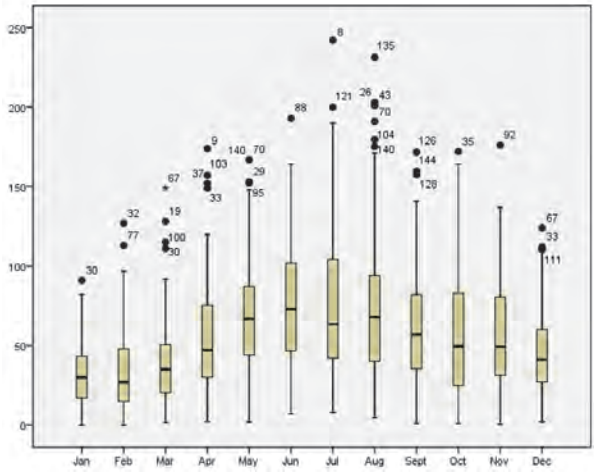

Fig. 8. Box-plot of monthly datasets by SPSS.

The amount of precipitation in April and October show a significant decrease between 1871 and 2014 (–14 mm/100 years and 23.5 mm/100 years, respectively), but any other monthly sum does not show significant modification (*Table 4*). In every month, the linear function has lower relative standard error than the exponential trend, so linear trend is fitting the data better. This result enhances the previous researches: between 1871 and 2000, the decreasing tendency was –25.1 mm in 100 years in October (*Kocsis,* 2008). The new

finding is that the extended dataset shows significant decrease also in April. This phenomenon might be unfavorable for the agricultural cultivation, because the fall of the precipitation sum could have a critical effect on the germination of the crops.

Table 4. The slope of the linear trend and empirical significance level (p-value) of the monthly data series (*indicates significant modification at the 5% probability level) and standard errors of the linear and exponential trends, respectively (For January and February data, exponential trend cannot be fitted)

Month	Slope (LIN)	p-value (%)	V_e LIN (%)	V_e EXP (%)
I	0.03	44.4	60.93	None
II	0.06	24.2	72.59	None
III	–0.06	26.1	64.00	67.12
IV	**–0.14**	**3.1***	59.83	62.71
V	–0.12	8.9	49.03	51.00
VI	0.01	90.1	48.47	50.52
VII	–0.05	54.1	59.82	62.27
VIII	–0.03	74.4	61.22	64.36
IX	–0.02	79.3	57.99	61.26
X	**–0.24**	**0.3***	66.54	71.66
XI	0.01	85.0	59.81	62.96
XII	0.05	35.9	56.75	59.55

The monthly analysis of variability gives the evidence that changes can be statistically determined in the absolute deviation of the monthly average values only in September (*Table 5*). Previously, in any cases of monthly variability changes cannot be detected (*Kocsis,* 2008). Between 1871 and 2014, significant increasing variability, can be reported in September. Suspected increase in variability due to the rise of the frequency of extreme weather events cannot be proved clearly.

Table 5. The slope of the linear trend of variability and empirical significance level (p-value) of the monthly data series (*indicates significant modification at the 5% probability level)

Month	Variability (slope LIN)	Variability (p-value) (%)
I	0.01	69.8
II	0.03	35.1
III	–0.01	87.6
IV	–0.04	28.9
V	–0.02	58.1
VI	0.04	34.4
VII	–0.04	48.2
VIII	0.09	10.2
IX	**0.09**	**3.8***
X	–0.07	13.5
XI	–0.01	70.8
XII	–0.03	37.1

4. Discussion and conclusions

Our previous and latest results are summarized in *Table 6*, and it can be stated that new analysis enhanced the previous findings. Significant decreasing tendency can be experienced in spring, which is parallel with the findings of *Szalai et al.* (2005) and *Lakatos* and *Bihari* (2011), that highest precipitation decrease occurred in the spring in Hungary. The new result in case of Keszthely is that significant decreasing tendency can be detected also in April, and the variability is significantly increasing in September. Changing tendencies of the meteorological element are rarely linear, but linear trend is the most commonly used method to describe them. Climate normal was used also and showed declining tendency in annual precipitation during the 20th century.

Table 6. Summary of the results and previous findings

	Significant tendency in 100 years		
	1871–2000 (*Kocsis,* 2008)	1871–2010 (*Kocsis,* 2015)	1871–2014
Changes in annual sum	none	none	none
Changes in seasonal sums	Spring (–35 mm)	Spring (–29 mm)	Spring (–31.5 mm)
Changes in monthly sums	October (–26 mm)	October (–25 mm)	April (–14 mm) and October (–23.5 mm)
Changes in variability	none	none	September (+)

To describe the tendencies in time series, several types of trends can be used, but linear and exponential ones are easily interpretable. In case of linear trend it is easier to decide about significance than in case of exponential one. *Lakatos* and *Bihari* (2011) communicated that changes shown in percent (exponential trend) are more suitable to interpret average changes per time unit in the tendencies of precipitation sums than interpret in mm (linear trend). But no mention can be found about the standard error of the approaches that can prove the decision in favor to exponential trend interpretation. Mathematically it should be more correct to compute the standard errors of the linear and exponential trends, respectively, and interpret the function that has lower error. In this work, relative standard error was counted in all cases, and it can be concluded that linear trend fitted the data sets better, and it had lower error than exponential trends.

References

Barhtoly, J. and *Pongrácz, R.,* 2005: Extremes of ground-based and satellite measurements in the vegetation period for the Carpathian Basin. *Phys. Chem. Earth 30*, 81–89.

Barhtoly, J. and *Pongrácz, R.,* 2007: Regional analysis of extreme temperature and precipitation indices for the Carpathian Basin from 1946 to 2001. *Glob. Planet. Change 57*, 83–95.

Bartholy, J., Mika, J., Pongrácz, R., and *Schlanger, V.,* 2005: Climatic specialties of global warming in the Carpathian Basin. In: (Ed.: *Takács-Sánta, A*.) Éghajlatváltozás a világban és Magyarországon, Budapest, 105–139. (in Hungarian)

Bartholy, J. and *Pongrácz, R.,* 2010: Analysis of precipitation conditions for the Carpathian Basin based on extreme indices in the 20th century and climate simulation for 2050 and 2100. *Phys. Chem. Earth 35*, 43–51.

Bartholy, J., Pongrácz, R., and *Gelybó, Gy.,* 2007: Regional climate change in Hungary for 2071-2100. *Appl. Ecol. Environ. Rese 5*, 1–17.

Bartholy, J., Pongrácz, R., Gelybó, Gy., and *Szabó, P.,* 2008: Analysis of expected climate change in the Carpathian Basin using the PRUDENCE results. *Időjárás 112*, 249–264.

Bartholy, J., Pongrácz, R., Gelybó, Gy., and *Szabó, P.* 2009: Analysis of expected climate change in the Carpathian Basin using the PRUDENCE results. *Időjárás 112,* 249–265.

Bartholy, J., Pongrácz, R., and *Kiss, A.* 2015: Projected changes of extreme precipitation using multi-model approach. *Időjárás 119,* 129–142.

Bartholy, J., Pongrácz, R., Matyasovszky, I., and *Schlanger, V.,* 2004: A XX. században bekövetkezett és a XXI. századra várható éghajlati tendenciák Magyarország területére. *AGRO-21 Füzetek 33*: 3–18. (in Hungarian)

Bodri, L. 2004: Tendencies in variability of gridded temperature and precipitation in Hungary (during the period of instrumental record). *Időjárás 108,* 141–153.

Boyles, R.P. and *Raman, S.,* 2003: Analysis of climate trends in North Carolina (1949–1998). *Environ. Internat. 29*, 263–275.

Hungarian Meteorological Service, 2010: Klímamodellezési tevékenység – Eredmények (2010). (in Hungarian)

IPCC, 2007: Summary for Poicymakers. In (Eds: *Solomon, S., D. Qin, M. Manning, Z. Chen, M. Marquis, K.B. Averyt, M.Tignor and H.L. Miller*) Climate Change 2007: The Physical Science Basis. Contribution of Working Group I to the Fourth Assessment Report of the Intergovernmental Panel on Climate Change. Cambridge University Press, Cambridge, United Kingdom and New York, NY, USA, www.ipcc.ch: 5, 7.

IPCC, 2013: Summary for Policymakers. In: (Eds.: *Stocker, T.F., D. Qin, G.-K. Plattner, M. Tignor, S.K. Allen, J. Boschung, A. Nauels, Y. Xia, V. Bex* and *P.M. Midgley*) Climate Change 2013: The Physical Science Basis. Contribution of Working Group I to the Fifth Assessment Report of the Intergovernmental Panel on Climate Change. Cambridge University Press, Cambridge, United Kingdom and New York, NY, USA.

Kiss, A., Pongrácz, R., and *Bartholy, J.* 2014 Magyarországra becsült csapadéktrendek: hibakorrekció alkalmazásának hatása. *Légkör 59,* 117–120. (in Hungarian)

Kocsis, T., 2008: Az éghajlatváltozás detektálása és hatásainak modellezése Keszthelyen. PhD Thesis (in Hungarian)

Kocsis, T., 2015: Climate-statistical analyses of precipitation sums at Keszthely between 1871 and 2010. 10th Hungarian Congress of Ecologists, Veszprém, Hungary

Kocsis, T. and *Anda, A.,* 2006: A keszthelyi meteorológiai megfigyelések története. Published by University of Pannonia Georgikon Faculty, Keszthely. (in Hungarian)

Lakatos, M. and *Bihari, Z.*, 2011: Temperature- and precipitation tendencies observed in the recent past. In (Eds: *Bartholy, J., Bozó, L., Haszpra, L.*) Klímaváltozás-2011: 159–169. (in Hungarian)

Olichwer, T. and *Tarka, R.,* 2015: Impact of climate change on the groundwater run-off in south-west Poland. *Open Geosci. 7,* 1–14.

Péczely, Gy. 1998: Éghajlattan. Nemzeti Tankönyvkiadó Rt., Budapest. (in Hungarian)

Pongrácz, R., Bartholy, J., and *Miklós, E.,* 2011: Analysis of projected climate change for Hungary using ENSEMBLES simulations. *Appl. Ecol. Environ. Res. 9,* 387–398.

Pongrácz, R., Bartholy, J., and *Kiss, A.* 2014: Estimation of future precipitation conditions for Hungary with special focus on dry periods. *Időjárás 118,* 305–321.

Prista, G.O., Agostinho, R.J., and *Cachao, M.,A.,* 2015: Observing the past to better understand the future: a synthesis of the Neogene climate in Europe and its perspectives on present climate change. *Open Geosci. 7*, 65–83.

Szalai, S. 2011: Magyarország hidroklimatológiai jellemzése. *KLÍMA-21 Füzetek 65*: 17-28. (in Hungarian)

Szalai, S., Bihari, Z, Lakatos, M., and *Szentimrey, T.,* 2005: Magyarország éghajlatának néhány jellemzője 1901-től napjainkig. Hungarian Meteorological Service (in Hungarian)

Varga-Haszonits, Z. 2003: Az éghajlatváltozás mezőgazdasági hatásának elemzése, éghajlati scenáriók. *AGRO-21 Füzetek 31*: 9.-28. (in Hungarian)

Website of the Hungarian Water Inspectorate, https://www.vizugy.hu/index.php?module=content&programelemid=42 (01.07.2016.)

IDŐJÁRÁS

Quarterly Journal of the Hungarian Meteorological Service
Vol. 121, No. 1, January – March, 2017, pp. 79–99

Tourism climatic conditions of Hungary – present situation and assessment of future changes

Attila Kovács[1*], **Ákos Németh**[2], **János Unger**[1] and **Noémi Kántor**[1]

[1]*Department of Climatology and Landscape Ecology, University of Szeged, 2 Egyetem str., H-6722 Szeged, Hungary*

[2]*Hungarian Meteorological Service, P.O. Box 38, H-1525 Budapest, Hungary*

[*]*Corresponding author E-mail: kovacsattila@geo.u-szeged.hu*

(Manuscript received in final form September 13, 2016)

Abstract—This paper provides insight into the tourism-related outcomes of the Hungarian CRIGiS project, which was conducted in 2015. Based on tourism climatic indicators, this study aims at assessing the exposure of tourism sector to climate change. The widely known Tourism Climatic Index (*TCI*) is applied for the quantification of the climatic potential in Hungary in its original and modified form. This adjusted index version is suitable to reflect the seasonally different thermal perception patterns of Hungarian residents. These indicators were calculated based on past observations, and on the other hand, they rely on the outputs of regional climate model projections. The spatial distribution of the index values in Hungary is presented on a monthly basis and on district level, which is an administrative territorial unit in Hungary. The results indicate that, according to both versions of *TCI*, tourism climate conditions will likely to improve in the shoulder seasons and deteriorate in summer, remaining still at least acceptable for outdoor tourism purposes. The project outcomes are available for public use in the National Adaptation Geo-information System (NAGiS) developed in Hungary.

Key-words: climate change, tourism climatic potential, Tourism Climatic Index, spatial pattern, subjective thermal perception, districts of Hungary

1. Introduction

Climate constitutes an essential natural resource for tourism industry – it can promote or constrain certain tourist activities and tourism development (*de Freitas,* 2003; *Gómez Martín,* 2005; *Scott* and *Lemieux,* 2010; *Scott et al.,* 2012). Climate is an important driver of tourist motivation (*Crompton,* 1979; *Morgan et al.,* 2000; *Kozak,* 2002; *Hübner* and *Gössling,* 2012) as well as of destination choice and other decision-making mechanisms, either before trip or under holiday (*Hamilton* and *Lau,* 2005; *Gössling et al.,* 2006; *Scott et al.,* 2008, 2012; *Moreno,* 2010; *Scott* and *Lemieux,* 2010). In addition, climate has a significant impact on overall attractiveness of a target area (*Hu* and *Ritchie,* 1993; *Kozak,* 2002; *Moreno,* 2010). Tourism industry and destination products are highly sensitive to climate variability and climate change. The impacts of climate change are expected to vary geographically and seasonally (*IPCC,* 2014).

Climate change will directly affect tourism sector by altering the temporal and spatial distribution of climate resources for tourism, and thus, the main domestic and international tourism flows and expenditures (*Scott et al.,* 2004, 2012; *Rutty* and *Scott,* 2014). Climatic resources – considering their global level distributions – are projected to shift towards higher latitudes. Namely, northern parts (of Europe and America) are expected to improve of climate conditions, while southern regions (Mediterranean and Caribbean) are likely to become 'too hot' in summer. On the other hand, spring and autumn months will likely to improve in the latter case. As a result, northern European tourists might stay in their home country or neighboring areas in summer due to climate change. These features were emphasized or concluded by many research studies in the field of tourism climatology (*Morgan et al.,* 2000; *Scott* and *McBoyle,* 2001; *Scott et al.,* 2004; *Hamilton et al.,* 2005; *Amelung* and *Viner,* 2006; *Amelung et al.,* 2007; *Nicholls* and *Amelung,* 2008; *Hein et al.,* 2009; *Perch-Nielsen et al.,* 2010; *Amengual et al.,* 2012; *Amelung* and *Moreno,* 2012). However, some studies have questioned these results, because they have not considered what tourists perceive to be thermally unacceptable for their activities.

According to *Rutty* and *Scott* (2010), it is unlikely that the above mentioned southern regions will become 'too hot' for coastal tourism for the next decades. They concluded this assertion according to a survey of university students conducted in northern Europe, which examined their climate preferences for beach and urban tourism concerning the Mediterranean region. *Moreno* and *Amelung* (2009) similarly concluded that relatively modest shifts in climatic attractiveness will likely to be found over the coming 50 years, and the Mediterranean region is likely to remain Europe's prime region for summer vacation. They used the Beach Climate Index of *Morgan et al.* (2000), which was developed by using interviews with tourists. Using questionnaires with northern travellers, *Moreno* (2010) found that large majority of tourists would

still travel to the Mediterranean even if ideal coastal weather conditions were occur in their home country as a result of climate change.

These are only three examples, which question the main research opinion – i.e., the tourist activities may decrease in the Mediterranean because of the projected warming tendencies –, subjective reactions of people actually may not follow the projected trends concluded from purely objective investigations. In fact, direct consultation with travellers on their climate assessments (perception, preferences, and tolerances) is more important than ever, as emphasized by a large number of studies (e.g., *Gómez Martín,* 2005, 2006; *de Freitas et al.,* 2008; *Scott et al.,* 2008; *Gössling et al.,* 2012). These investigations, with focusing on human assessments, allow us on the one hand to explore tourists perception and preferences of weather parameters, to define the 'ideal' or 'unfavorable' climatic conditions and to determine the perceived importance of different climate parameters, or even to explore the role and importance of climate (or climate change) as a destination attribute. On the other hand, several studies analyse tourism climate potential of destination areas with climate evaluation tools (indices, rating systems). Travellers' assessment patterns should be incorporated into these tools.

Understanding the way climate change affects tourism industry and the subjective assessments and behavioral reactions of tourists remains limited. Effectiveness of adaptation to climate change and adaptive capacity of tourists remain largely unexplored as well (*Scott et al.,* 2009, 2012; *Gössling et al.,* 2012). By identifying the quantitative impacts of climatic conditions and climate change on tourism, we can facilitate the development of objective strategies, decision-making processes, and planning for climate change adaptation. Several tourism climatological evaluation tools have been developed to quantify the climate potential and climate change impacts on tourism sector; however, they are most regardless of local residents' or tourists' climatic assessments. It is widely accepted in the field of tourism (bio)climatology that the tourism climate evaluation tools should be adjusted to the local residents' or tourists' subjective assessments (*de Freitas,* 2003; *Scott et al.,* 2004, 2008; *de Freitas et al.,* 2008). To prepare targeted and sustainable adaptation strategies in response to climate change, it is indispensable to reveal climate potential with empirically tested approaches.

This study provides insight into the results related to tourism climate potential of the project '*Vulnerability/impact studies with a focus on tourism and critical infrastructures*' (*CRIGiS,* 2016). This project was conducted in 2015, with the main aim to develop methodologies that could be used to objectively quantify the effects of climate change in exposure, vulnerability, and adaptation capacity for various sectors in Hungary. In the frame of the project, the exposure of the tourism sector to the climate change was quantified. For this purpose, we applied the widely used Tourism Climatic Index in its original form (*TCI*; *Mieczkowski,* 1985) and in its modified form that is adjusted to the Hungarians'

subjective thermal assessments (*mTCI*; *Kovács et al.,* 2016), as well as the recently developed so-called second generation tourism climatic index – Climate Index for Tourism (*CIT*; *de Freitas et al.,* 2008). In this paper, we present some outcomes on the basis of *TCI* and *mTCI* patterns.

2. Methods

2.1. Tourism Climatic Index

TCI is a widely used measure that evaluates the suitability of a particular climate for general outdoor tourism activities like sightseeing and shopping or other light physical activities (e.g., *Mieczkowski,* 1985; *Scott et al.,* 2004; *Amelung* and *Viner,* 2006; *Amelung et al.,* 2007; *Farajzadeh* and *Matzarakis,* 2009; *Hein et al.,* 2009; *Perch Nielsen et al.,* 2010; *Amelung* and *Moreno,* 2012; *Amelung* and *Nicholls,* 2014; *Roshan et al.,* 2016).

In Hungary, *TCI* has been used only by a few studies so far. *Németh* (2013) quantified climate potential for Lake Balaton Region for the climate normal periods 1961–1990, 1971– 2000, and 1981–2010. *Kovács et al.* (2015) analyzed the annul course of *TCI* for Budapest (the capital of Hungary) and Siófok (the main resort on the shore of Lake Balaton) for the period 1996–2010. *Hódos* (2014) presented first time the spatial distribution of *TCI* in the region of Hungary. She determined *TCI* per month for the Carpathian Region (44–50°N and 17–27°E) for the normal periods 1961–1990, 1971–2000, 1981–2010, and 2001–2010. The changes between the periods 1981–2010 and 1961–1990 were also analyzed. The study region covered the target area of the CarpatClim project, which final outcome was a 0.1° spatial resolution, quality controlled, homogenized, cross border harmonized, and gridded dataset on daily scale for several basic meteorological variables and derived climate indicators from 1961 to 2010 (*Szalai et al.,* 2013). For homogenization the MASH (Multiple Analysis of Series for Homogenization; *Szentimrey,* 2011), for interpolation the MISH (Meteorological Interpolation based on Surface Homogenized data basis; *Szentimrey* and *Bihari,* 2007) procedure were applied; both of them were developed at the Hungarian Meteorological Service.

The original form of the *TCI* consists of five sub-indices, which in turn are based on monthly values of seven basic climate parameters (*Table 1*). From the seven basic parameters, three ones – monthly precipitation sum, daily sunshine duration, and daily mean wind speed – are rated in itself with different score values, from zero (unfavorable) to five (optimal), forming sub-indices *R*, *S,* and *W*, respectively (*Table 1*, *Fig. 1*). In the case of *R*, the rating system is monotonically decreasing with the increase of precipitation sum (*Fig. 1a*), while the score values of *S* ascend monotonically as the number of sunshine hours increases (*Fig. 1b*). In the case of *W*, four distinct rating systems were introduced by *Mieczkowski* (1985) depending on specific air temperature ranges (*Fig. 1c*).

Table 1 The sub-indices of Tourism Climatic Index, their rating score ranges, and their weights (based on *Mieczkowski,* 1985)

Monthly values of basic climate parameters		***TCI* sub-indices**	**Scores**	**Weight**
daily maximum temperature (°C)	daytime effective temperature (°C)	*CId* – daytime comfort index	–3 to +5	40%
daily minimum relative humidity (%)				
daily mean temperature (°C)	daily effective temperature (°C)	*CIa* – daily comfort index	–3 to +5	10%
daily mean relative humidity (%)				
monthly precipitation sum (mm)		*R* – precipitation index	0 to +5	20%
daily sunshine duration (hour)		*S* – sunshine duration index	0 to +5	20%
daily mean wind speed (km/h)		*W* – wind speed index	0 to +5	10%

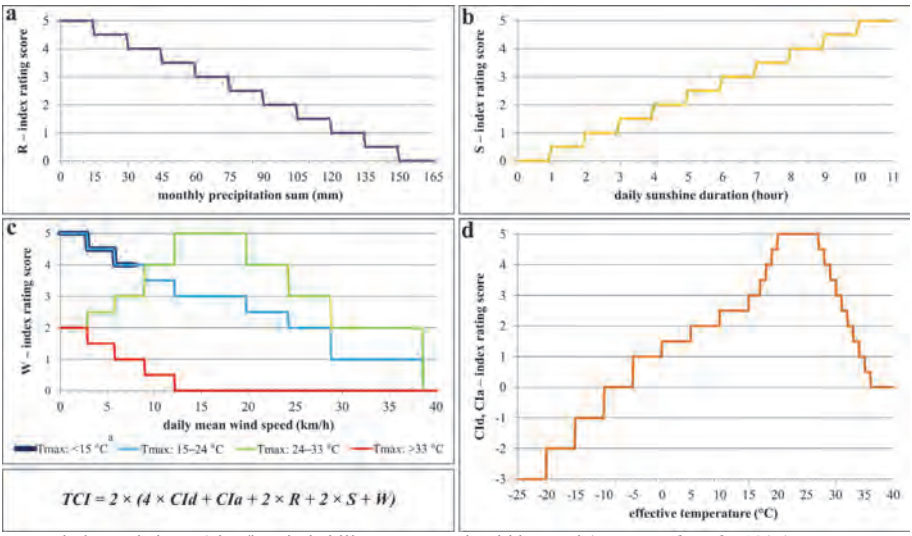

[a] For wind speed above 8 km/h, wind chill nomogram should be used (see *Mieczkowski,* 1985)

Fig. 1. Rating score systems for each sub-index in the Tourism Climatic Index (based on the rating systems of *Mieczkowski,* 1985).

The remaining two sub-indices of *TCI* were designated to describe the thermal comfort conditions – one of them refers to the whole day (*CIa* – daily comfort index), while the other characterizes the thermal conditions at the warmest period of the day (*CId* – daytime comfort index). Correspondingly, *CIa* is derived from the daily mean values of air temperature and relative humidity, while *CId* rates the combined effect of the daily maximum air temperature and minimum relative humidity (*Table 1*) (*Mieczkowski,* 1985). In fact, the rating system of *CIa* and *CId* relies on one of the earliest thermal indices, the so-called Effective Temperature (*ET*). *ET* is a simple empirical index, which expresses the combined effect of air temperature and relative humidity on thermal comfort (*Houghten* and *Yaglou,* 1923). *Mieczkowski* (1985) defined the *ET* range of 20–27 °C as optimal zone with a rating score of five; then reduced the points gradually on both sides of the optimal zone according to an arbitrarily assigned set of ordinal values (*Fig. 1d*).

It is worth noting that in contrast to the score values of *R, S,* and *W, Mieczkowski* (1985) assigned minus score points to the lowest *ET* values (i.e., to the coldest environmental conditions) (*Fig. 1*) in the case of *CIa* and *CId*.

Finally, each sub-index is weighted with certain factors that express their relative importance within the overall climate evaluation (*Table 1*). The value of *TCI* is obtained as the weighted sum of the sub-indices (*Mieczkowski,* 1985):

$$TCI = 2(4CId + CIa + 2R + 2S + W). \quad (1)$$

The *TCI* measures the climate's overall suitability for tourism activities on a scale of minus twenty to hundred, with higher values indicating more favorable climate potentials for outdoor activities (*Mieczkowski,* 1985; *Table 2*).

Table 2. Tourism climatic index rating system (*Mieczkowski,* 1985)

***TCI* scores**	**Descriptive categories**
90 – 100	ideal
80 – 89	excellent
70 – 79	very good
60 – 69	good
50 – 59	acceptable
40 – 49	marginal
30 – 39	unfavorable
20 – 29	very unfavorable
10 – 19	extremely unfavorable
–20 – 9	impossible

2.2. *Modified form of Tourism Climatic Index*

Although *TCI* has been the most widely applied tourism climate index over the past 30 years (*Scott et al.,* 2012), a number of limitations have been identified or emphasized by several research studies (e.g., *Scott et al.,* 2004; *Amelung* and *Viner,* 2006; *de Freitas et al.,* 2008; *Farajzadeh* and *Matzarakis,* 2009; *Moreno* and *Amelung,* 2009; *Perch-Nielsen et al.,* 2010; *Kovács* and *Unger,* 2014a). The modified form of *TCI* used in CRIGiS project overcomes two of the major shortcomings of the index.

One of the main limitations of the index is that its thermal components are theoretically unsound according to the recent human thermo-physiological knowledge. In fact, the thermal comfort sub-indices, *CId* and *CIa*, rely on *ET*, which is based on air temperature and humidity data only. However, several biometeorological studies have indicated that the thermophysiological effect of the atmospheric environment on the human body depends on the combination of four climate parameters (air temperature, air humidity, wind velocity, and thermal radiation) and on personal factors, such as clothing and human activity (*Jendritzky,* 1993; *Matzarakis* and *Mayer,* 1996; *Höppe,* 1999; *Mayer,* 2008). Several studies have proposed modification of the *TCI*'s thermal comfort sub-indices (*Scott* and *McBoyle,* 2001; *Scott et al.,* 2004; *Amelung* and *Viner,* 2006; *Perch-Nielsen et al.,* 2010). Instead of using effective temperature, *Kovács et al.* (2016) proposed the integration of the Physiologically Equivalent Temperature (*PET*) into the thermal comfort sub-indices of the *TCI*. The advantage of the biometeorological index *PET* is that it considers the physiological effect of both climate and human factors (*Höppe,* 1999; *Kántor et al.,* 2016a).

The other essential shortcoming of *TCI* is that the rating and weighting schemes of each of its sub-indices are arbitrary – they were defined according to Mieczkowski's personal expert opinion, which was based on former, obsolete (biometeorological) literature. These rating systems had never been tested empirically against the perceptions and preferences of real tourists (*Mieczkowski,* 1985; *Scott et al.,* 2004; *Amelung* and *Viner,* 2006; *de Freitas et al.,* 2008; *Farajzadeh* and *Matzarakis,* 2009; *Moreno* and *Amelung,* 2009; *Perch-Nielsen et al.,* 2010).

Adaptation of some tourist climate evaluation tools has already begun in Hungary. The process focused mainly on the adjustment of the thermal parts of *TCI* by incorporating *PET* (*Kovács* and *Unger,* 2014a, 2014b) and making the score-system suitable to express the subjective thermal assessment patterns of the Hungarian population (*Kovács et al.,* 2016).

From the different aspects of subjective thermal evaluation, in this paper we are focusing on the most evident assessment – the thermal perception (thermal sensation). A new *PET* rating system is developed and integrated into the thermal sub-indices of the *TCI*, which reflect the thermal perception patterns of Hungarian residents. This modification improves the credibility of the

thermal rating scores of *TCI,* and thus, enhances the potential of *TCI* to evaluate the thermal aspect of climate.

In order to reveal the subjective thermal assessment patterns, we used questionnaire surveys and simultaneous meteorological measurements in open air urban environments. We utilized data from a 3-year-long outdoor thermal comfort campaign, conducted on 78 days in 2011, 2012, and 2015 in six public spaces of Szeged, Hungary. Corresponding to the outdoor activities of people in this climate zone, the interviews and the meteorological measurements were carried out during spring, summer, and autumn. (More information on the Hungarian thermal comfort surveys is available in *Kántor et al.,* 2011, 2012, 2016b; *Kovács et al.,* 2016; *Kántor,* 2016.)

In frame of the surveys we recorded the thermal perception of people on a 9-point scale (thermal sensation vote, *TSV*). The applied *TSV* scale ranged from –4 to 4, corresponding to the perception of very cold to very hot. Then the thermal sensation votes were paired with the measured atmospheric parameters according to the exact time when the *TSV* data were recorded. From the meteorological data (air temperature, relative humidity, wind velocity, and mean radiant temperature), *PET* values were calculated with the RayMan software (*Matzarakis et al.,* 2010). Then we used the obtained 5805 *TSV–PET* datapairs to reveal the subjective thermal sensation patterns of Hungarians in different seasons.

In order to develop a new *PET* rating system, at first, *TSV* responses were plotted against *PET*. Instead of the usage of the actual TSVs, mean thermal sensation votes (*MTSV*) were used, which were calculated according to 1°C-wide bins of *PET* values (*Fig. 2*). It should be emphasized that MTSVs were weighted with the number of cases per *PET*-bin, similarly to the method of *Nakano* and *Tanabe* (2004) and *Yang et al.* (2013). Then, we performed regression analyses between the subjects' MTSVs and *PET*. The analyses were implemented separately for each evaluated season. The number of data pairs were 2792 in spring, 1097 in summer, and 1916 in autumn.

In every season, statistically significant regression equations ($p = 0.000$) were obtained, and quadratic model was found to increase the value of determination coefficient (R^2) compared to linear regression. Thus, we present only the quadratic functions in this study and use them for further analysis. The slope of the regression lines represents the 'thermal sensitivity' of subjects against the changes of *PET*. All of the obtained equations indicate that Hungarians react more sensitively to one unit increment of *PET* in the cooler parts of the *PET*-scale, than in the warmer end, revealing an enhanced heat tolerance (*Fig. 2*).

The presented seasonal *MTSV* vs. *PET* quadratic regression functions formed one of the main pillars of the next step of our study, that is, the development of a *PET*-based rating system for *TCI*. Beside the regression equations, we defined a new relationship, where sub-index rating scores from

zero (unfavorable) to five (optimal) were assigned to *PET* values. For providing full details on the conceptual and methodological aspects of the modification and adjustment of *TCI*, see *Kovács et al.* (2016).

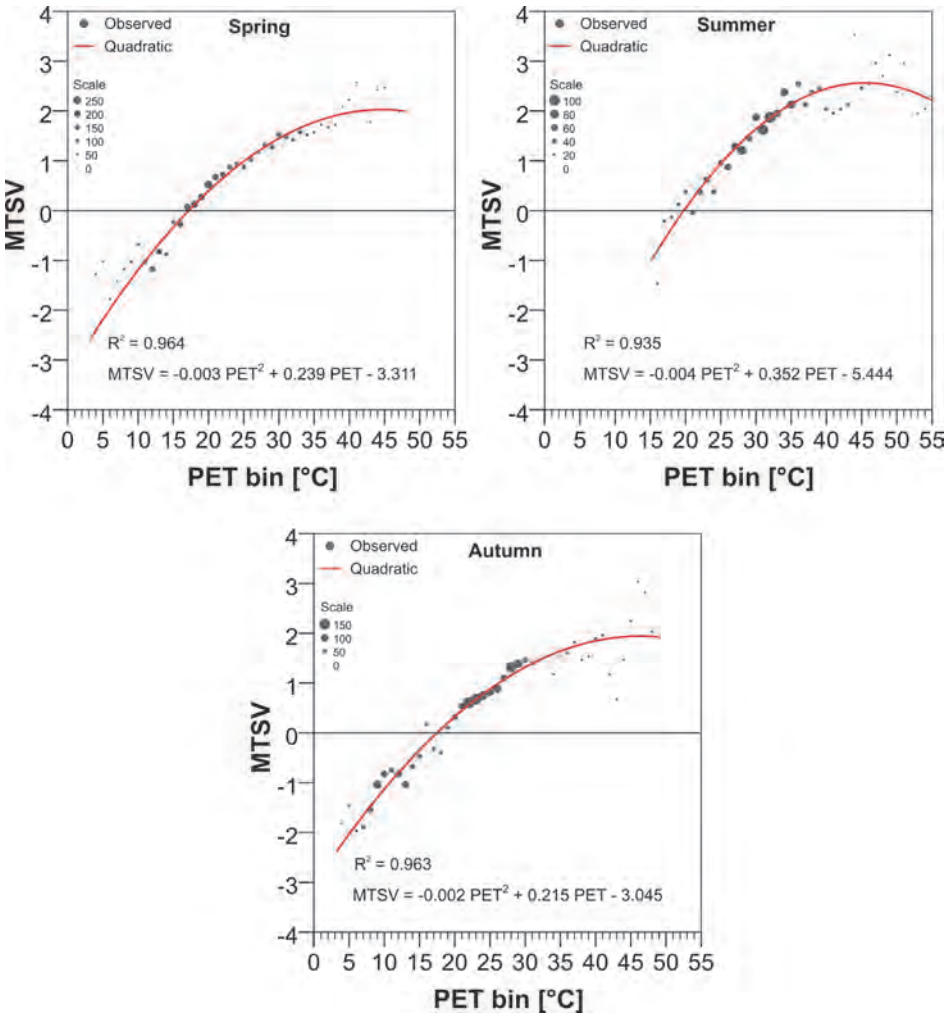

Fig. 2. Quadratic regression between the mean thermal sensation votes of Hungarians vs. the physiologically equivalent temperature (*PET*) in spring, summer, and autumn.

Fig. 3 illustrates the derived seasonal relationships between *PET* and the rating scores. Each *PET* value takes a score between zero and five. These relationships

are utilized in the new *CId* and *CIa* thermal comfort sub-indices to rate *PET* values (instead of to rate the *ET* values with the scores in the case of the original *TCI*, see *Fig. 1*). In practice, the new *CId* and *CIa* sub-indices are derived utilizing daytime maximum and daytime average *PET* values. The rating systems of the precipitation (*R*), sunshine (S*)*, and wind speed (*W*) sub-indices were not modified and are used in accordance with the rating methods of *Mieczkowski* (1985) (*Fig. 1*).

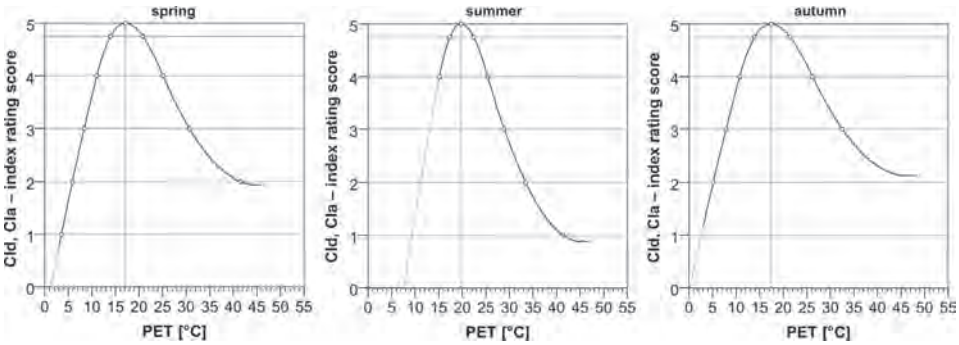

Fig. 3. The derived *PET* rating scores for the thermal sub-indices (*CId* and *CIa*) of modified *TCI* in different seasons based on the thermal sensation votes of Hungarians.

2.3. Quantifying the impact of climate change on tourism potential

The CRIGiS project, which constitutes the base of the present study, was the part of a broader program called '*Adaptation to Climate Change*' (*ACC,* 2016). Beyond establishing assessment methodologies, the program aimed at installing a system providing reliable database for supporting development of domestic adaptation activities to climate change. The implementation of the program started with the establishment of the National Adaptation Geo-information System (NAGiS) (*NAGiS,* 2016). The NAGiS aimed at supporting strategic planning and decision-making on the adaptation to climate change through development and operation of a multipurpose, geo-information database, which could merge several data sources derived from diverse sectors, such as hidrology, agriculture, and natural ecosystems. The CRIGiS project was initiated to extend the NAGiS with new data layers to further sectors. This extension includes indicators of exposure, sensitivity, and adaptive capacities in the tourism sector, as well as in the critical infrastructure sectors. One of the main goals of the tourism-related part of CRIGiS was to allow the outcomes usable for analyses aiming to estimate the effects of climate change on tourism potential. Such investigations can contribute to help in impact assessments and

resilience tests related to climate change in tourism sector. Ultimately, the results can be usable promoting sustainable tourism development.

The new, tourism-related data layers (i.e., original and modified *TCI*) were established for different time periods. First of all, based on observational data, they were calculated for the period of 1961–1990. On the other hand, future values of these indices were obtained from regional climate model projections for the periods of 2021–2050 and 2071–2100. The observational data were derived from the database used in CarpatClim project (as well as in *Hódos,* 2014), homogenized and interpolated with the methods MASH and MISH. However, the target area was extended to the whole area of Hungary (covering 45.8–48.6°N and 16–27°E). The climate projections were provided by the ALADIN-Climate, a regional climate model (RCM) applied at the Hungarian Meteorological Service (*Csima* and *Horányi,* 2008). The model run relied on A1B emission scenario described in the Special Report on Emissions Scenarios (SRES; *Nakicenovic et al.,* 2000), which concerns average future changes in socioeconomic conditions and population.

The climate projections did not contain information about the future values of sunshine duration, which are, however, required to calculate *TCI* and *mTCI*. Thus, sunshine duration was obtained from daily cloud cover data according to the method suggested by *Monteith* (1965) and adopted by several studies calculating *TCI* from climate model data (*Amelung,* 2006; *Perch-Nielsen et al.,* 2010; and *Mailly et al.,* 2014).

The original *TCI* values were determined according to the rating schemes and formula of *Mieczkowski* (1985) (see *Section 2.1.*). For the modified *TCI*, daily values of the observational and model data were applied instead of monthly values; moreover, calculation of *PET* required daily averages of total cloudiness as well. We determined daily *PET* values from air temperature, relative humidity, wind velocity, and cloud cover data by utilizing RayMan. For the new *CId* sub-index of *TCI* (which relies on daily maximum *PET*), the daily maximum temperature, daily minimum relative humidity, daily average wind speed, and daily average cloud cover data were used. For the new *CIa* sub-index (which relies on daily average *PET*), daily average temperature, relative humidity, wind speed, and cloud cover data were used. From the daily maximum PETs, daily average PETs, and the other necessary variables (precipitation, sunshine duration, and wind speed), monthly averages were taken and then monthly *mTCI* values were calculated.

For future exposure analysis, the so-called delta-method was applied. This means that the changes between the modeled future outcomes (2021–2050, 2071–2100) and the past model data (1961–1990) were determined, and the differences between them were added to the observational data (1961–1990). The reason for using delta method was to filter the systematic errors of model results. It should be emphasized that this method was used not for the raw model results but for the exposure assessment outcomes (i.e., for *TCI* and *mTCI* data).

The outcomes, therefore, combined past 'exposure observations' and changes occurring in the 'exposure' (*Fig. 4*).

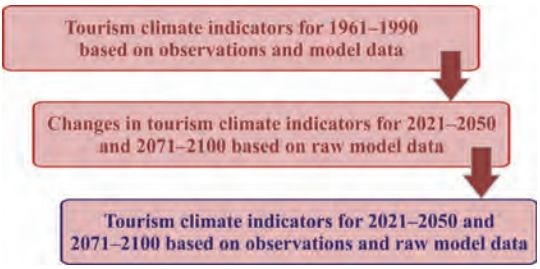

Fig. 4. Process of determining tourism climate indicators based on observations and model data.

The climate indicators were calculated on a 0.1°×0.1° (about 10 km) horizontal resolution grid of the observational and climate model data, for a total of 1104 grid points in Hungary. In order to display of tourism climate indices on maps, district averages were calculated from the grid point data as this provides more beneficial results for the users, such as tourists and tourism professionals. The district is an administrative territorial unit in Hungary. The spatial distribution of *TCI* and *mTCI* are presented on a monthly basis and on district level.

3. Results

In this paper, the results of the middle months of the seasons, April, July, and October are presented. We classified *TCI* and *mTCI* values according to the rating categories in *Table 2*, with the only exception of *TCI* values below 40, which were merged into a category 'unfavorable', if at all.

First, the results based on observational data are presented for the two indicators (*Figs. 5a–10a*). In April, according to original *TCI*, some western and northern districts are characterized with acceptable conditions (range of 50–59), while in the other parts of the country, including the whole Great Hungarian Plain, good conditions occur (60–69) (*Fig. 5a*). Modified *TCI* indicates more favorable conditions, generally by two categories: very good (70–79) conditions are found in Transdanubia and the northern regions, while the climate potential is excellent (80–89) in most parts of the Great Plain (*Fig. 6a*). Almost every district are characterized with at least excellent climatic conditions in July according to *TCI*, moreover, in most parts of the Great Plain, the climatic conditions reach the ideal category (90–100) (*Fig. 7a*). The *mTCI* pattern

usually signals less pleasant conditions by two categories, and its distribution is slightly more diverse. It is worth mentioning that this means still good or very good circumstances (*Fig. 8a*). October shows similar results as April concerning both the category level and the spatial distribution of *TCI* and *mTCI* (*Figs. 9a–10a*).

Turning our attention for future assessments through climate model results, considerable changes will not be probable for the mid-century according to *TCI* in April *(Fig. 5b)*. For the end of the century, most parts of the country will likely to be characterized with good conditions; only some mountainous districts remain acceptable, while in a few districts in the Great Plain, very good conditions are displayed (*Fig. 5c*). In the case of *mTCI*, only a slight redistribution will be probable for the mid-century (*Fig. 6b*). However, for the end of the century, large parts of the country may experience an improvement in climatic circumstances, that is, the conditions in Transdanubia and the northern districts may become excellent like in the Great Plain (*Fig. 6c*).

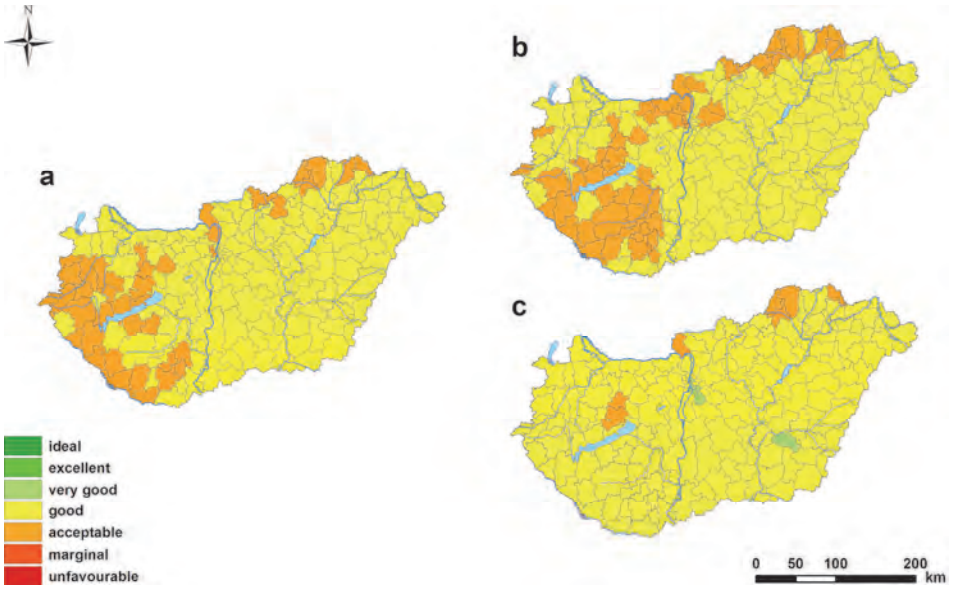

Fig. 5. Spatial distribution of *TCI* categories in April by districts for 1961–1990 (a), 2021–2050 (b), and 2071–2100 (c).

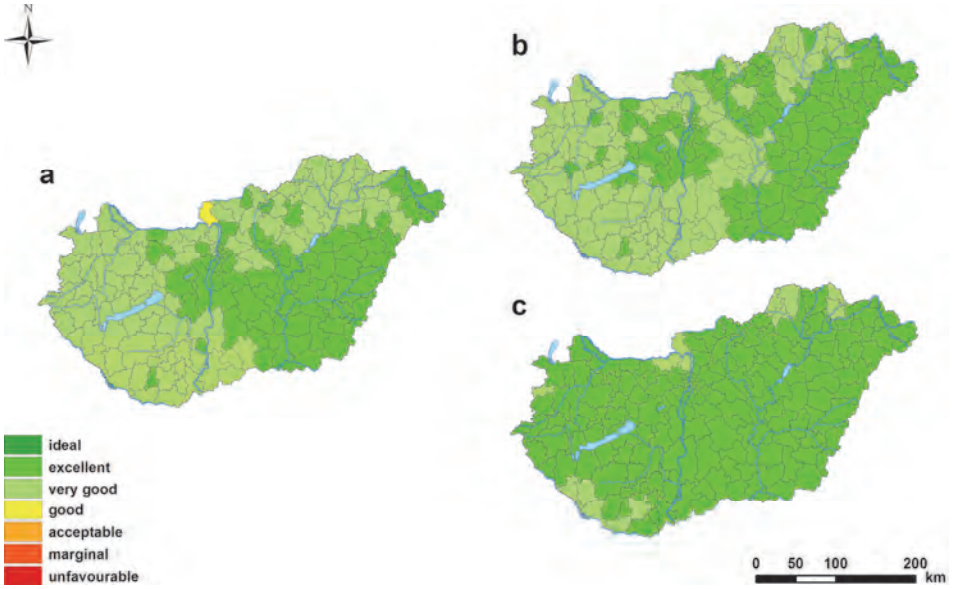

Fig. 6. Spatial distribution of *mTCI* categories in April by districts for 1961–1990 (a), 2021–2050 (b), and 2071–2100 (c).

The tendencies are similar for the future periods in the case of both indicators in July. Both of them indicate considerable changes but for unfavorable direction *(Figs. 7–8)*. According to *TCI*, ideal conditions may not occur at all, and the ratio of excellent areas may decrease for the mid-century *(Fig. 7b)*. At the end of the century, very good conditions are probable in the northern part of the country, while good conditions are displayed in the Great Plain and southwestern part of Transdanubia (*Fig. 7c*). According to *mTCI* patterns, the ratio of the very good conditions may decrease for the mid-century, and good conditions may dominate in most parts of the country. Moreover, in the southwestern part of Transdanubia, acceptable conditions are displayed *(Fig. 8b)*. For the end of the century, *mTCI* pattern indicates acceptable conditions in greater parts of the country, mainly in the whole southwestern part of Transdanubia and southern Great Plain (*Fig. 8c*). The spatial pattern of *mTCI* categories at the end of the century is similar to the case of *TCI* but they indicate less favorable conditions for light outdoor activities.

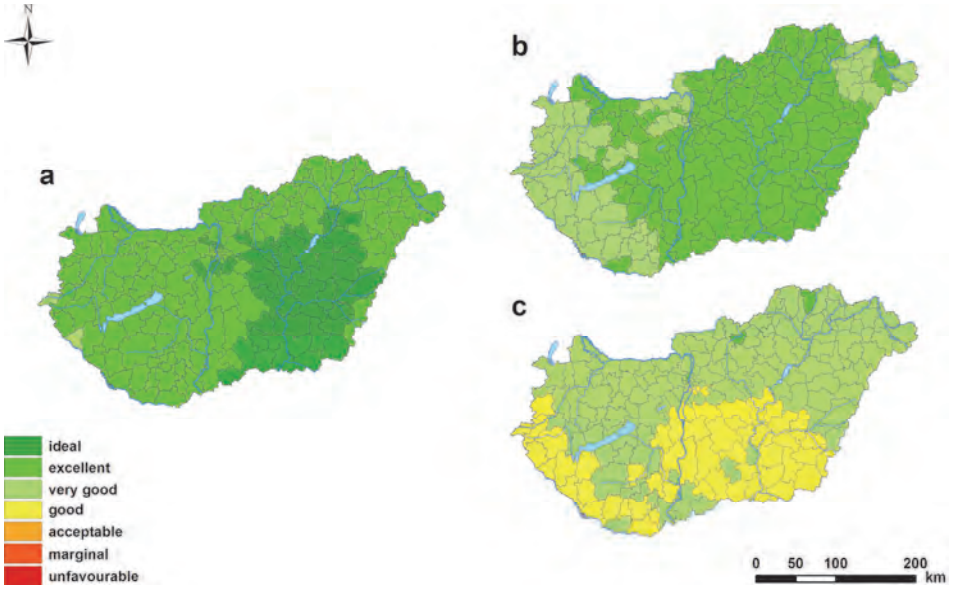

Fig. 7. Spatial distribution of *TCI* categories in July by districts for 1961–1990 (a), 2021–2050 (b), and 2071–2100 (c).

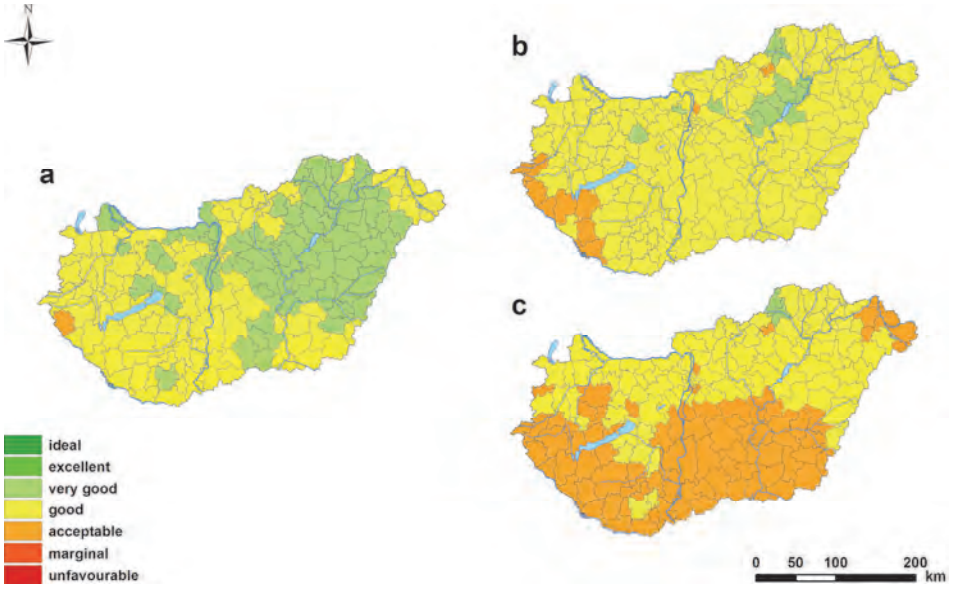

Fig. 8. Spatial distribution of *mTCI* categories in July by districts for 1961–1990 (a), 2021–2050 (b), and 2071–2100 (c).

In October, according to *TCI*, more remarkable improvement in climate potential is probable than in April, which already refers to the mid-century period (*Fig. 9b*). For this period, most parts of the country will likely to be characterized with good conditions, moreover, a remarkable part of the Great Plain may become very good. The improvement continues to the end of the century, moreover, at this time excellent conditions will be probable in a few southeastern districts of the Great Plain (*Fig. 9c*). The *mTCI* patterns indicate unchanged conditions or an improvement by a category (*Fig. 10*). Here, in the mid-century, already excellent conditions are indicated in most parts of the country, which was not the case in April.

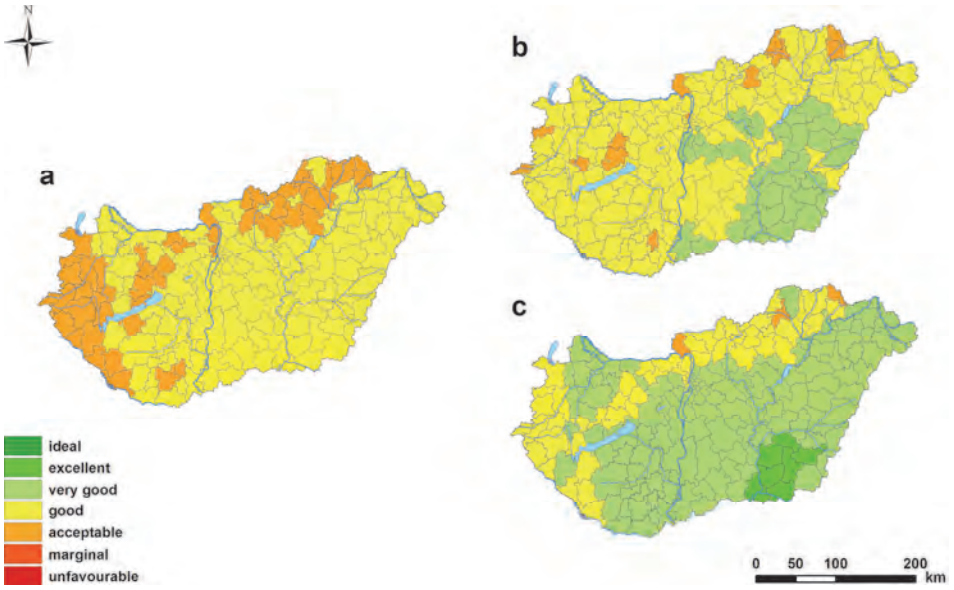

Fig. 9. Spatial distribution of *TCI* categories in October by districts for 1961–1990 (a), 2021–2050 (b), and 2071–2100 (c).

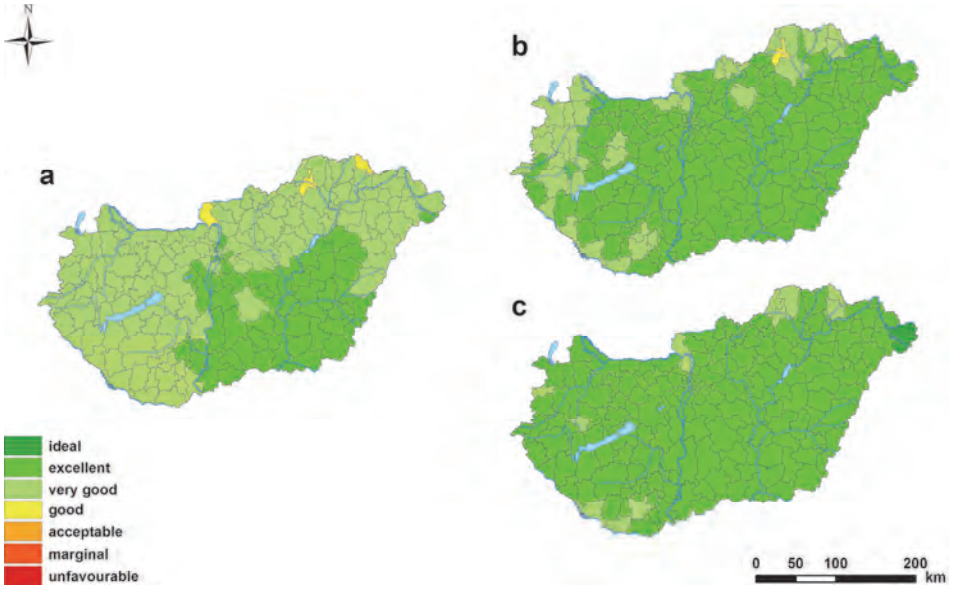

Fig. 10. Spatial distribution of *mTCI* categories in October by districts for 1961–1990 (a), 2021–2050 (b), and 2071–2100 (c).

4. Summary and concluding remarks

The study presented some tourism-related outcomes of the CRIGiS project based on the original *TCI* as well as on a modified form of *TCI*, that was adjusted to the subjective thermal assessment of Hungarian residents. According to the district-based spatial patterns of *TCI* and *mTCI* through observational data, the following outlines can be drawn for the three selected months:

– In the shoulder months (April and October), the Great Hungarian Plain as well as some northern and eastern parts of Transdanubia have more favorable climatic conditions by a category than the other parts of the country according to both indices. The *mTCI* pattern indicates more pleasant conditions than that of *TCI* generally by two categories.

– July has more favorable conditions than April and October according to *TCI*, however, *mTCI* indicates less pleasant circumstances in July compared to the shoulder months.

According to the climate model outcomes, the tourism climate potential changes for the end of the century are as follows:

– In April, the climatic conditions in Transdanubia and the northern parts of the country will likely to improve by a category and may become the same as in the Great Plain concerning both indices. The conditions may remain unchanged in most parts of the Great Plain.
– October shows an improvement by a category according to *TCI*, moreover, some southeastern districts in the Great Plain may expect two *TCI* categories improvement. According to *mTCI* patterns, the climatic conditions in Transdanubia and the northern parts may improve by a category and become the same as in the Great Plain.
– In July, most parts of the country may become less favorable for tourism. Both indices signal that climatic conditions are likely to deteriorate mostly at the southwestern part of the country and at the southern part of the Great Plain. The climatic conditions will still remain at least acceptable even from the Hungarian assessment point of view.

It should be borne in mind when considering the results, that the tourism climate potential of an area is associated with the features how tourism sector is affected by the present and future climatic circumstances. However, the competitiveness and economic success of tourism businesses and destinations are highly influenced by several socioeconomic mechanisms and factors (e.g., budget, accessibility and distance, presence of markets) and by natural or cultural landscape elements affecting tourist decision-making (e.g., geology, hidrology, vegetation, historical monuments, celebrations) as well (*de Freitas,* 2003; *Gómez Martín,* 2005).

Since one of the most important objectives of project CRIGiS was to develop a methodology for impact and vulnerability assessments, they were based on the outputs of a single regional climate model (RCM) simulation. Nevertheless, in a further step, the investigations have to be repeated using more RCM results to quantify the uncertainties of the projection for the users (in the absence of this, outcomes of any impact study cannot be properly interpreted).

In order to accomplish the other comprehensive goal of the project, i.e., to install a geo-information system providing reliable database, the datasets (i.e., *TCI* and *mTCI* data layers) were prepared to be compatible with the NAGiS system. Thus, the outcomes could be established in the datasets of NAGiS to be ready for use. The results are available for public use since May, 2016 (*NAGiS,* 2016).

Acknowledgement: This paper has been published with the support of Iceland, Liechtenstein and Norway through the EEA Grants and the Regional Environmental Centre.

References

ACC, 2016: Program 'Adaptation to Climate Change'. http://eea.rec.org/index.php?page=home-en (last accessed 23 May, 2016)

Amelung, B., 2006: Global (environmental) change and tourism. Issues of scale and distribution. PhD Dissertation, Universitaire Pers Maastricht. Amelung Publishers, Maastricht

Amelung, B. and *Viner, D.,* 2006: Mediterranean tourism: exploring the future with the tourism climatic index. *J. Sustainable Tour. 14,* 349–366.

Amelung, B., Nicholls, S. and *Viner, D.,* 2007: Implications of global climate change for tourism flows and seasonality. *J. Travel Res. 45,* 285–296.

Amelung, B. and *Moreno, A.,* 2012: Costing the impact of climate change on tourism in Europe: results of the PESETA project. *Climatic Change 112,* 83–100.

Amelung, B. and *Nicholls, S.,* 2014: Implications of climate change for tourism in Australia. *Tourism Manage. 41,* 228–244.

Amengual, A., Homar, V., Romero, R., Alonso, S. and *Ramis, C.,* 2012: Projections of the climate potential for tourism at local scales: application to Platja de Palma, Spain. *Int. J. Climatol. 32,* 2095–2107.

CRIGiS, 2016: Project '*Vulnerability/impact studies with a focus on tourism and critical infrastructures*'. http://www.met.hu/KRITeR/en/kezdo/ (last accessed 23 May, 2016)

Crompton, J.L., 1979: Motivations for pleasure vacation. *Ann. Tourism Res. 6,* 408–424.

Csima, G. and *Horányi, A.,* 2008: Validation of the ALADIN-Climate regional climate model at the Hungarian Meteorological Service. *Időjárás 112,* 155–177.

De Freitas, C.R., 2003: Tourism climatology: evaluating environmental information for decision making and business planning in the recreation and tourism sector. *Int. J. Biometeorol. 48,* 45–54.

De Freitas, C.R., Scott, D. and *McBoyle, G.,* 2008: A second generation climate index for tourism (*CIT*): specification and verification. *Int. J. Biometeorol. 52,* 399–407.

Farajzadeh, H. and *Matzarakis, A.,* 2009: Quantification of climate for tourism in the northwest of Iran. *Meteorol. Appl. 16,* 545–555.

Gómez Martín, B., 2005: Weather, climate and tourism. A geographical perspective. *Ann. Tourism Res. 32,* 571–591.

Gómez Martín, B., 2006: Climate potential and tourist demand in Catalonia (Spain) during the summer season. *Climate Res. 32,* 75–87.

Gössling, S., Bredberg, M., Randow, A., Sandström, E. and *Svensson, P.,* 2006: Tourist perceptions of climate change: A study of international tourists in Zanzibar. *Curr. Issues. Tourism 9,* 419–435.

Gössling, S., Scott, D., Hall, C.M., Ceron, J-P. and *Dubois, G.,* 2012: Consumer behaviour and deman response of tourists to climate change. *Ann. Tourism Res. 39,* 36–58.

Hamilton, J.M. and *Lau, M.A.,* 2005: The role of climate information in tourist destination choice decision-making. In (*Gössling, S.* and *Hall, C.M.* (Eds.)) Tourism and global environmental change. Routledge, London, 229–250.

Hamilton, J.M., Madisson, D.J. and *Tol, R.S.J.,* 2005: Climate change and international tourism: a simulation study. *Glob. Environ. Change 15,* 253–266.

Hein, L., Metzger, M.J. and *Moreno, A.,* 2009: Potential impacts of climate change on tourism; a case study for Spain. *Curr. Opin. Environ. Sustain. 1,* 170–178.

Houghten, F.C. and *Yaglou, C.P.,* 1923: Determining equal comfort lines. *J. Am. Soc. Heat. Vent. Eng. 29,* 165–176.

Hódos, R., 2014: A turisztikai klímapotenciál alakulása a Kárpát-régióban 1961–2010 között. Bachelor's thesis, Eötvös Loránd University, Budapest. http://nimbus.elte.hu/tanszek/docs/BSc/2014/HodosRita_2014.pdf (last accessed 1 September, 2016) (In Hungarian)

Höppe, P., 1999: The physiological equivalent temperature – an universal index for the biometeorological assessment of the thermal environment. *Int. J. Biometeorol. 43,* 71–75.

Hu, Y. and *Ritchie, J.R.B.,* 1993: Measuring destination attractiveness: A contextual approach. *J. Travel Res. 32,* 25–34.

Hübner, A. and *Gössling, S.,* 2012: Tourist perceptions of extreme weather events in Martinique. *J. Destin. Mark. Manage 1,* 47–55.

IPCC, 2014: Climate change 2014: Impacts, adaptation, and vulnerability. Part A: Global and sectoral aspects. Contribution of Working Group II to the Fifth Assessment Report of the Intergovernmental Panel on Climate Change (*Field, C.B. et al.* (Eds.)). Cambridge University Press, Cambridge, United Kingdom and New York, NY, USA, 1132.

Jendritzky, G., 1993: The atmospheric environment – an introduction. *Experientia 49,* 733–738.

Kántor, N., Égerházi, L.A. and *Gulyás, Á.,* 2011: Assessments of the outdoor thermal conditions in Szeged, Hungary: perceptions and preferences of local individuals. In (*Gerdes, A.*, *Kottmeier, C.* and *Wagner, A.* (Eds.)) Climate and Constructions International Conference. Karlsruher Institut für Technologie, Karlsruhe, 307–314.

Kántor, N., Égerházi, L.A. and *Unger, J.,* 2012: Subjective estimation of thermal environment in recreational urban spaces – part 1: investigations in Szeged, Hungary. *Int. J. Biometeorol. 56,* 1075–1088.

Kántor, N., 2016: Differences between the evaluation of thermal environment in shaded and sunny position. *Hung. Geogr. Bull. 65,* 139–153.

Kántor, N., Kovács, A. and *Takács, Á.,* 2016a: Small-scale human-biometeorological impacts of shading by a large tree. *Open Geosci. 8,* 231–245.

Kántor, N., Kovács, A. and *Takács, Á.,* 2016b: Seasonal differences in the subjective assessment of outdoor thermal conditions and the impact of analysis techniques on the obtained results. *Int. J. Biometeorol. 60*, 1615–1635.

Kovács, A. and *Unger, J.,* 2014a: Modification of the tourism climatic index to central European climatic conditions – examples. *Időjárás 118,* 147–166.

Kovács, A. and *Unger, J.,* 2014b: Analysis of tourism climatic conditions in Hungary considering the subjective thermal sensation characteristics of the south-Hungarian residents. *Acta Clim. Chorol. Univ. Szegediensis 47–48,* 77–84.

Kovács, A., Unger, J. and *Szépszó, G.,* 2015: Adjustment of tourism climatological indicators for the Hungarian population in assessing exposure and vulnerability to climate change. In (*Demiroğlu, O.C., de Freitas, C.R., Scott, D., Kurnaz, M.L.* and *Ünalan, D.* (Eds.)) Proceedings of the 4th International Conference on Climate, Tourism and Recreation – CCTR2015. Istanbul Policy Center, Istanbul, Turkey, 71–76.

Kovács, A., Unger, J., Gál, C.V. and *Kántor, N.,* 2016: Adjustment of the thermal component of two tourism climatological assessment tools using thermal perception and preference surveys from Hungary. *Theor. Appl. Climatol 125,* 113–130.

Kozak, M., 2002: Comparative analysis of tourist motivations by nationality and destinations. *Tourism Manage. 23,* 221–232.

Mailly, D., Abi-Zeid, I. and *Pepin, S.,* 2014: A multi-criteria classification approach for identifying favourable climates for tourism. *J. Multi-Crit. Decis. Anal. 21,* 65–75.

Matzarakis, A. and *Mayer, H.,* 1996: Another kind of environmental stress: thermal stress. *WHO Newsl. 18,* 7–10.

Matzarakis, A., Rutz, F. and *Mayer, H.,* 2010: Modelling radiation fluxes in simple and complex environments: basics of the RayMan model. *Int. J. Biometeorol. 54,* 131–139.

Mayer, H., 2008: KLIMES – a joint research project on human thermal comfort in cities. *Ber. Meteor. Inst. Albert-Ludwigs-Univ. Freiburg 17,* 101–117.

Mieczkowski, Z.T., 1985: The tourism climatic index: a method of evaluating world climates for tourism. *Can. Geogr. 29,* 220–233.

Monteith, J.L., 1965: Evaporation and environment. In: The state and movement of water in living organism. Proceedings of the Symposia of the Society for Experinmental Biolology 19. Cambridge University Press, Cambridge, 205–234.

Moreno, A. and *Amelung, B.,* 2009: Climate change and tourist comfort on Europe's beaches in summer: a reassessment. *Coast. Manage. 37,* 550–568.

Moreno, A., 2010: Mediterranean tourism and climate (change): a survey based study. *Tour. Hosp. Plan. Dev. 7,* 253–265.

Morgan, R., Gatell, E., Junyent, R., Micallef, A., Özhan, E. and *Williams, A.T.,* 2000: An improved user-based beach climate index. *J. Coast. Conserv. 6,* 41–50.

NAGiS, 2016: National Adaptation Geo-information System. http://nater.mfgi.hu/en (last accessed 23 May, 2016)

Nakano, J. and *Tanabe, S-I.,* 2004: Thermal comfort and adaptation in semi-outdoor environments. *ASHRAE Trans. 110,* 543–553.

Nakicenovic, N., Alcamo, J., Davis, G., de Vries, B., Fenhann, J., Gaffin, S., Gregory, K., Grübler, A., Jung, T.Y., Kram, T., La Rovere, E.L., Michaelis, L., Mori, S., Morita, T., Pepper, W., Pitcher, H., Price, L., Riahi, K., Roehrl, A., Rogner, H-H., Sankovski, A., Schlesinger, M., Shukla, P., Smith, S., Swart, R., van Rooijen, S., Victor, N., and *Dadi, Z.,* 2000: *IPCC special report on emissions scenarios*. Cambridge University Press, Cambridge

Németh, Á., 2013: Estimation of tourism climate in the Lake Balaton Region, Hungary. *J. Environ. Geogr. 6,* 49–55.

Nicholls, S. and *Amelung, B.,* 2008: Climate change and tourism in Northwestern Europe: Impacts and adaptation. *Tourism Anal. 13,* 21–31.

Perch-Nielsen, S.L., Amelung, B. and *Knutti, R.,* 2010: Future climate resources for tourism in Europe based on the daily Tourism Climatic Index. *Climatic Change 103,* 363–381.

Roshan, G., Yousefi, R. and *Fitchett, J.M.,* 2016: Long-term trends in tourism climate index scores for 40 stations across Iran: the role of climate change and influence on tourism sustainability. *Int. J. Biometeorol. 60,* 33–52.

Rutty, M. and *Scott, D.,* 2010: Will the Mediterranean become "too hot" for tourism? A reassessment. *Tour. Hosp. Plan. Dev. 7,* 267–281.

Rutty, M. and *Scott, D.,* 2014: Thermal range of coastal tourism resort microclimates. *Tourism Geogr. 16,* 346–363.

Scott, D. and *McBoyle, G.,* 2001: Using a 'tourism climate index' to examine the implications of climate change for climate as a natural resource for tourism. In (*Matzarakis, A.* and *de Freitas, C.R.* (Eds.)) Proceedings of the First International Workshop on Climate, Tourism and Recreation. International Society of Biometeorology, Commission on Climate, Tourism and Recreation, Halkidi, Greece, 69–88.

Scott, D., McBoyle, G. and *Schwartzentruber, M.,* 2004: Climate change and the distribution of climatic resources for tourism in North America. *Climate Res. 27,* 105–117.

Scott, D., Gössling, S. and *de Freitas, C.R.,* 2008: Preferred climates for tourism: case studies from Canada, New Zealand and Sweden. *Climate Res. 38,* 61–73.

Scott, D., de Freitas, C.R. and *Matzarakis, A.,* 2009: Adaptation in the tourism and recreation sector. In (*Ebi, K.L., Burton, I.* and *McGregor, G.R.* (Eds.)) Biometeorology for adaptation to climate variability and change. Springer Netherlands, Dordrecht, 171–194.

Scott, D. and *Lemieux, C.,* 2010: Weather and climate information for tourism. *Proc. Environ. Sci. 1,* 146–183.

Scott, D., Hall, C.M., and *Gössling, S.,* 2012: *Tourism and climate change: impacts, adaptation and mitigation.* Routledge, Abingdon

Szalai, S., Auer, I., Hiebl, J., Milkovich, J., Radim, T., Stepanek, P., Zahradnicek, P., Bihari, Z., Lakatos, M., Szentimrey, T., Limanowka, D., Kilar, P., Cheval, S., Deak, Gy., Mihic, D., Antolovic, I., Mihajlovic, V., Nejedlik, P., Stastny, P., Mikulova, K., Nabyvanets, I., Skyryk, O., Krakovskaya, S., Vogt, J., Antofie, T. and *Spinoni, J.* (2013): Climate of the Greater Carpathian Region. Final Technical Report. www.carpatclim-eu.org/ (last accessed 1 September, 2016)

Szentimrey, T. and *Bihari, Z.,* 2007: Manual of interpolation software MISHv1.02. Hungarian Meteorological Service, Budapest

Szentimrey, T., 2011: Manual of homogenization software MASHv3.03. Hungarian Meteorological Service, Budapest

Yang, W., Wong, N.H. and *Jusuf, S.K.,* 2013: Thermal comfort in outdoor urban spaces in Singapore. *Build. Environ. 59,* 426–435.

INSTRUCTIONS TO AUTHORS OF *IDŐJÁRÁS*

The purpose of the journal is to publish papers in any field of meteorology and atmosphere related scientific areas. These may be

- research papers on new results of scientific investigations,
- critical review articles summarizing the current state of art of a certain topic,
- short contributions dealing with a particular question.

Some issues contain "News" and "Book review", therefore, such contributions are also welcome. The papers must be in American English and should be checked by a native speaker if necessary.

Authors are requested to send their manuscripts to

Editor-in Chief of IDŐJÁRÁS
P.O. Box 38, H-1525 Budapest, Hungary
E-mail: journal.idojaras@met.hu

including all illustrations. MS Word format is preferred in electronic submission. Papers will then be reviewed normally by two independent referees, who remain unidentified for the author(s). The Editor-in-Chief will inform the author(s) whether or not the paper is acceptable for publication, and what modifications, if any, are necessary.

Please, follow the order given below when typing manuscripts.

Title page: should consist of the title, the name(s) of the author(s), their affiliation(s) including full postal and e-mail address(es). In case of more than one author, the corresponding author must be identified.

Abstract: should contain the purpose, the applied data and methods as well as the basic conclusion(s) of the paper.

Key-words: must be included (from 5 to 10) to help to classify the topic.

Text: has to be typed in single spacing on an A4 size paper using 14 pt Times New Roman font if possible. Use of S.I. units are expected, and the use of negative exponent is preferred to fractional sign. Mathematical formulae are expected to be as simple as possible and numbered in parentheses at the right margin.

All publications cited in the text should be presented in the *list of references*, arranged in alphabetical order. For an article: name(s) of author(s) in Italics, year, title of article, name of journal, volume, number (the latter two in Italics) and pages. E.g., *Nathan, K.K.,* 1986: A note on the relationship between photosynthetically active radiation and cloud amount. *Időjárás 90,* 10-13. For a book: name(s) of author(s), year, title of the book (all in Italics except the year), publisher and place of publication. E.g., *Junge, C.E.,* 1963: *Air Chemistry and Radioactivity.* Academic Press, New York and London. Reference in the text should contain the name(s) of the author(s) in Italics and year of publication. E.g., in the case of one author: *Miller* (1989); in the case of two authors: *Gamov* and *Cleveland* (1973); and if there are more than two authors: *Smith et al.* (1990). If the name of the author cannot be fitted into the text: *(Miller,* 1989); etc. When referring papers published in the same year by the same author, letters a, b, c, etc. should follow the year of publication.

Tables should be marked by Arabic numbers and printed in separate sheets with their numbers and legends given below them. Avoid too lengthy or complicated tables, or tables duplicating results given in other form in the manuscript (e.g., graphs).

Figures should also be marked with Arabic numbers and printed in black and white or color (under special arrangement) in separate sheets with their numbers and captions given below them. JPG, TIF, GIF, BMP or PNG formats should be used for electronic artwork submission.

More information for authors is available: journal.idojaras@met.hu

Published by the Hungarian Meteorological Service

Budapest, Hungary

INDEX 26 361

HU ISSN 0324-6329